The Auroral Large Imaging System
—Design, operation and scientific results

Akademisk avhandling

som med vederbörligt tillstånd av rektorsämbetet vid Umeå universitet för avläggande av filosofie doktorsexamen i rymdfysik framlägges till offentligt försvar i IRF:s aula, fredagen den 13 juni 2003, kl.9' (09.15.00). Disputationsakten kommer att äga rum på engelska.

av

Urban Brändström, Institutet för rymdfysik, Kiruna

Fakultetsopponent

Dr. Kirsti Kauristie, Meteorologiska institutet, Helsingfors, Finland.

Sammanfattning: Ett gemensamt skandinaviskt markbaserat nät av automatiserade stationer för avbildande norrskensstudier föreslogs 1989 av Åke Steen. Systemet gavs namnet ALIS efter engelskans "Auroral Large Imaging System". De huvudsakliga vetenskapliga motiven för detta återfanns inom norrskensfysiken, men möjligheten att använda ALIS för andra ändamål som tex. studier av polära stratosfärsmoln, meteorer och liknande fenomen insågs tidigt.

Denna avhandling fokuserar på konstruktion och drift av en svensk prototyp till ALIS bestående av sex obemannade fjärrstyrda stationer i norra Sverige som är inplacerade i ett rutnät med ungefär fem mils sida. Vidare ges en sammanfattning av de vetenskapliga resultaten.

Varje station är utrustad med en känslig, högupplösande (1024×1024 bildelement) icke-bildförstärkt avbildande monokromatisk CCD detektor. Ett filterhjul med plats för sex smalbandiga interferensfilter möjliggör avbildande spektroskopiska absolutmätningar av tex. norrskensemissioner. Stationernas inbördes avstånd (ca. 50 km) och synfält (ca. 50°–60°) är anpassade så att synfälten överlappar varandra. Detta gör det möjligt att använda triangulering och tomografiska metoder för att ta fram höjdinformation för de observerade fenomenen.

ALIS var troligen ett av de första instrumenten som utnyttjade icke-bildförstärkta högkvalitativa CCD detektorer för spektroskopiska avbildande flerstationsstudier av ljussvaga fenomen som tex. norrskensemissioner. Därvid är absolutkalibrering av de avbildande instrumenten ett lika viktigt som svårt problem.

Även om ALIS huvudsakligen byggdes för norrskensstudier, så kom, helt oväntat, merparten av de vetenskapliga resultaten från ett annat näraliggande område, nämligen radio-inducerade optiska emissioner. ALIS gjorde de första otvetydiga observationerna av detta fenomen på hög latitud samt den första inversionen (med tomografiliknande metoder) av höjdprofiler från dessa data. Övriga vetenskapliga resultat inkluderar uppskattningar av norrskenets elektronspektra med tomografiska metoder, resultat från koordinerade mätningar med satelliter och radarsystem samt studier av polära stratosfärsmoln. En ALIS-detektor användes vidare i ett samarbetsprojekt som resulterade i de första markbaserade norrskensbilderna tagna under dagtid. Nyligen gjorde ALIS observationer av ett meteorspår från en Leonid där en preliminär studie ger vissa belägg för att vatten observerats i meteorspåret.

Nyckelord: Flerstationsmätningar, Norrsken, Polära stratosfärsmoln, Radio-inducerade optiska emissioner, Rymdfysik, Spektroskopiskt avbildande mätningar, Tomografi.

The
Auroral Large Imaging System
—Design, operation and scientific results

Urban Brändström
Swedish Institute of Space Physics
Kiruna

April, 2003

Soli Deo Gloria

"Har jag i min tid något godt kunnat uträtta, gifwen derföre Gudi äran! Hwad jag af mensklig swaghet felat, förlåten mig för Christi skull."

Ur konung Gustaf 1:s afskedstal till rikets ständer d. 16 juni 1560

Sammanfattning

Ett gemensamt skandinaviskt markbaserat nät av automatiserade stationer för avbildande norrskensstudier föreslogs 1989 av Åke Steen. Systemet gavs namnet ALIS efter engelskans "Auroral Large Imaging System". De huvudsakliga vetenskapliga motiven för detta återfanns inom norrskensfysiken, men möjligheten att använda ALIS för andra ändamål som tex. studier av polära stratosfärsmoln, meteorer och liknande fenomen insågs tidigt.

Denna avhandling fokuserar på konstruktion och drift av en svensk prototyp till ALIS bestående av sex obemannade fjärrstyrda stationer i norra Sverige som är inplacerade i ett rutnät med ungefär fem mils sida. Vidare ges en sammanfattning av de vetenskapliga resultaten.

Varje station är utrustad med en känslig, högupplösande (1024×1024 bildelement) icke-bildförstärkt avbildande monokromatisk CCD detektor. Ett filterhjul med plats för sex smalbandiga interferensfilter möjliggör avbildande spektroskopiska absolutmätningar av tex. norrskensemissioner. Stationernas inbördes avstånd (ca. 50 km) och synfält (ca. $50°$–$60°$) är anpassade så att synfälten överlappar varandra. Detta gör det möjligt att använda triangulering och tomografiska metoder för att ta fram höjdinformation för de observerade fenomenen.

ALIS var troligen ett av de första instrumenten som utnyttjade icke-bildförstärkta högkvalitativa CCD detektorer för spektroskopiska avbildande flerstationsstudier av ljussvaga fenomen som tex. norrskensemissioner. Därvid är absolutkalibrering av de avbildande instrumenten ett lika viktigt som svårt problem.

Även om ALIS huvudsakligen byggdes för norrskensstudier, så kom, helt oväntat, merparten av de vetenskapliga resultaten från ett annat näraliggande område, nämligen radio-inducerade optiska emissioner. ALIS gjorde de första otvetydiga observationerna av detta fenomen på hög latitud samt den första inversionen (med tomografiliknande metoder) av höjdprofiler från dessa data. Övriga vetenskapliga resultat inkluderar uppskattningar av norrskenets elektronspektra med tomografiska metoder, resultat från koordinerade mätningar med satelliter och radarsystem samt studier av polära stratosfärsmoln. En ALIS-detektor användes vidare i ett samarbetsprojekt som resulterade i de första markbaserade norrskensbilderna tagna under dagtid. Nyligen gjorde ALIS observationer av ett meteorspår från en Leonid där en preliminär studie ger vissa belägg för att vatten observerats i meteorspåret.

Nyckelord: Flerstationsmätningar, Norrsken, Polära stratosfärsmoln, Radioinducerade optiska emissioner, Rymdfysik, Spektroskopiskt avbildande mätningar, Tomografi.

Abstract

The Auroral Large Imaging System (ALIS) was proposed in 1989 by Åke Steen as a joint Scandinavian ground-based network of automated auroral imaging stations. The primary scientific objective was in the field of auroral physics, but it was soon realised that ALIS could be used in other fields, for example studies of Polar Stratospheric Clouds (PSC), meteors and other atmospheric phenomena.

This report describes the design, operation and scientific results from a Swedish prototype of ALIS consisting of six unmanned remote-controlled stations located in a grid of about 50 km in northern Sweden. Each station is equipped with a sensitive high-resolution (1024×1024 pixels) unintensified monochromatic CCD-imager. A six-position filter-wheel for narrow-band interference filters facilitates absolute spectroscopic measurements of, for example, auroral and airglow emissions. Overlapping fields-of-view resulting from the station baseline of about 50 km combined with the station field-of-view of $50°$ to $60°$ enable triangulation as well as tomographic methods to be employed for obtaining altitude information of the observed phenomena.

ALIS was probably one of the first instruments to take advantage of unintensified (i.e. no image-intensifier) scientific-grade CCDs as detectors for spectroscopic imaging studies with multiple stations of faint phenomena such as aurora, airglow, etc. This makes absolute calibration a task that is as important as it is difficult.

Although ALIS was primarily designed for auroral studies, the majority of the scientific results so far have, quite unexpectedly, been obtained from observations of HF pump-enhanced airglow. ALIS made the first unambiguous observation of this phenomenon at high latitudes and the first tomography-like inversion of height profiles of the airglow regions. The scientific results so far include tomographic estimates of the auroral electron spectra, coordinated observations with satellite and radar, as well as studies of polar stratospheric clouds. An ALIS imager also participated in a joint project that produced the first ground-based daytime auroral images. Recently ALIS made spectroscopic observations of a Leonid meteor trail and preliminary analysis indicates the possible detection of water in the Leonid.

Keywords: Aurora, Artificial Airglow, HF pump-enhanced airglow, Multistation measurements, Polar Stratospheric clouds, Radio-Induced optical emissions, Space physics, Spectroscopic imaging observations, Tomography.

Preface

> "Vi få ej välja ramen för vårt öde. Men vi ge den dess innehåll. Den som vill äventyret skall också uppleva det — efter måttet av sitt mod. Den som vill offret skall offras — efter måttet av sin renhet." *Dag Hammarskjöld*

It is a great privilege to have the opportunity to finish this work that is an attempt to provide a comprehensive compilation of material related to the Auroral Large Imaging System (ALIS). ALIS was conceived by Åke Steen, who had visions extending far beyond this work, and nothing of what is reported here would have been made possible without his vision, enthusiasm, stubbornness and ability to acquire the necessary funding. His efforts, however, would have been impossible without the altruism and excellent leadership of Bengt Hultqvist, who was director of the Swedish Institute of Space Physics (IRF) 1957–1994. Bengt Hultqvist also read a draft of this work and provided much valuable advice. I also want to thank the present director of IRF, Rickard Lundin, as well as Stanislav Barabash and Jan Pohjanen, for ensuring me the excellent undisturbed working conditions that enabled me to complete this thesis. Thanks to Ingrid Sandahl for taking care of ALIS since 2001.

To make a complete list of acknowledgements is virtually impossible, yet I feel obliged to attempt to list at least some names as representatives for a much larger group. I begin by specially thanking Lars Wittikko for many years of hard work in the ALIS project, and also as a representative of all those who deserved an acknowledgement, but have never received one. My apologies for those painful, but equally unavoidable omissions! I also apologise now if I have, despite my best efforts, failed to provide proper references and credits anywhere.

A very special acknowledgement to Takehiko Aso and Masaki Ejiri, for their friendship, humble attitude, enthusiastic support of ALIS, inspiration and excellent ideas that kept me from giving up many times. "Domo arrigato!"

I acknowledge Carl-Fredrik Enell, Björn Gustavsson, Peter Rydesäter, Tima Sergienko and Asta Pellinen-Wannberg for their efforts with ALIS and ALIS data as well as for countless hours of proofreading encouragement and much more. I am also very much indebted to Carol Norberg and Rick McGregor who had the tedious task of correcting my English and also provided many valuable comments. I thank Lars Nilsson as a personification of those with the special gift of mastering the Art of computer programming.

I would also like to thank the past and present staff of IRF, ANS, EISCAT, ESRANGE, NIPR, etc. represented by this far too short and incomplete list of names: Vesa Alatalo, Nils-Åke Andersson, Göran Axelsson, Peter Bergquist, Göte Johansson, Hugo Johansson, Jan Johansson, Magnus Johansson, Christer Jurén, Juha Liikamaa, Aarne Luiro, Torbjörn Lövgren, Mats Luspa, Arne Moström, Olle Norberg, Jonas Olsen, Walter Puccio, Markus Rantakeisu, Akira Urashima, Bengt Wanhatalo and Masatoshi Yamauchi. As representatives of the many co-authors and colleagues around the world I would like to acknowledge Viktor Alpatov, Laila Andersson, Anasuya Aruliah, Paul Bernhardt, Mikael Hedin, Ingemar Häggström, Jouni Jussila, Kari Kaila, Oleg Kornilov, Mike Kosch, Shu Lai, Hans Lauche, Thomas Leyser, William McNeil, Edmond Murad,

Contents

List of Figures

List of Tables

Chapter 1

Introduction

Stig min klang mot sol mot norrskensbågar vida,
Väck sovande fjäll, slumrande myr och mo!
Vig åt arbete in fält, som fruktsamma bida,
Vig dem till sist en gång åt den eviga tystnadens ro!

Albert Engström

"And I looked, and, behold, a whirlwind came out of the north, a great cloud, and a fire infolding itself, and a brightness was about it, and out of the midst thereof as the colour of amber, out of the midst of the fire."
Ezekiel 1:4

"Norr-skenets rätta hemvist, det högsta av vår atmospher, är för oss och alla våra undersökningar otilgängeligt. Ögat och synen äro de ende medel, hvilka til röns inhämtande därvid kunna användas. Men äfven dem är ej tillåtit, at skåda Norr-skenen sådane som de äro i sig sjelfve, utan endast så, som de, på långt håll, visa sig för våra bedrägliga omdömen." *Wilcke [1778]*

The colourful and highly dynamic northern lights are one of the most fascinating and beautiful phenomena seen in the night sky. For as long as there have been people present at suitable locations, they have probably postulated over the origin and purpose of the aurora, first in terms of myths, superstitious interpretations, or religious beliefs and later on in terms of scientific methods. Ancient works by *Aristotle* [ca. 340 B.C.]; *Pliny* [ca. 77] and *Seneca* [ca. 63] with vivid descriptions of low latitude aurora are reported by *Chamberlain* [1995]. It is sometimes speculated if some ancient biblical texts might contain early descriptions of auroral events, such as, for example the vision of Ezeikel around 593 B.C., as quoted above [*Siscoe et al.*, 2002; *Raspopov et al.*, 2003, and references therein].

Many sources report that the name: "Aurora Borealis" (northern lights) was assigned by *Gassendi* [1651], however, research by *Siscoe* [1978] indicates that these terms existed earlier, and that they might be traceable to Galileo Galilei or his disciple Guiducci [*Eather*, 1980, p. 51].

When modern science emerged, explanations of the aurora began to be formulated. Initially only visual observations were available [for example *Gassendi*, 1651; *Celsius*, 1733; *de Mairan*, 1733]. In a speech to the king (Gustav III) and then, technology has improved considerably and there exists a plethora of auroral imagers based on television type cameras, often in a combination with an image intensifier. An example of a modern television-type imager is the excellent Portable Auroral Imager (PAI) intended for high-resolution auroral imaging [*Trondsen*, 1998]. A few more examples of television-type imagers are mentioned in Section 3.2.1.

Space-borne optical imagers simplified the monitoring of large-scale auroral features. The Viking imager [*Anger et al.*, 1987] may serve as an excellent example of this [see *Pellinen and Kaila*, 1991, for a more complete listing of space-borne imagers]. Polar/VIS[§] is a more recent example of the versatile capabilities of space-borne auroral imaging techniques. For global auroral imaging, the capability to use UV-emissions to measure sunlit day-side aurora is a great advantage [*Steen*, 1989]. However, auroral imaging from space *does not* make ground-based and rocket-borne studies obsolete, they are both powerful and complementary methods that should not be underestimated. For example, small- and medium-scale phenomena are difficult to study from space due to the spatial smearing caused by the orbital motion, as well as imprecisely known value of the effective albedo [*Steen*, 1989]. Furthermore the orbital motion prohibits continuous studies in a certain local time sector, as well as along a certain magnetic field-line. The best results tend to emerge when different observing methods are combined.

1.1.1 Auroral height estimations

The number of reliable height estimations of the aurora before those obtained from photographic methods are very few [*Størmer*, 1955]. The first measurement of the height of an aurora was made between 1726 and 1730 by *de Mairan* [1733] resulting in an estimated height of about 400–1300 km. Further reading on early height determinations is found in the works of *Wilcke* [1778]; *Størmer* [1955], and references therein.

By obtaining auroral photographs simultaneously from two or more locations, it is possible to employ triangulation techniques to estimate the height of the aurora. The first results from this method were obtained by *Størmer* [1911]. Later on the methods were improved and simplified [for example *Vegard and Krogness*, 1920], as described in the cornerstone work by *Størmer* [1955].

For examples of more recent height-determinations of the aurora see *Brandy and Hill* [1964]; *Romick and Belon* [1967]; *Brown et al.* [1976]; *Stenbaek-Nielsen and Hallinan* [1979]; *Kaila* [1987]; *Steen* [1988a,b]; *Aso et al.* [1990]; *Jones et al.* [1991]; *Aso et al.* [1993, 1994]; *Frey et al.* [1996], and references therein. However, embarking onto a detailed discussion of the many recent measurements extend far beyond the scope of this introduction.

1.1.2 Spectroscopic techniques

The auroral signal contains a considerable amount of spectral information. The first measurements of the auroral spectra were carried out by *Ångström* [1868, 1869]. He also named the convenient unit Ångström (1 Å = 0.1 nm). Another

[§] `http://eiger.physics.uiowa.edu/~vis/`

Chapter 2

ALIS, the Auroral Large Imaging System.

> "One of the symptoms of an approaching nervous breakdown is the belief that one's work is terribly important." *Bertrand Russell*

The first proposal for an Auroral Large Imaging System (ALIS), [*Steen*, 1989] suggested a net of 28 auroral imaging stations in northern Scandinavia spaced 100 km apart and with an average field-of-view (FoV) of 90° (Figure 2.1). It was anticipated that ALIS would be jointly funded and operated by the participating countries. In a later publication, [*Steen et al.*, 1990], the Swedish part of ALIS (Swe-ALIS) was considered in more detail. Here the station baseline was reduced to 50 km for 14 stations within Sweden with an average field-of-view of 60° (Figure 2.2). In 1990 funding for the costs for an initial subset of Swe-ALIS was received. This "mini-ALIS" would consist of four to eight stations (corresponding to stations numbered 1–8 in Figure 2.2). As design and construction work commenced, it became practice to use the acronym "ALIS" instead of "mini-ALIS" or "Swe-ALIS". As the title suggests, this practice will be adhered to also in this thesis. However, it is useful to remember that the present work represents only a first small step towards the auroral large imaging system that was originally envisioned [*Steen*, 1989; *Steen et al.*, 1990].

Design work on ALIS started in the fall of 1990. Construction work on the basic infrastructure started in 1991. The first camera became operational at the end of 1993 and the first auroral observations were carried out with it during early 1994. Later in 1995 ALIS consisted of 3 complete stations (and 3 stations without cameras), and participated for the first time in a scientific campaign [*Aso et al.*, 1998a,b]. During this campaign two additional intensified CCD-cameras were operated, giving a total of five observing sites. At this time most ALIS stations had no filter-wheels or camera positioning systems. In the following years, ALIS expanded to six fully-equipped stations. Table 2.1 shows the ALIS time-line.

This chapter focuses on the basic scientific and technical considerations affecting the design of the six-station ALIS, which was in full operation until April 2001.

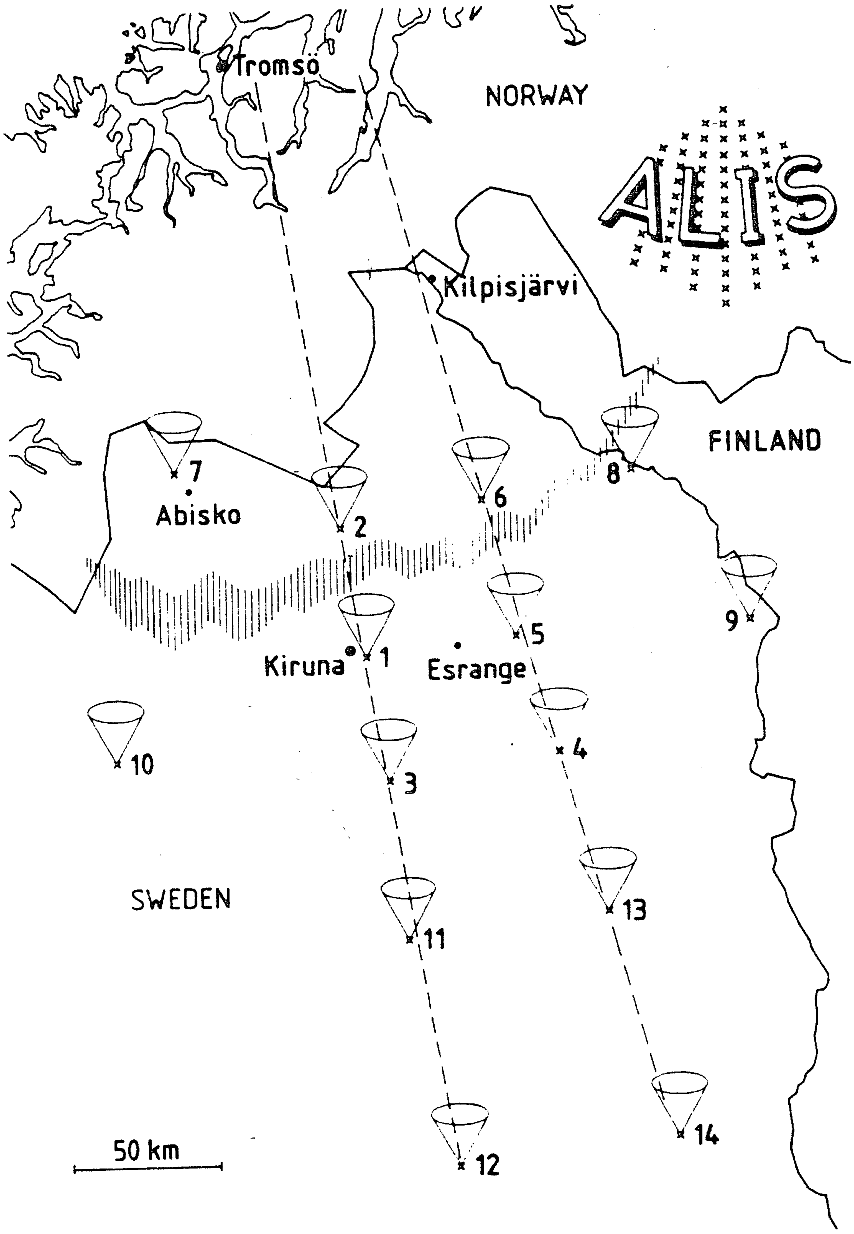

Figure 2.2: A proposed layout for the Swedish part of ALIS (Swe-ALIS). This layout was partly followed when deciding the final sites for the ALIS stations as given in Figure 2.4 and Table 2.3. [after *Steen et al.*, 1990]

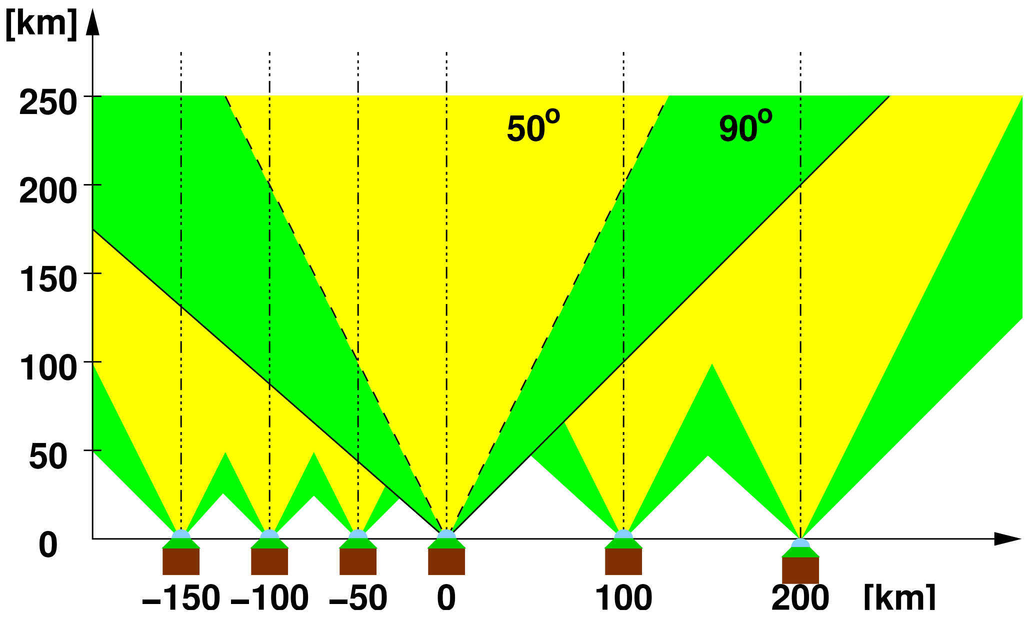

Figure 2.3: At a 50 km baseline (left) stations looking into zenith with a field-of-view of 90° (green) have overlapping fields-of-view from about 25 km. Limiting the field-of-view to about 50° (yellow) raises the height of overlap to 50 km. Increasing the station baseline to 100 km (right), the fields-of-view overlaps from about 50 km at 90°, and from about 100 km at about 50° field-of-view. It is furthermore seen that it is desirable to have steerable cameras in order to image a common volume with as many stations as possible (see also Figure 3.11).

				latitude			longitude			h
No.	Adr.	Site name	Acronym	$^\circ$	$'$	$''N$	$^\circ$	$'$	$''E$	m
1	S01	IRF	KRN	67	50	26.6	20	24	40.0	425
1	S01	Knutstorp	KRN	67	51	20.7	20	25	12.4	418
2	S02	Merasjärvi	MER	67	32	50.7	21	55	12.3	300
3	S03	Silkkimuotka	SIL	68	1	47.0	21	41	13.4	385
4	S04	Tjautjas	TJA	67	19	57.8	20	45	2.9	474
5	S05	Abisko	ABK	68	21	20.0	18	49	10.5	360
6	S06	Nikkaluokta	NIL	67	51	6.7	19	0	12.4	495
7	S07	Kilvo	KIL							
8	S08	Nytorp	NYT							
9	S09	Frihetsli	FRI							
10	S10	Mobile	BUS							

Table 2.3: Geographical coordinates of the ALIS stations. Notes: Station No. 1 moved in the summer of 1999, see text. Stations No. 7–8 were deployed on site but never used. Station No. 9 was never deployed. Station No. 10 is mobile.

tions, thereafter expansions towards east and west were desired. Practical considerations led to the stations being deployed in the following order (see Figure 2.4): (1) Kiruna, (2) Merasjärvi, (3) Silkkimuotka, (4) Tjautjas, (5) Abisko and (6) Nikkaluokta. After that, an expansion southward was planned with stations (7) Kilvo and (8) Nytorp. This was mainly in order to accommodate measurements of southward expansion of the auroral oval during the upcoming solar maxima. Later the plans were changed in favour of one station in Norway, (9) Frihetsli, to be possibly followed by a station at the EISCAT site at Ramfjordmoen, Norway. The motivation for this change of plans was to give a better support to combined measurements with EISCAT. Awaiting this expansion northward, a tenth mobile station provided zenith coverage along the Tromsø magnetic field-line during active experiments with HF pump-enhanced airglow and the EISCAT radar facility (Section 6.4). A summary of site numbers, names, acronyms and geographic coordinates is found in Table 2.3 and in Figure 2.4.

Station (1) Kiruna was initially located in the optical laboratory at IRF, Kiruna but had to be moved a couple of kilometres (to Knutstorp, close to the Kiruna EISCAT-site) in the fall of 1999 due to ongoing construction work and rising levels of man-made light pollution at the original site.

2.2 IT hardware and infrastructure

As might be expected, an unmanned large-scale remote-controlled facility like ALIS requires considerable amounts of Information Technology (IT), both in terms of computers and datacommunication infrastructure. As work on ALIS was initiated, much of what is taken for granted today simply did not exist, or was far too expensive. In other cases the technical evolution took unexpected turns, making some choices of technology appear awkward and obsolete today.

2.2.1 Computers

A variety of computer architectures and operating systems were available when work on ALIS started. At an early stage command and control functions were separated from image processing, data storage and transmission. The first specification of the computer systems for ALIS [*Brändström and Steen*, 1992] included a main computer and a dedicated Image Processing Computer (IPC) in the control centre. At the stations, one computer would be responsible for controlling the station, while a special dedicated unit, called the Near-sensor Interface and Processing Unit (NIPU), would handle the large amounts of data ($\geq$ 2 Mbytes/s) created by the imagers.

A Hewlett Packard HP-755 PA-RISC workstation was selected as the control centre main computer. Budgetary constraints prohibited the use of similar computers at the stations. Therefore it was decided to use IBM-PC compatible machines (i486). Due to the fast development of computer hardware, the station computers have been replaced after typically 3 years of operation. The current system still uses various PCs (ranging from i486 to Pentium III). At the control centre the HP-755 computer lasted until 1999 when it was replaced by two PCs. The aim of having a dedicated image processing computer has not been realised as no real-time data is yet available due to the absence of high-speed lines to the stations. Dataanalysis is performed on various workstations.

2.2.2 The NIPU

The datahandling, image processing and data storage at the stations were supposed to be handled by a dedicated computer. Around 1990, a very promising device for this purpose was the Transputer, a parallel processing device communicating with other devices over four serial links. Another interesting device was the Intel I860 floating-point processor. A prototype system was built using the T222 and T800 Transputers. Apart from the imager itself it was also desirable to control the Camera Positioning System (CPS) as well as the filter-wheel from the NIPU. In this way the NIPU would control all subsystems related to the imager. The ALIS imager would produce over 2 Mbytes/s, which was too fast for the T222/T800 Transputer links (capable of 20 Mbits/s). However a new Transputer, the T9000, was expected to be released around 1992. This device would have enhanced links capable of 100 Mbits/s and increased processing power (25 MFLOPS), and would thus be well-suited for demanding image-processing applications [*Pountain*, 1991]. Designs were made for this device, but its release was postponed several times due to technical problems. Since the camera controller for the ALIS-Imager (Chapter 3) was also based on a Transputer, the T222, a T800 in the NIPU was chosen as an intermediate solution for handling the incoming image data. Due to the limitations of the link-speed of these Transputers, data was to be transferred to the NIPU over a 16-bit parallel interface. Six NIPUs of this design were built (Figure 2.5).

Meanwhile the fast development of the PCs eventually made the Transputers obsolete, and around 1997 it was decided that a second PC would take over the responsibilities of the NIPU. A prototype PCI-board with a DSP was designed and tested, but during this work technical problems with the parallel read-out from the camera controller were discovered (Section 3.3.4). Since these problems could not be resolved, the resulting decrease of the maximum imager frame-rate made both the NIPU and the second PC for receiving image data superfluous. Therefore the six already existing NIPUs ended up as rather over-designed controllers for the camera-positioning system (Section 3.6) and the filter-wheels (Section 3.5.1).

2.2.3 Communication systems

When design work on ALIS began, the fastest off-the-shelf modem available was at 2400 bits/s, and with a special, rather expensive, leased-line one could attain 9600 bits/s. The first ALIS paper [*Steen*, 1989] specified a ≥ 10 Mbits/s communication link capable of near real-time image transfer to the control centre. A network of microwave links was considered but deemed far too expensive, as was the case with the fibre-optic lines passing near two of the stations (Merasjärvi, Silkkimuotka, see below).

Dial-up telephone lines were too slow, and faster means of communication too expensive. It was anticipated that the fast technological development in this field would make faster communication lines available at a reasonable cost. Thus it was decided that ALIS would use slow dial-up modem lines for command, status information and to transmit reduced quick-look images to the control centre. A future "to be defined" high-speed link to the control centre would provide the high-speed communication required for real-time transfer of raw image data. Meanwhile, local data storage, and on-site image processing of the data would be employed at the stations.

The dial-up lines were one of the major sources of trouble in ALIS during the early years. This was mainly due to bad telephone lines and old electromechanical telephone switching equipment. This led to extensive efforts to troubleshoot modem lines and to develop reliable communications software. Also the modem technology and quality of the telephone lines improved considerably over the years. Today the dial-up lines are capable of reliable 28800 bits/s communication, using the standard Point-to-Point Protocol (ppp) [*Simpson*, 1994].

The high-speed link remains to be defined. The optimal solution would be optical fibres (> 100 Mbits/s), but other solutions are also possible, such as ADSL (500 kbits/s), ISDN (< 128 kbits/s), radio-links (> 1 Mbits/s), etc.

Stations (2) Merasjärvi and (3) Silkkimuotka are located in the proximity of nodes for high bandwidth fibre-optic communication lines. (5) Abisko is located close to the Abisko Scientific Station (ANS) which recently acquired high-speed fibre optic Internet connection.

Presently only the Kiruna station has a 2 Mbits/s Ethernet connection to Internet realised by a microwave-link to IRF, the rest of the stations are connected by means of 28 kbits/s dial-up modem lines. The rapidly increasing demand for high-speed Internet subscriptions among the general public might speed up the process of getting faster communication lines for all ALIS stations at a reasonable cost.

reluctantly chosen remaining option was to use MS-DOS at the stations. This lead to limitations in the flexibility of the system.

Some years later highly reliable and free operating systems such as Free-BSD and GNU/Linux emerged. It was immediately realised that a change to one of these operating systems at the stations would be necessary to meet the required data-handling specifications. In 1997 all stations had changed operating systems to Debian GNU/Linux, and in the fall of 1999 the HP-UX operating system in the control centre was also changed to GNU/Linux as the old HP workstation was replaced.

2.3 The ALIS control centre

The ALIS control centre (CC), is located in the optical laboratory of IRF in Kiruna (Figure 2.6). In the CC there are computers for controlling ALIS, commu-

Figure 2.6: The ALIS control centre at the optical laboratory as it looked around 1993. To the left are workstations and the station computer for the Kiruna station. The station overview map and console for the HP-755 workstation are seen in the center-right part of the photo. The two racks to the right contains monitors for the low-light TV-cameras, video recorders and timing systems.

nication equipment (e.g. modem pools for dial up connections) and workstations for running ALIS (Figure 2.7). In 1999, as ALIS station (1) Kiruna was moved (Section 2.1.2) a secondary point for controlling ALIS, an Operations Centre (OC) was established at the same place as station 1 (Figure 2.8). This was done in order to minimise disturbances from construction work at the CC. It is desirable to be able to run supporting low-light instruments and to make visual observations

Figure 2.8: The ALIS operations centre that was established at Knutstorp (close to the EISCAT-site in Kiruna) in 1999. Two low-light TV-cameras (one with all-sky, and one with $\approx 40°$ field-of-view) are used to give the operator a real-time display of the sky. These images are displayed on the monitors in the upper left part of the photograph. Below are two video tape recorders. The six ALIS stations are monitored and controlled from the computer terminals below, and some quick-look images from ALIS are seen on the screens.

when running ALIS. While most ALIS operations have been undertaken from the CC or OC, it is worth noting that ALIS can be controlled from almost any computer with a suitable Internet connection. During unattended operations, a pager call can be used to alert the operator on duty of abnormal conditions. The pager is also used for alarm messages (for example fire, trespass, power-failures, etc.) from the housekeeping units at the stations during non-measuring periods.

In the beginning, there were many technical requirements on the CC [for example *Steen*, 1989; *Steen et al.*, 1990]. As ALIS evolved the requirements on the CC were relaxed, and if, all stations obtain high-speed Internet connections, it will be completely superfluous, at least from a technical point of view. On the other hand, experience has shown that a dedicated centre for running ALIS campaigns, where scientists and staff can gather and run the observations, review results as well as solve problems, yields far better results as compared to if one single person runs ALIS from home or an office. Therefore it is probably important to have a dedicated operations centre for ALIS, despite the fact that ALIS can be run from almost anywhere.

Chapter 3

The ALIS Imager

> "For now we see through a glass, darkly; but then face to face: now I know in part; but then shall I know even as also I am known." *1 Cor. 13:12*

> "Orten, hvarifrån de [Norr-skenen] åskådas; tiden då de visa sig; deras ställning på himmelen; ombyteliga figur och vackra färgor; äro nästan de ende omständligheter, som därvid, äfven med svårighet, kunna i akt tagas. Ögat, pennan och den snällaste Målares pensel, äro för senfärdige, att teckna alla deras förändringar. Deras fladdrande ombyten förvilla imaginationen, och man bör vara god geometra, at skilja utseendet och figuren ifrån själva tingen, för at ej med allmänheten och forntiden däraf tillskapa tusende syner och vidunder, uti blotta luften." *Wilcke [1778]*

Spectroscopic measurements of auroral and airglow emissions have belonged to the realm of photometer measurements, while imaging techniques mainly have been tools for studies of morphology and dynamics. This chapter will discuss the required specifications for the ALIS imager in order to enable absolute spectroscopic measurements of column emission rates. Calibration issues will be discussed in Chapter 4.

3.1 Some basic concepts

There exist a number of textbooks [for example *Theuwissen*, 1995; *Holst*, 1998, and references therein], reports [for example *Eather*, 1982; *Lance and Eather*, 1993], and articles [for example *Janesick et al.*, 1987, and references therein] on solid-state imaging with CCD detectors. This section will provide a short summary of some fundamental concepts required to specify a CCD-imaging system suitable for the needs of auroral and airglow imaging.

Holst [1998] defines the term *radiometry,* as the *"energy or power transfer from a source to a detector"* while *photometry* is defined as *"the transfer from a source to a detector where the units of radiation have been normalised to the spectral sensitivity of the eye."*

3.1.1 Spectral radiant sterance (radiance)

The basic quantity from which all other radiometric quantities can be derived is spectral radiant sterance, L. Given a source area, A_s, radiating a radiant flux, *chosen to make interpretation convenient."* The spectral radiant sterance (L_γ) in Equation 3.2 can be obtained from the column emission rate I (in Rayleighs) according to *Baker and Romick* [1976]:

$$L_\gamma = \frac{10^{10} I}{4\pi} \left[\frac{\text{photons}}{\text{s m}^2 \text{ sr}}\right] \tag{3.6}$$

Although not a proper SI-unit, the Rayleigh is often used in the field of auroral and airglow measurements. It is also frequently misunderstood and abused. It is important to remember that *the Rayleigh only is usable when the wavelength is specified.* Due to the plethora of Rayleigh definitions [*Baker and Romick*, 1976], it is always wise to state the definition of the unit before using it. In the following text, the Rayleigh will be used according to the original definition [*Hunten et al.*, 1956, but in SI-units] as defined above.

Using the recommended column emission rates in Rayleighs for the International Brightness Coefficients (IBC) as an example, the following spectral radiant sterances are obtained [*Chamberlain*, 1995, App. II]: IBC-I aurora, corresponding to 1 kR at 5577 Å is often described as the lowest column emission rate detectable by the unaided human eye. Usually this is compared to the luminous incidence of a moonless cloudy night which is about 10^{-4} Lux*. By the use of Equations 3.2 and 3.6, the spectral radiant sterance in energy units (L_E) can be calculated:

$$L_E(1\ [\text{kR}]) = \frac{10^{13} hc}{4\pi\lambda} = \frac{10^3 hc}{4\pi \times 5577} \approx 300 \left[\frac{nW}{\text{s m}^2 \text{ sr}}\right] \tag{3.7}$$

Similarly the brightest IBC-IV corresponding to 1 MR at 5577 Å, which is often compared to the luminous incidence of the full-moon of about 10^{-1} Lux* becomes:

$$L_E(1\ [\text{MR}]) \approx 300 \left[\frac{\mu W}{\text{s m}^2 \text{ sr}}\right] \tag{3.8}$$

3.1.3 Spectral radiant incidence (irradiance)

Spectral radiant incidence (irradiance), E, is defined as radiant power incident per unit area onto a target, in this case typically the effective aperture of the optics, A_{app}, image area, A_i, area of CCD-detector, A_{CCD}, or the area of a CCD pixel, A_{pix}.

The transmittance, $T(\lambda, ...)$, of an optical system is a function of many parameters, for example wavelength λ, viewing angle, temperature, etc., and must be experimentally determined (See Chapter 4). Here it is enough to state that the total transmittance is given by the product of the individual transmittances of the various components of the optical system:

$$T = \prod_{\forall X} T_X = T_a T_o T_f \ldots \tag{3.9}$$

Where T_X is exemplified by T_a, T_o and T_f which are the transmittance of the atmosphere, optics and filter, respectively. In the following text T will denote the product of appropriate transmittances according to Equation 3.9.

*According to *Holst* [1998, p. 28]

3.1.4 Number of incident photons

Using Equation 3.17 the number of photons reaching the image plane, n_{γ_i}, can be calculated:

$$n_{\gamma_i} = E_{\gamma_i} t_{int} A_i = T t_{int} A_i \frac{10^{10} I}{16 f_{\#}^2} \text{ [photons]} \tag{3.18}$$

Here t_{int} is the integration time in seconds. The number of photons hitting the CCD, $n_{\gamma_{CCD}}$, are:

$$n_{\gamma_{CCD}} = n_{\gamma_i} T_w T_{CCD} \frac{A_{CCD}}{A_i} \text{ [photons]} \tag{3.19}$$

Here T_w is the transmittance of the optical window protecting the CCD, and T_{CCD} is the transmittance of the CCD substrate (in the case of a back-side illuminated CCD). Likewise, the number of photons hitting an individual pixel, $n_{\gamma_{pix}}$, is:

$$n_{\gamma_{pix}} = n_{\gamma_{CCD}} \frac{A_{pix}}{A_{CCD}} = T t_{int} A_{pix} \frac{10^{10} I}{16 f_{\#}^2} \text{ [photons]} \tag{3.20}$$

(using Equations 3.18–3.19 and Equation 3.20). Again, please remember the caution at the end of Section 3.1.3

3.1.5 The CCD as a scientific imaging detector

"During the past couple of decades the Charge Coupled Device (CCD) sensor has gradually replaced the tube type sensors, such as the vidicon, due to its advantages in size, weight, power consumption, noise characteristics, linearity, dynamic range, photometric accuracy, spectral responsitivity, geometric stability, reliability, and durability" [*Janesick et al.*, 1987]. As an auroral imager, the CCD is thus almost an ideal detector for ground-based as well as for space-borne instruments. The CCD can be used either as the primary photon detector, or in an Intensified CCD (ICCD) configuration. Whether to use a CCD or an ICCD is mainly a matter of requirements on temporal resolution and signal-to-noise ratio, *SNR*. This section will begin with a short review of a number of parameters describing the performance of a CCD detector.

3.1.6 Quantum efficiency

The quantum efficiency, Q_E, is a measure of the number of electrons generated per incident photon:

$$Q_E = \eta_E Q_{EI} \left[\frac{e^-}{\text{photons}}\right] \tag{3.21}$$

where η_E is the effective quantum yield (electrons generated, collected, and transferred per interacting photon per pixel) and Q_{EI} is the interacting quantum efficiency (interacting photons per incident photons per pixel) [*Janesick et al.*, 1987]. However, for the purpose of this text it is only needed to consider Q_E, which for the purpose of this text, is the same as the detective quantum efficiency (DQE).

Quantum efficiency for a CCD is wavelength dependent, and is of no value unless the wavelength is specified. High performance scientific thinned, back-side illuminated anti-reflection coated CCD devices might have as high quantum

Additional noise sources include: reset noise, on-chip and off-chip amplifier noise (1/f-noise and white noise). Of particular interest for low-light applications is that the 1/f-noise, which is the main source of the read noise ("noise-floor"), increases in proportion to the square root of the read-out frequency ("pixel-clock"), thus requiring a suitable compromise between noise performance and frame-rate. The analogue-to-digital converter has a quantisation noise, also switching transients coupled through the clock signals, electro-magnetic interference, etc., sums up to the total noise. There is pattern noise due to differences in dark-current and photo response non-uniformities [*Holst*, 1998]. At high signal levels the total noise is dominated by pattern noise (pixel to pixel sensitivity variations within the CCD) for most CCDs, at low signal levels the read noise ("noise floor") dominates [*Janesick et al.*, 1987]. Many of these noise sources can be reduced to negligible levels by good electronic design practices. In particular, the dark-current (and reset noise) is reduced by cooling the CCD. By the use of Double Correlated Sampling (DCS) the reset noise can be almost eliminated. The quantisation noise is eliminated by using a sufficiently high resolution ADC. It is, however, beyond the scope of this work to embark onto a detailed analysis of the noise-sources in CCD imagers, instead a simplified noise model from *Holst* [1998] is adopted:

$$\langle n_{e^-_{CCD}} \rangle = \sqrt{\langle n_{e^-_s} \rangle^2 + \langle n_{e^-_r} \rangle^2 + \langle n_{e^-_p} \rangle^2} \;\; [e^-_{RMS}] \tag{3.24}$$

The standard deviation of the noise floor (or read noise), $\langle n_{e^-_r} \rangle$, is usually stated in the imager specification as 'read noise', or easily obtained from a zero exposure. This noise source increases with the square-root of the pixel clock frequency, which imposes an *SNR* constraint onto the frame-rate.

The pattern noise, $\langle n_{e^-_p} \rangle$, is the sum of Fixed Pattern Noise (FPN), resulting from pixel-to-pixel variations in the dark-current, and Photo Response Non-Uniformities (PRNU). An approximate worst case value is provided by *Holst* [1998]:

$$\langle n_{e^-_p} \rangle = \sqrt{\langle n_{e^-_{FPN}} \rangle^2 + \langle n_{e^-_{PRNU}} \rangle^2} \approx \langle n_{e^-_{PRNU}} \rangle \approx U \overline{n}_{e^-_\gamma} \approx \frac{\overline{n}_{e^-_\gamma}}{\sqrt{n_{e^-_{max}}}} \;\; [e^-_{RMS}] \tag{3.25}$$

However, for the low signal levels considered here, pattern noise is neglected. Then the total noise approximation for a bare CCD becomes (by substituting Equation 3.23 into Equation 3.24):

$$\langle n_{e^-_{CCD}} \rangle \approx \sqrt{\overline{n}_{e^-_\gamma} + \overline{n}_{e^-_d} + \langle n_{e^-_r} \rangle^2} \;\; [e^-_{RMS}] \tag{3.26}$$

It should be remembered that this equation is an approximation.

3.1.8 Signal-to-noise ratio

The measured signal-to-noise ratio in terms of the digital output, DN, or in terms of root-mean-square electrons e^-_{RMS} is defined as follows:

$$SNR_{CCD} = \frac{DN_{signal}}{DN_{noise}} \approx \frac{\overline{n}_{e^-_\gamma}}{\langle n_{e^-_{CCD}} \rangle} \tag{3.27}$$

As with the CCD (see Equation 3.23), the photo-cathode produces both photon-noise and dark-current noise :

$$\langle n_{e^-_{s,pc}} \rangle = \sqrt{\langle n_{e^-_{\gamma,pc}} \rangle^2 + \langle n_{e^-_{d,pc}} \rangle^2} \;\; [\mathrm{e}^-_{\mathrm{RMS}}] \tag{3.34}$$

Another noise source, unique to the ICCD, is the electron multiplication noise, which is due to the statistical distribution of the number of secondary photoelectrons[‡]. Taking this uncertainty in $\overline{g}$ into account, the combined variance with the photon noise becomes:

$$\langle n_{e^-_{\gamma,pc}} \rangle^2 = k_{MCP}\, \overline{g}^2\, \overline{n}_{e^-_{\gamma,pc}} \approx 2\overline{g}^2\, \overline{n}_{e^-_{\gamma,pc}} \tag{3.35}$$

Here, k_{MCP} is the microchannel excess noise. The photo-cathode dark-current noise, is also dependent on $\overline{g}$ in the same way:

$$\langle n_{e^-_{d,pc}} \rangle^2 = 2\overline{g}^2\, \overline{n}_{e^-_{d,pc}} \tag{3.36}$$

Taking Equation 3.26 as an approximation for the total CCD noise, and inserting into it Equations 3.35 and 3.36, for the ICCD noise sources, leads to the following expression for the total noise for the ICCD, $\langle n_{e^-_{ICCD}} \rangle$:

$$\langle n_{e^-_{ICCD}} \rangle \approx \sqrt{2\overline{g}^2\, (\overline{n}_{e^-_{\gamma,pc}} + \overline{n}_{e^-_{d,pc}}) + \overline{n}_{e^-_d} + \overline{n}_{e^-_r}} \tag{3.37}$$

By applying Equations 3.33 and 3.37 into Equation 3.27 the following approximation for the *SNR* of an ICCD, SNR_{ICCD}, emerges:

$$SNR_{ICCD} \approx \frac{\overline{g}\, \overline{n}_{e^-_{\gamma,pc}}}{\sqrt{2\overline{g}^2\, (\overline{n}_{e^-_{\gamma,pc}} + \overline{n}_{e^-_{d,pc}}) + \overline{n}_{e^-_d} + \overline{n}_{e^-_r}}} \tag{3.38}$$

As seen, increasing the gain of the image intensifier makes the CCD noise-sources negligible, but *does not* increase the *SNR*. For very high gain, Equation 3.38 is reduced to:

$$SNR_{ICCD} \approx \frac{\overline{n}_{e^-_{\gamma,pc}}}{\sqrt{2(\overline{n}_{e^-_{\gamma,pc}} + \overline{n}_{e^-_{d,pc}})}} \tag{3.39}$$

3.1.10 Threshold of detection and maximum signal

The threshold of detection is usually defined as $SNR = 2$ while the Noise Equivalent Exposure, *NEE*, is obtained when $SNR = 1$. The maximum signal, or Saturation Equivalent Exposure (SEE) is obtained when the charge well capacity, $n_{e^-_{max}}$, is reached. This occurs when:

$$n_{e^-_\gamma} \geq n_{e^-_{max}} - n_{e^-_d} \tag{3.40}$$

In most cases the maximum charge-well capacity, DN_{SEE}, is matched to the maximum ADC output DN_{max}. For the ICCD case, apart from the condition above, there is also a saturation level for the image intensifier to be considered. On the other hand, the high-voltage for the intensifier can be gated, acting like an electronic shutter.

[‡] A more detailed discussion of this noise source is found in works by *Holst* [1998, pp. 195–200], *Trondsen* [1998, p. 48], *Csorba* [1985, pp. 120–124] and *Hertel* [1989].

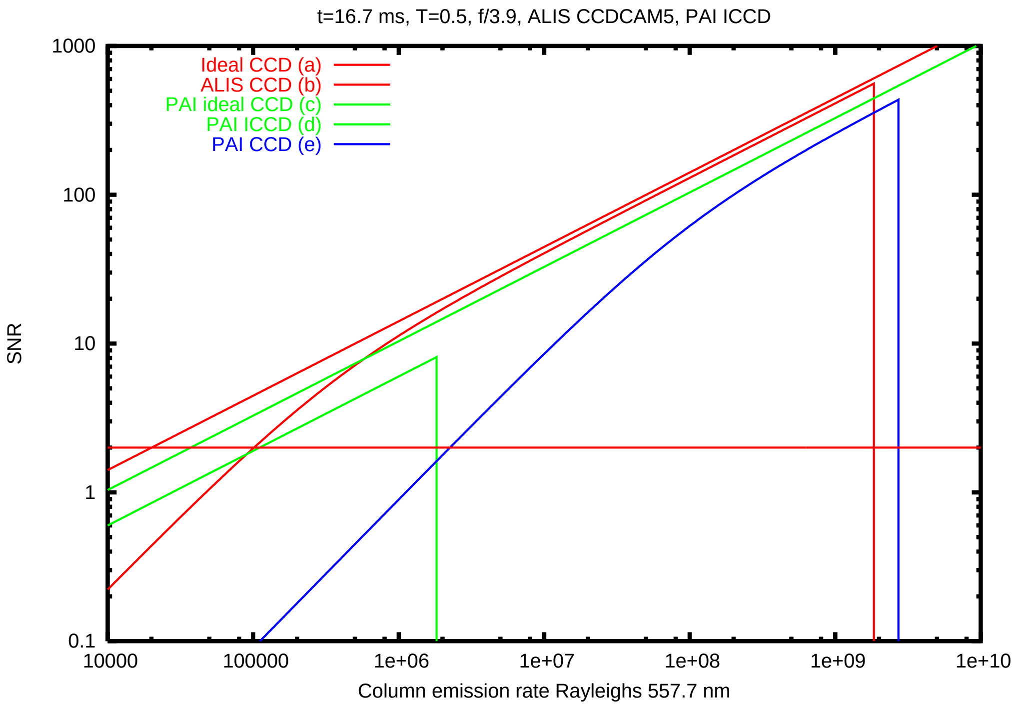

Figure 3.2: *SNR* vs. column emission, for f/3.9 optics with $T \approx 0.5$ and 16.7 ms on-chip integration time. (a) Ideal photon detector (Equation 3.29) with $A_{pix} = 576\,\mu m^2$ (ALIS). (b) Equation 3.28 for ALIS `ccdcam5` (Table 3.2). (c) Same as (a) but $A_{pix} = 310\,\mu m^2$ (PAI). (d) Equation 3.38 for the PAI ICCD (Table 3.1). (e) Same as (b) but for the PAI CCD without image intensifier. The horizontal line indicates the threshold of detection at $SNR = 2$.

Parameter	Symbol	`PAI`	Unit	Notes
MCP mean gain (medium)	$\overline{g}$	1500		
Photo-cathode dark-current	$\overline{n}_{e^-_{d,pc}}$	0.1	nAm^{-2}	
Photo-cathode quantum efficiency	$Q_{E_{pc}}$	28	%	at 5577 Å
CCD read noise	$\langle n_{e^-_r} \rangle$	80	e^-_{RMS}	
CCD dark current	$\overline{n}_{e^-_d}$	0.1	nAm^{-2}	b) at 21°C
CCD full well (anti-blooming off)	$N_{e^-_{max}}$	80	ke^-	a)
CCD quantum efficiency	$Q_{E_{CCD}}$	67	%	at 5577 Å
CCD pixel area	A_{pix}	11.7×27.0	μm^2	
Fibre-optic minification ratio	M_{FO}	1.55		

Table 3.1: ICCD parameters for the portable auroral imager (PAI) obtained from *Trondsen* [1998, Table 4.1 p.51]. All values at room temperature. Notes: a) Value from data-sheet of the CCD. b) *Trondsen* has confirmed the value of 0.1mAm^{-2} to be a typo.

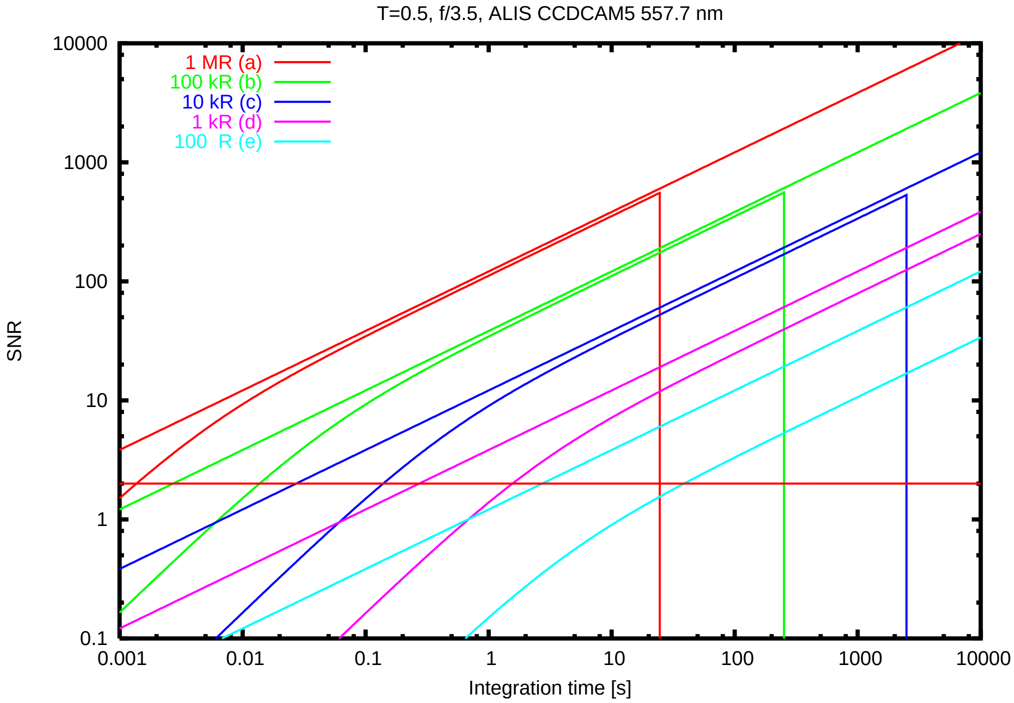

Figure 3.3: *SNR* versus integration time for (a) 1 MR IBC-IV (b) 100 kR IBC-III, (c) 10 kR IBC-II, (d) 1 kR, IBC-I and (e) 100 R. All at 5577 Å.

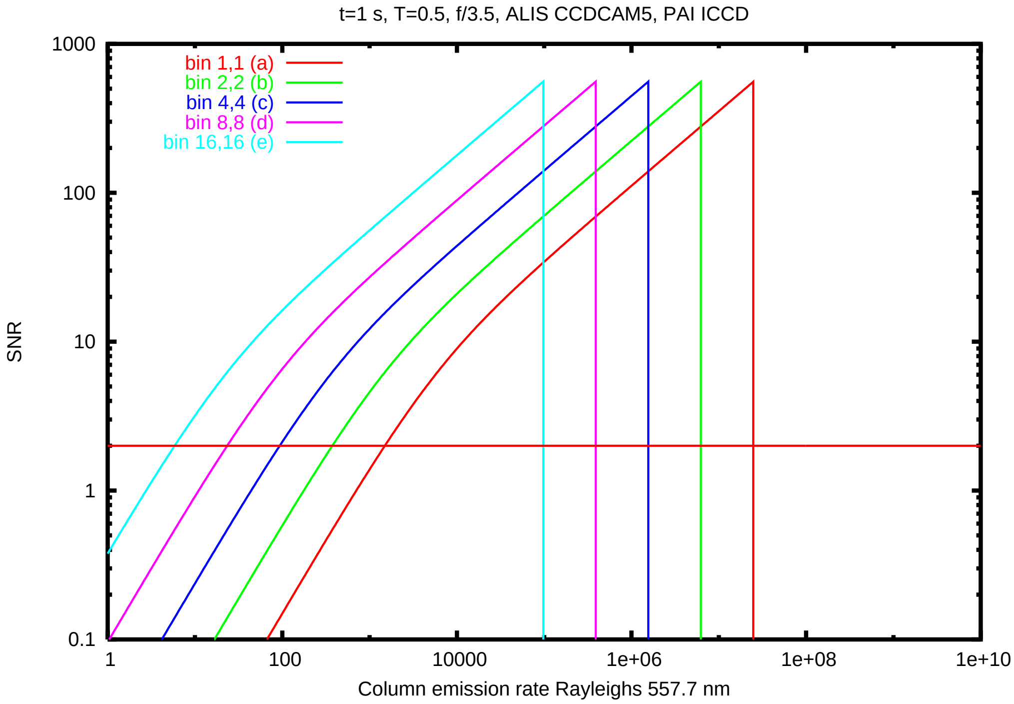

Figure 3.4: SNR vs. column exposure rates at 1 s integration time ($f_{\#} = 3.5, T = 0.5$) with binning factors: (a) 1×1, (b) 2×2, (c) 4×4, (d) 8×8 and (e) 16×16.

3.3 The CCD imager for ALIS

Based on the discussion in the previous sections, it might be concluded that an ICCD imager is better for video-rate observations, mainly due to the long read-out time of a full-frame CCD. On the other hand, the large dynamic range, linearity and long time stability of a scientific-grade unintensified CCD make it an interesting choice for absolute spectroscopic imaging measurements of column emission rates down to about 1 s time resolution. Therefore it was decided to select a thinned back-side illuminated quad-read-out CCD for the ALIS imagers. At the time of specification no commercially available imager met the requirements of temporal resolution. One company was willing to modify their dual-read-out CCD camera head to a quad-read-out system, resulting in the imager system finally procured for ALIS. This section presents a short summary of some of the most important technical details of the six imagers. For further technical information about the imager hardware, etc., see *Preston* [1993, 1995]; *AstroMed Ltd.* [1993] and *AstroCam Ltd.* [1995]

3.3.1 The camera head

The CCD camera head (CCH) is of dimensions $125 \times 140 \times 144\ mm^3$ (Figure 3.6). A slightly larger front plate ($155 \times 170\ mm^2$) enables mounting the camera head

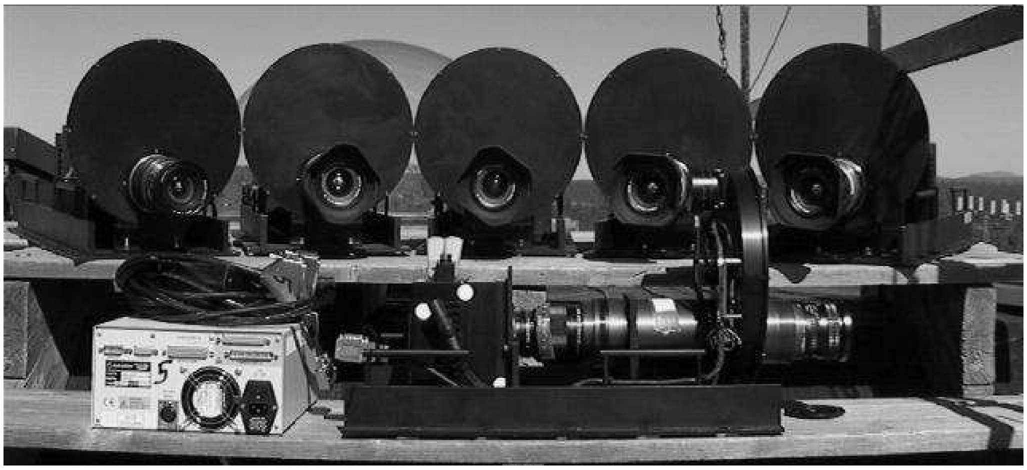

Figure 3.6: The six ALIS imagers. In the right forefront a sideview of an imager is shown. The front lens, telecentric part with filter wheel, and camera lens connected to the CCD camera head are seen. The white box on the left is a camera control unit.

to the structure supporting the camera head, optics and filter-wheel. Centred on the front plate is the optical interface, which consists of a removable ring with a Canon lens-mount. By replacing the ring, the lens-mount can be reconfigured to a Nikon lens-mount. Thus it is possible to attach a wide variety of standard objective lenses. The thinned back-side illuminated quad-read-out CCD is mounted onto a Peltier cooler inside a hermetically sealed compartment filled with an inert gas under low-pressure. Light enters through the front-plate hole, a mechanical shutter, and a high-quality optical window onto the CCD inside the

`ccdcam`	pixels	$\frac{\mu s}{\text{pixel}}$	$\overline{n}_{e_r^-}$ $[e^-_{RMS}]$	$t_{read}[s]$	Notes
1	1124 × 1024	6	12–14	1.7	a)
1	1124 × 1024	8	9–12	2.3	a)
1	1124 × 1024	13	8–9	3.7	a) default
1	1124 × 1024	23	7	6.6	
2	1124 × 1024	1.6	28	0.5	
2	1124 × 1024	2.5	11	0.7	
2	1124 × 1024	4.1	10	1.2	
2	1124 × 1024	10.5	8	3.0	default
3	1124 × 1024	1.6	25	0.5	
3	1124 × 1024	2.5	13	0.7	
3	1124 × 1024	4.1	10	1.2	
3	1124 × 1024	7.0	9	2.0	default
4	1124 × 1024	1.6	25	0.5	b)
4	1124 × 1024	3.8	13	1.1	b)
4	1124 × 1024	6.7	10	1.9	b)
4	1124 × 1024	12.5	9	3.6	b) default
5	1056 × 1024	1.6	28	0.4	
5	1056 × 1024	2.5	11	0.7	
5	1056 × 1024	4.1	10	1.1	
5	1056 × 1024	10.5	8	2.8	default
6	1076 × 1024	1.6	25	0.4	
6	1076 × 1024	3.8	13	1.0	
6	1076 × 1024	6.7	10	1.8	
6	1076 × 1024	12.5	9	3.4	default

Table 3.3: CCD-read noise at various pixel clocks for the six ALIS imagers. The values are from the vendor-provided configuration files for the imagers.

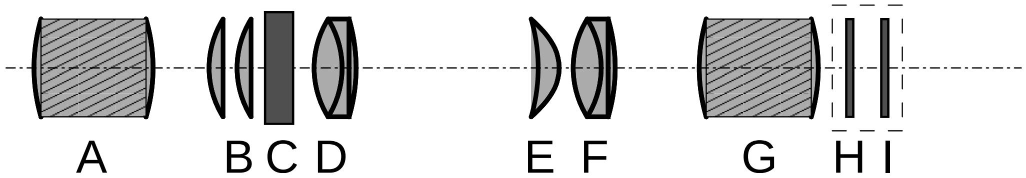

Item	`ccdcam`	Description
A	1,6	Front objective: Mamiya Sekor C 35 mm $f_{\#} = 3.5$
A	2–5	Front objective: Mamiya Sekor C 45 mm $f_{\#} = 2.8$
B	1–6	Two plano-convex telecentric lenses (plano side to rear)
C	1–6	$3''$ interference filter.
D	1–6	Field lens: Achromat, (lowest curvature side to rear)
E	1–6	Close-up lens 1: Meniscus, reverse configuration (convex side to rear)
F	1–6	Close-up lens 2: Achromat, reverse configuration (lowest curvature side to rear)
G	1–6	CCD camera lens: Canon FD 85 mm $f_{\#} = 1.2$
H	1–6	Window of the hermetically sealed CCD enclosure (inside CCD camera head)
I	1–6	CCD (inside CCD camera head)

Figure 3.7: Schematic diagram of the optical system for an ALIS imager. The two front objectives give a diagonal field-of-view of about 90° and 70° respectively. Information about the optical elements and their orientation after *Keo Consultants* [1994, 1997]

3.4 The optical system

To fully exploit the detector performance, a very fast custom designed optical system would need to be designed for ALIS. Ideally this would include a set of replaceable front-lenses, preferably mounted on a rotating disc in front of the filter-wheel, resulting in a remotely selectable field-of-view. As narrow-band interference filters are to be used, a telecentric lens system is required to have nearly parallel rays through the filters (see Section 3.5 for details). It was realised early that the requirement of changeable field-of-view had to be dropped due to reliability as well as budgetary constraints. Therefore, given the station separation, a field-of-view of approximately 50°–90° would be the best compromise (See also Figure 2.3 in Chapter 2). Following quotations from various optical manufacturers in the field, it was also quickly realised that the cost of *one* custom designed optical system would quickly exceed the entire project budget. Therefore a commercial telecentric optical system, frequently used in this field, was selected.

This system consists of a replaceable front-objective (A), two plano-convex telecentric lens-elements (B), a $3''$ filter holder (C, replaced by the IRF-designed filter-wheel Section 3.5.1), a field-lens (D), two close-up lenses (E,F) and a camera objective(G) (Figure 3.7). As discussed in Section 2.1.1, the station separation baseline was selected for a moderate field of view of about 50°–90°. For the first four imagers, the 45 mm front-objective resulted in a diagonal field-of-view of

3.5.1 The filter wheel

The filter wheel (Figure 3.8) has six positions for 76.2 mm (3″) interference filters

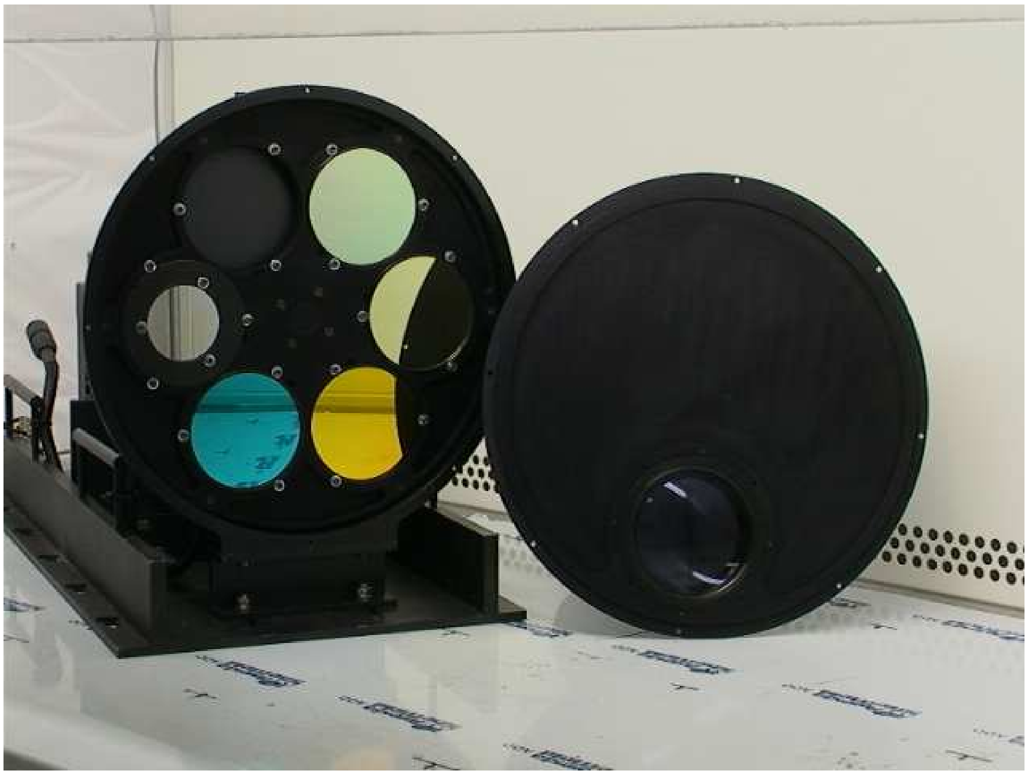

Figure 3.8: The six-position filter wheel with cover removed exposing the filter compartment. Starting at filter position zero (approximately five o'clock in the photo) filters for: $O(^1S)$ 5577 Å, $O(^1D)$ 6300 Å, 6230 Å (background), white light (empty), 5324 Å (a smaller filter in an adaptor ring intended for LIDAR studies), and finally in position five, the N_2^+ 1Neg. 4278 Å auroral filter. To the right the cover with the back end of the front lens is seen. A stepping motor attached to the rear top side of the filter wheel enclosure (not shown) actuates the filter wheel by a small cog-wheel driving cogs in the inner perimeter of the filter wheel. An angular encoder is attached to the filter wheel axis on the rear side of the enclosure (not shown).

numbered 0–5. Temperature stabilisation is achieved through a heating blanket and temperature sensors inside the filter compartment. Positions 0, 1, 3 and 5 have standardised filter assignments (Table 3.4), and the remaining two positions have been used for various other filters (Table 3.5). A stepping motor actuates cogs along the perimeter of the filter wheel. An angular encoder on the filter wheel axis senses the filter position. The filter change time is 1–2 s. The filter wheel cover, which also supports the front lens, is easily removable for filter changes etc. However, the cover should only be removed in a clean room, to avoid dust in the filter compartment. The power-supply and stepping motor drive electronics are mounted in a 19″ enclosure, the Filter Wheel Control unit (FWC) (Figure 3.9 and the block diagram in Figure 3.12).

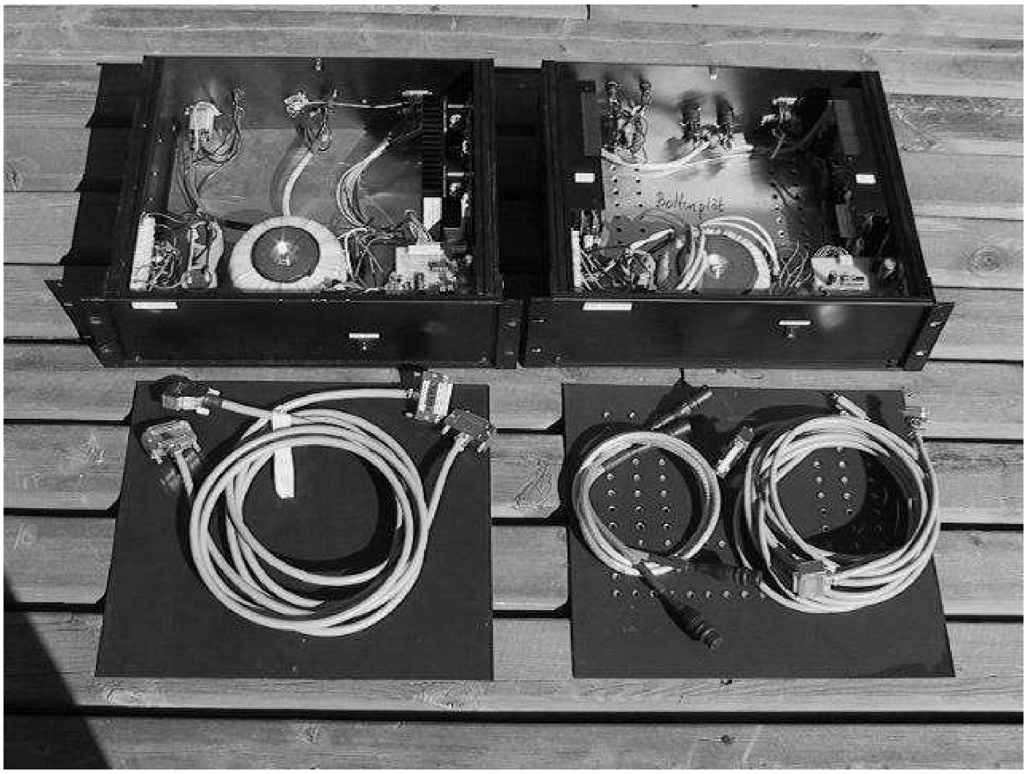

Figure 3.9: Left: Power supply, stepping motor drive circuits, cables etc. for the filter wheel. Right: The same equipment, but doubled for the camera positioning system (2 axes). See also Figure 3.12.

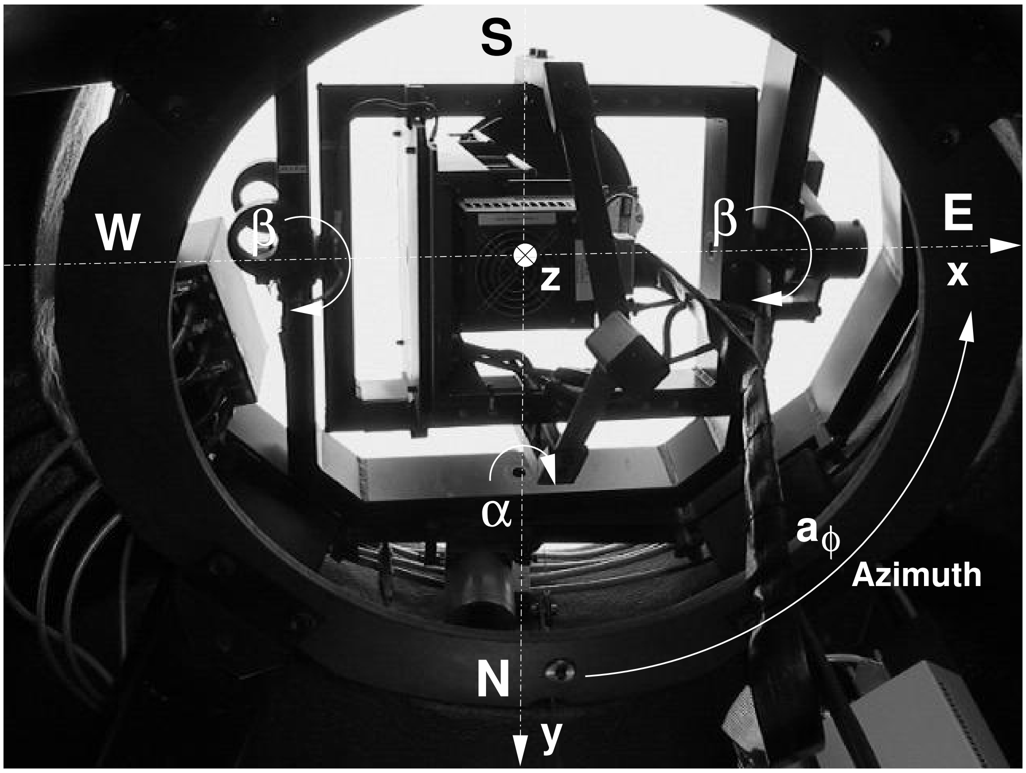

Figure 3.10: Bottom view of the camera positioning system at ALIS station 4 (Tjautjas). North is downward and east is to the left in the figure. Azimuth (a_{ϕ}) is 0° towards north and 90° towards east, as indicated by the arrow in the lower left part of the picture. Zenith angle (z_{θ}) is 0° in zenith and increases as the optical axis of the lens is lowered towards the horizon (decrease in elevation). α is zero in zenith and positive when tilting eastward. β is zero in zenith and positive southward (for $\alpha = 0$). The back end of the CCD camera head of an ALIS imager (`ccdcam1`) is mounted in the innermost frame, rotating about the β-axis. This frame is in turn mounted in the middle frame, rotating about the perpendicular α-axis, which, in turn, is attached to the outermost fixed frame. The stepping motors and gear boxes for the axes are seen in the lower middle, and right side of the photograph. Incremental angular encoders are at the opposite side of each axis. A part of the camera control unit is seen at the lower right-hand side. The unit is mounted on one of the four iron legs supporting the outermost frame. The plywood ring, together with the counter-weight at the bottom of the innermost frame serve as an emergency-stopping device for out-of-bounds CPS movements.

	1 KRN		2 MER		3 SIL		4 TJA		5 ABK		6 NIL	
	a_ϕ	z_θ	a_ϕ	z_θ	a_ϕ	z_θ	a_ϕ	z_θ	a_ϕ	z_θ	a_ϕ	z_θ
`core` — Centred on a volume above Kiruna	0°	0°	298°	24°	249°	28°	346°	20°	130°	24°	90°	20°
`eiscat` — Optimised for field-aligned EISCAT studies	0°	39°	348°	42°	350°	32°	0°	42°	20°	35°	15°	42°
`E-W` — Optimise east-west field-of-view	0°	39°	0°	15°	0°	32°	0°	42°	0°	35°	0°	15°
`heating` — Optimised for HF-pump enhanced airglow	346°	37°	340°	40°	330°	37°	345°	44°	5°	25°	5°	40°
`mag-Z` — Local magnetic zenith	180°	12°	180°	12°	180°	12°	180°	12°	180°	12°	180°	12°
`north` — Centred on a volume north of Kiruna	0°	30°	330°	33°	311°	25°	355°	33°	85°	22°	44°	26°
`south` — Centred on a volume south of Kiruna	180°	30°	250°	23°	215°	28°	260°	7°	148°	31°	135°	23°
`surv` — Optimised for maximum field-of-view	225°	20°	100°	14°	45°	12°	115°	15°	30°	14°	270°	20°

Table 3.6: ALIS preset camera positions. The columns give azimuth and zenith angles for the six stations. See also Figure 3.11.

have been encountered so far. Future CPS units will need a slight re-design of the hardware and a micro-controller replacing the obsolete NIPU. The existing devices will need upgraded electronics including new angular encoders as part of normal system maintenance.

3.7 Summary

This chapter has discussed the selection and design of the ALIS imager and its associated subsystems. In summary these systems consist of the following items:

ALIS imager: consisting of Optics (Section 3.4), filter-wheel (Section 3.5.1), with interference filters (Section 3.5) and the CCD Camera Head (CCH) mounted together as a removable unit. Six ALIS imagers exist to date, and they are denoted `ccdcam 1–6` (See Section 3.3.1 and Tables B.1–B.6 in Appendix B. *It is important not to confuse these numbers with the station numbers* (Table 2.3).

Camera Control Unit (CCU) : containing power-supply and electronics for the camera head. The CCUs are individually adapted for each camera head and must not be used with a different camera head.

Filter-Wheel Control unit (FWC) : containing power-supply and electronics for the filter-wheel (Figure 3.9).

Camera Positioning System (CPS) : Supports the ALIS Imager and provides the possibility to remotely point the camera to any desired region of the sky. The CPS is attached to the camera-stand (Section 3.6).

Chapter 4

Calibrating ALIS

> "Gör vad du kan — och uppgiften skall vila lätt i din hand, så lätt att du med förväntan sträcker dig mot det svårare prov som kan följa.
>
> Det är när morgonglansen bytts i middagströtthet, när benmusklerna skälva vid anspänningen, vägen tycks oändlig och plötsligt ingenting vill gå riktigt som du önskar — det är då du *inte* får tveka." *Dag Hammarskjöld*

Calibration is the process of answering the following two basic questions:

1. What physical value does the pixel represent?

2. How is each pixel mapped to the observed object?

Answering these two rather simple questions is often no simple task.

In the case of a classical photometer, there is only one detector with a relatively narrow field-of-view. For an ALIS imager there are about 10^6 individual detectors (pixels) covering a moderate field-of-view (50°–60°). Calibrating image data is therefore a considerably more complex issue compared to calibrating a photometer.

An ALIS Imager produces two-dimensional images of size $m \times n$ pixels. Each pixel is represented by a signed 16-bit integer value (-32768–32767). This value is often referred to as digital output, DN_{ij}. The indices are pixel columns, i, and pixel rows, j, These go from the first to the last pixel in each direction (Figure 4.1). Note that the number of pixels in each direction should be divided by the on-chip binning factors (Section 3.2.1). Supplemental information is contained in the image header (for example azimuth, zenith-angle, integration time, filter, etc.).

4.1 Removing the instrument signature

First it is necessary to remove the instrument signature from the image data. This task is sometime called "data reduction". The procedure is to a large extent similar to that followed when reducing astronomical CCD image data [for example *Massey*, 1992]. In most cases the reduction is carried out first by removing additive effects, and then proceeding with multiplicative effects.

4.1.1 Bias removal

The simplest way to remove the bias is to subtract an image obtained with zero integration time (usually called bias-frame or zero-exposure). However as the bias-frame is subject to the same read noise (Section 3.1.7) as the object-image, this will generally increase the noise by a factor of $\sqrt{2}$. Preparing a bias-correction image by averaging many bias-frames together reduces this problem. As the bias varies over time it would severely impair the temporal resolution if a large number of zero exposures needed to be taken at regular intervals. To remedy this most CCDs are equipped with some extra pixels at the edge of each line. These pixels are shaded from light and thus provide bias information for each line for each image read-out. In the case of the ALIS imager, there are bias-pixels (also called reference pixels, or overscan-strip) for each line of each quadrant on the CCD as indicated in Figure 4.1.

For each pixel, the bias (or DC-level), B_{ij}, can be expressed as follows:

$$B_{ij} = B_{Lj} + B_{\overline{Z}ij} + B_q + B_0 \ \text{[counts]} \tag{4.1}$$

Here B_0 is the black-level (or preset bias), as given in Table 4.1. This value is set in the CCD configuration file (Section 3.3.3).

ccdcam	Preset bias B_0
1	−25000
2	−30758
3–4	−30768
5–6	−31768

Table 4.1: Preset bias-levels (black-levels) for the ALIS imagers. The values are obtained from the configuration files for the imagers.

Bias variations between the four read-out channels can be equalised by subtracting the quadrant bias, B_q, for each quadrant $(0 \cdots 3)$. This value can be found by averaging pixels from either zero exposure or from the bias-pixels.

B_{Lj} is the overscan-strip correction, which is obtained by selecting good bias-pixels (not all are usable) and averaging them together on each line. The number of bias-pixels varies between the CCDs, as indicated in Table 4.2. The number of

ccdcam	Total pixels $(m \times n)$	Bias-pixels
1–4	1124×1024	$50 \times 512 \times 4$
5	1056×1024	$16 \times 512 \times 4$
6	1076×1024	$26 \times 512 \times 4$

Table 4.2: Total number of pixels and bias-pixels for the six ALIS imagers. The bias-pixels are given per quadrant. The number of imaging pixels is 1024×1024 for all six CCDs.

usable bias-pixels varies even more. A suitable smooth function can then be fitted to this averaged bias-column, although this is not done in the current version of the software.

One ALIS imager (`ccdcam6`) has actually been calibrated in the integrating sphere facility at National Institute of Polar Research, Japan [*Okano et al.*, 1997]. The results from this calibration (using white light) are described by *Urashima et al.* [1999]. Due to the considerable distance to this facility it would be difficult to perform flat-field calibrations for all cameras, as would be required. Therefore it is hoped that a similar calibration facility will be established in the proximity of the optical instruments in northern Scandinavia. This was proposed by *Steen* [1998]. Such a facility would be beneficial to many imaging devices in Europe.

So far no proper flat-field calibration are done on the ALIS images on a regular basis. Instead, the flat-field correction is solely based on a mathematical model of the vignetting in the optical system [*Gustavsson*, 2000, Chapter 5]. (This model resembles the "natural vignetting" of $\cos^4\theta$ discussed in Section 3.1.3). Despite the fact that this model does not take variations in filter-transmission, pixel-to-pixel sensitivity variations, etc. into account, it has proved to work reasonably well.

4.1.4 Bad-pixel correction

Defects are unavoidable in the production of a CCD, so defect-free chips are extremely rare and expensive. The CCDs used for the ALIS imagers are of scientific grade, allowing for only a few pixel-defects. The pixel-defects, and how to detect them, can be summarised as follows [after *Holst*, 1998]:

Point defect: Pixel with deviation of more than 6 % compared to adjacent pixels when illuminated to 70 % saturation. (Expose a white area to about 70 % of the dynamic range.)

Hot point defect: Pixels with extremely high output voltage. Typically a pixel whose dark-current is 10 times higher than the average dark-current. (Take a zero or dark image.)

Dead pixels: Pixels with low output voltage and/or poor responsitivity. Typically a pixel whose output is one half of the others when the background nearly fills the wells. (Expose a white area.)

Pixel traps: A trap interferes with the charge transfer process and results in either a partial or whole bad line, either all white or all dark. (Take a zero, dark or object image, depending on type of trap)

Column defect: Many (typically 10 or more) point defects in a single column. May be caused by pixel traps (see above).

Cluster defect: A cluster (grouping) of pixels with point defects (see above).

Although the CCDs in the ALIS imager are of scientific grade, there are a few pixel-defects present on each CCD. These defects have been identified by manually inspecting the images. The bad pixels are then removed by substituting interpolated values from adjacent pixels.

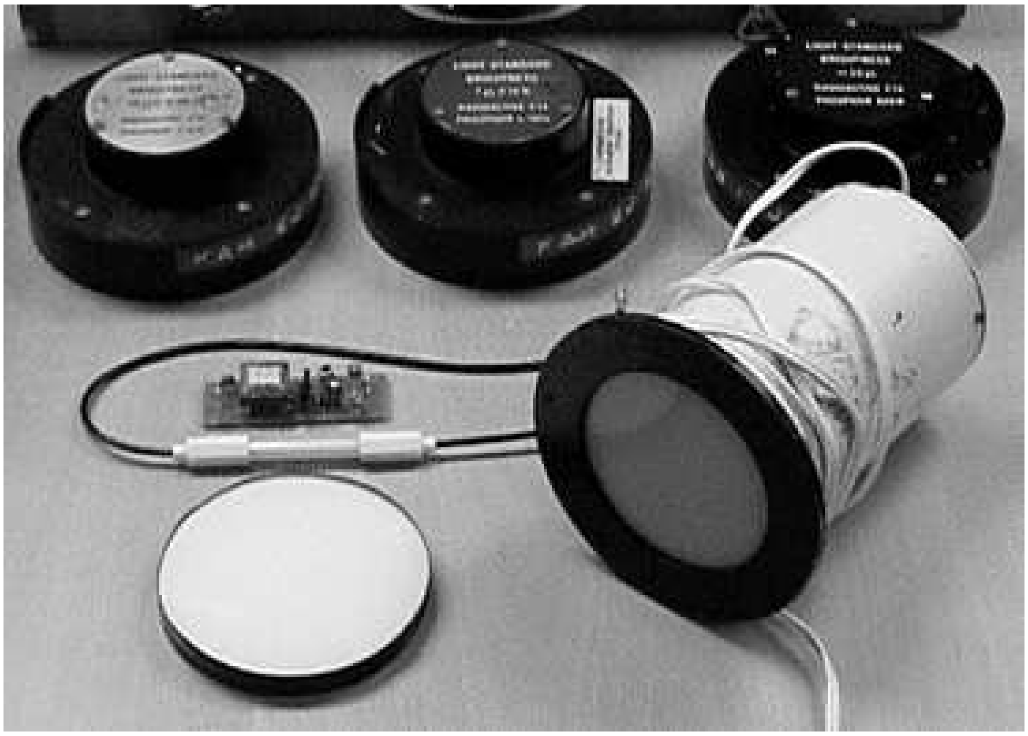

Figure 4.2: Top: The three ^{14}C phosphor light-standards with phosphor: Y-275, L-1614 and 920-B. Lower right: A calibration source with a tungsten lamp. (To the lower left are some parts from a calibration source based on a fluorescent light)

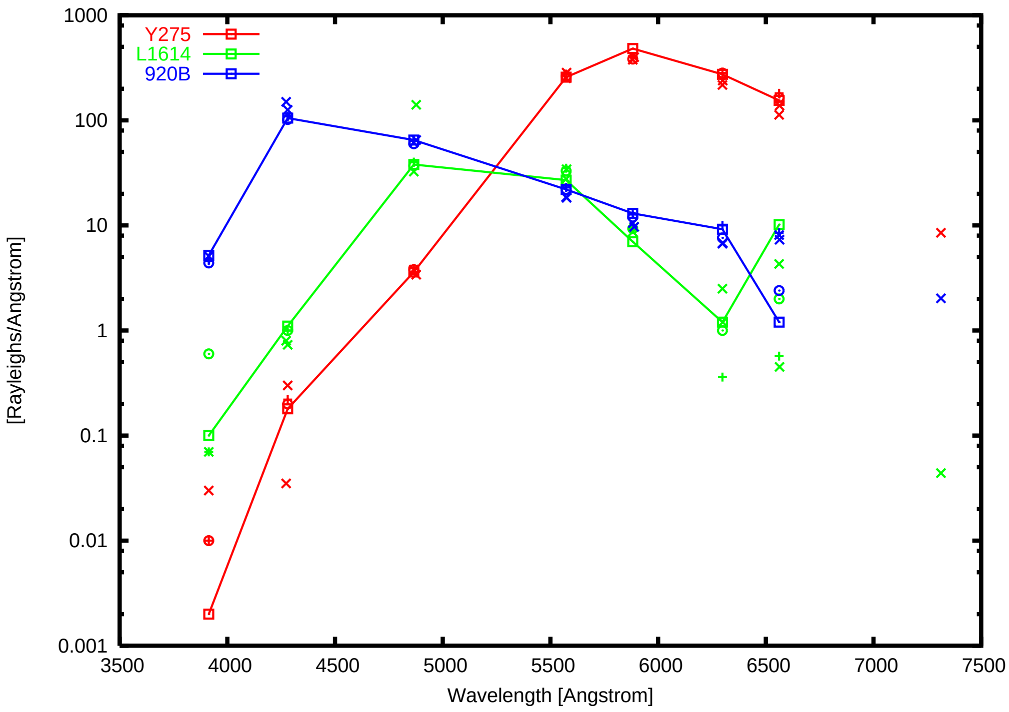

Figure 4.3: Column emission rates [R/Å] as a function of wavelength [Å] for the three radioactive ^{14}C light-standards with phosphor: 920-B (blue line), L-1614 (green line) and Y-275 (red line). These plots also include intercalibration results from the Aberdeen 1980 workshop [*Torr and Espy*, 1981]. These values are not shown in Table 4.3. Legend: Intercalibration sessions of 1981 'x' 1985 '+', 1999 '*', 2000 'o' , and 2001 '□'. The lines connect the results from the latest calibration workshop, held in Oulu 2001. (The last points on these lines for the L1614 and 920B calibrators are probably measurement errors)

Source	Year	column emission ratios (2001/year) at Filter [Å]						
		3914	4280	4866	5573	5882	6299	6562
y275	1985	0.07	0.60	0.95	**1.03**	1.28	**1.26**	1.37
y275	1999	0.20	0.90	0.95	**0.98**	1.26	**0.97**	0.94
y275	2000	0.20	0.82	0.92	**0.93**	1.19	**0.97**	0.86
l1614	1985	1.43	1.51	1.17	**0.97**	0.80	0.48	2.37
l1614	1999	0.17	1.10	1.03	**0.82**	0.75	1.20	5.10
l1614	2000	1.43	1.10	0.95	**0.77**	0.73	3.33	17.89
920b	1985	1.02	**0.83**	1.06	**1.18**	1.24	1.37	0.15
920b	1999	1.18	**1.03**	1.08	**1.00**	1.08	1.21	0.50
920b	2000	1.13	**0.96**	1.02	**0.96**	1.02	0.92	0.14

Table 4.4: Ratios of results from the latest calibration workshop [Oulu, 2002, see *Widell and Henricson*, 2001] to earlier calibration sessions. Bold face indicates results for wavelengths where the calibrators are most commonly used. See also Table 4.3 and Figure 4.3

In this case the modelled flat-field correction $F_{Mij\lambda}$ of Equation 4.6 is used together with a normalised filter transmittance function, $T'(\lambda)$, by integrating over the vendor-provided filter transmittance curve and normalising (i.e. set $T'(\lambda) = 1$) at peak filter transmittance (Figure 4.4). However for most filters

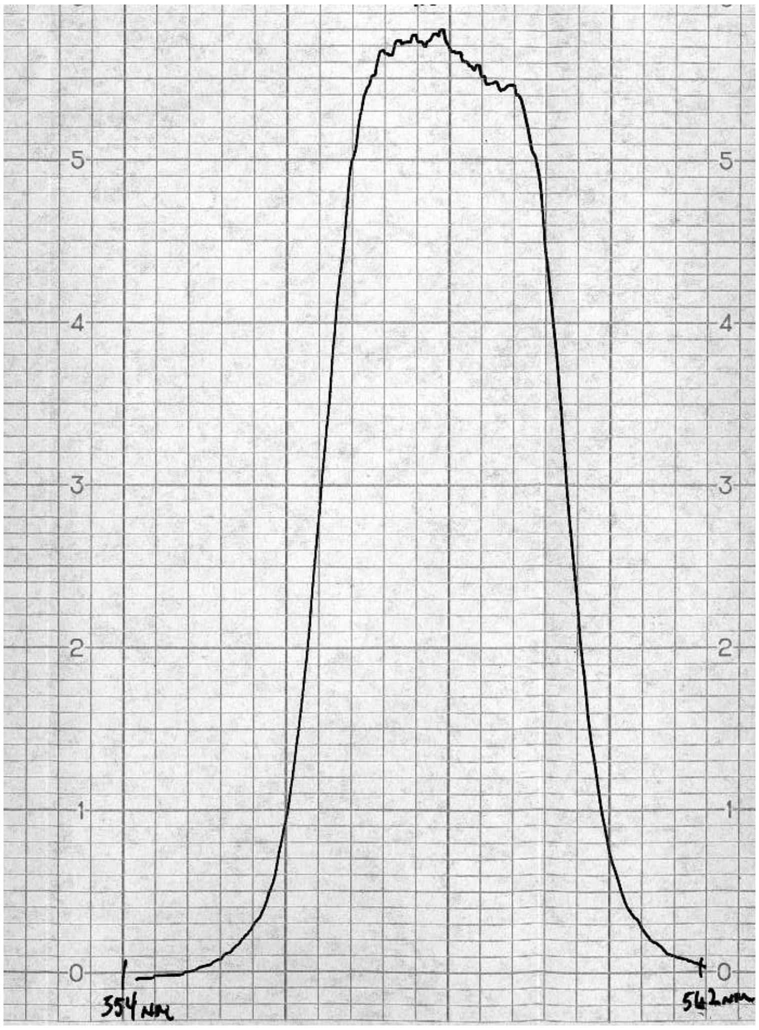

Figure 4.4: Example filter transmittance curve $T_f(\lambda)$ as measured by the filter manufacturer for a 40 Å wide 5590 Å filter (Lot. No. 3697). The measured peak transmittance of the filter is 0.6 and the centre wavelength at normal incidence (λ_{cw}) and filter bandwidth is measured to 5587.2 Å and 38.4 Å respectively. This filter is intended for the $O(^1S)$ 5577 Å auroral emission line. The deviation from normal incidence shifts the centre wavelength, which explains why a centre wavelength of 5590 Å was selected, (see Equation 3.45 in Section 3.5). As can be seen, this filter has a rather uniform transmittance in the passband.

it is acceptable to take $T'(\lambda) \approx 1$ over the entire filter-passband. Equations 4.5 and 4.11 yield the following equation (substituting Equation 4.10) to be used when a proper flat-field calibration is available:

$$C_{abs\lambda c} = \frac{1}{DN'_C} \int_{\lambda_1}^{\lambda_2} I_{ls}(\lambda)\, d\lambda \; \left[\frac{R}{\text{counts}}\right] \tag{4.13}$$

emission-line [*Gustavsson*, 2003]. This method would simplify the calibration procedures considerably. However this is a new method and these results have yet to be intercalibrated with the present calibration method. Regardless of whether the new method will be a verification procedure, or replace the present calibration procedure, it will no doubt represent a major improvement of the absolute calibration for ALIS.

Due to the inherent difficulties of absolute intensity calibration, an error of the order of 50 % is often regarded as acceptable. The largest errors appear to be related to the intercalibration of the light-standards (about 10–20 %, refer to Table 4.4). Furthermore, the calibration results appear to be fairly stable over one year (Table 4.5). On the other hand there are still many uncertain factors in the calibration procedure, most notably the absence of a uniform source needed for the flat-field calibration (Section 4.1.3). Therefore, to be on the safe side, it might be stated that the absolute calibration error lies in the range of 25–50 %. The intercalibration error of the ALIS imagers is probably much lower, at least for pixels in the central region of the image. For an imaging instrument, these errors are probably to be considered as acceptable. However improvements are still required.

Finally, the absolute calibration is applied to the object-images (DN'_{ij}, see Equations 4.5 and 4.6):

$$I_{ij} = C_{abs\lambda c} DN'_{ij} - I_{bg,ij} \ \ [R] \tag{4.15}$$

In this equation, I_{ij} is the calibrated pixel-value, and $I_{bg,ij}$ is the sky background correction.

4.2.2 Removing the background

Different schemes are employed to remove the sky background in Equation 4.15, depending on available data and the measurement situation. Therefore background removal is only outlined here.

In the case of HF pump-enhanced aurora, linear interpolation with time is sometimes used. Also a polynomial could be fitted line by line on each side of the emission region. In the most recent papers (Section 6.4) weighted sums of keograms through the emission region and on the side of it are used. This is done under the assumption that there is no aurora.

Regarding PSC studies (Section 6.6.1), brute-force median/min. filtering was applied [*Enell*, 2002].

For general auroral studies, background determinations are extremely difficult, as there is always some diffuse aurora present. In this case background images must be obtained by using a filter for a wavelength region with no auroral emissions. For the ALIS imagers, background filters are available: 5100 Å and 6230 Å. However these filters have seldom been used as they are only present at some stations (Section 3.5). For the future, permanent background photometers might be a solution of the problem.

transfer function is then used for calculating the field-of-view of each pixel of the CCD. Table 4.6 displays the fields-of-view of the ALIS imagers as calculated from the transfer-function.

	field-of-view			
`ccdcam`	FoV_o	FoV_x		FoV_y
1	90.4°	59.3°	×	60.5°
$\langle FoV \rangle$	1.2°	1.1°		0.9°
2	71.8°	48.5°	×	48.7°
$\langle FoV \rangle$	0.2°	0.1°		0.1°
3	71.7°	48.8°	×	48.8°
$\langle FoV \rangle$	0.1°	0.6°		0.3°
4	72.2°	49.9°	×	49.6°
$\langle FoV \rangle$	0.1°	0.1°		0.1°
5	71.8°	49.6°	×	49.1°
$\langle FoV \rangle$	0.2°	0.2°		0.1°
6	102.1°	66.1°	×	68.6°
$\langle FoV \rangle$	1.1°	0.4°		0.2°

Table 4.6: Measured fields-of-view for the ALIS imagers. These values are obtained from the geometrical calibration procedure using star images. Note that the CCD is a square inscribed in a circular field-of-view. Also note that the fields-of-view are calculated in a spherical geometry.

The optics used for the ALIS imagers is aberration limited, rather than diffraction limited. The effect of this aberration limited focus is shown in Figure 4.5. As can be seen the point spread function varies over the image plane, from 1–2 pixels in the centre to a few pixels at the edges. This will smoothen and widen images of sharp and narrow structures, in particular in the corners of the images. At the present no attempts are made to deblur/sharpen the effect of the PSF [*Gustavsson*, 2000, pp. 46–47].

Chapter 5

Controlling ALIS

> "For the highest payoff per dollar risked it should be remembered that communication system development is normally a ten year leadtime cycle process. Much better work in this field appears to result from a small number of people working for a long period of time than from a large massive crash effort attempting to generate a complete system within short time"
>
> *F. R. Collbohm*

Software for ALIS falls into two main categories: data analysis software (Section 6.2) and software for controlling ALIS. In the early phase of work on ALIS, initial ideas for how to develop the software for controlling ALIS were discussed by *Steen et al.* [1990]; *Johansson* [1991]; *Nilsson and Nyström* [1992] and *Nilsson* [1994]. While the main ideas for the control centre software have been in use until now, this is not the case for the station software.

ALIS is a complex and highly configurable instrument compared to traditional ground-based auroral imaging equipment. Someone once remarked that "comparing ALIS with a traditional all-sky camera is like comparing EISCAT with an ionosonde". ALIS is a campaign-orientated instrument and therefore needs more attention prior to measuring compared to traditional imagers. This gives large amount of flexibility for performing new types of scientific studies, but also introduces new problems. First of all, ALIS is a new instrument, with new and partly unexplored possibilities, and to learn those possibilities takes long time. While absolute measurements from photometers have been analysed for almost half a century, there is no common established practice to deal with such data expanded to two dimensions (not to mention three dimensions). Traditionally images have belonged to the realm of morphological measurements (some exceptions exist). Another concern is the tremendous increase in the amount of data produced, and how to process and analyse the data in a way that enables and improves the possibilities for physical interpretation. The point of this discussion is simply that it is difficult to develop a control system for something that is to a large extent new and unknown. Other difficulties arise from technical limitations, as well as from the rapid technical development, causing some components to become obsolete before they are finished and making it difficult to put priorities in the right order. (In the beginning of the project various proprietary programming environments had to be procured and learned, often at a high cost. Some years later, more standardised, reliable and free software emerged, partly making the earlier efforts

6. **Selecting temporal resolution:** The temporal resolution is currently limited to one image per 30–60 s at maximum resolution, and is generally never better than 30 images per minute at higher binning factors. These figures vary somewhat between the imagers. Also times for filter changes must be considered.

7. **Selecting spatial resolution and sensitivity:** This is generally a compromise between temporal resolution, sensitivity, framerate and disk-space. Note that increasing the temporal resolution by binning might lead to saturation problems due to the increase in sensitivity.

8. **Deciding on data storage strategies:** As the disk space at the stations is limited, it is advisable to estimate the amount of data produced and decide what data should be kept, when to retrieve the data and if deleting presumed unusable images should be allowed, etc.

9. **Coordination with other instruments:** Such as EISCAT measurements, satellite passes, rocket launches etc. This involves many considerations (for example when does a satellite pass occur? Should ALIS image along the foot-point of the satellite pass?). It is also essential to establish communication with the control centres of participating facilities.

10. **Selection of a suitable operational mode for the observation:** Available modes are: automatic, semiautomatic or manual, see Section 5.1.1. In order to increase the number of observations of a particular phenomenon it would be desirable to have more automatic runs, however, experiences indicate that at the present, the best results emerge from manned semiautomatic runs.

11. **Defining and testing the required configuration of ALIS:** No usable bug-free program exists. Therefore everything should be tested as thoroughly as possible before running the actual observation. It is also important to start up all systems in ALIS well in advance. The imagers need to be thermally stable and defrosting of the domes as well as booting subsystems at the stations might also take some time. (Estimate at least 1–2 days for testing a new measurement scheme, and 2–4 hours to start up ALIS.) It is also advisable to perform some rudimentary last checkout procedures about one hour prior to starting the measurements.

12. **Waiting for the right conditions:** This might be a long wait. In this phase, it is advisable to take images at all stations at regular intervals to check weather conditions and system performance. It is also a good practice to be prepared for many different kinds of observations. For example, if conditions for observing HF-pump enhanced airglow are not right, there might be an excellent auroral event instead.

13. **Run the observation:** During measurements many unexpected things can happen, so it is good to be well-prepared with alternatives. Two to three people in the control centre are the ideal for most measurements: one who takes care of technical problems and runs the system, one who concentrates

A-Alarms: Conditions causing the imaging to stop at one or several stations (power failures, filter-wheel problems, unrecoverable run-time errors, etc.).

B-Alarms: Other conditions affecting the quality of observations (timing problems, communication problems, over- or under-exposed images, etc.).

5.2 OPERA

The complete collection of software for controlling ALIS is called an OPERations system for ALIS (OPERA). The three main components of OPERA are briefly described below.

5.2.1 User interfaces

The main graphical user interface for ALIS is an X-windows application (`parsifal`) that has been supported on various computing platforms (HP-UX, Sun-OS (Solaris), GNU/Linux, Windows-95 and Java). It provides a user-friendly way to configure and run ALIS as well as to display quick-looks and status information. Commands can be sent to the system, either by user-defined menus or directly by typing them on a command line. From `parsifal` it is possible to monitor and control ALIS in many ways, to receive and view quick-look images, to communicate with other ALIS users, to upload experiment configurations, etc.. A text-only user interface, (`tosca`), is available for controlling ALIS over slow communication lines (implemented in Lisp as a major mode for the Emacs editor). From around 1999, as the stations become networked over ppp (Section 2.2.3) it also became possible to configure and control the stations over direct TCP/IP connections (for example by making a direct `telnet` login to the desired station computer). It is foreseen that the need for a dedicated control centre and special user-interfaces will vanish as it will be possible to control ALIS from an ordinary web-browser in the future.

5.2.2 AIDA

A central set of server processes, Alis Internal Data Administration (AIDA) runs at the control centre, accepting connections from user interfaces and directing user-commands to the desired set of stations. Furthermore, requests from the stations affecting users, or other stations, are routed to their proper destinations. AIDA also handles alarms and other exceptions and activates the paging system if no user-interface is online. The concept of AIDA as a central node (or crossbar-switch) has survived since the first implementation (around 1992), but is subject to change in the future as all stations become networked. When this happens, a central node is no longer required, as this functionality can be undertaken by any station. Therefore the need for a dedicated control centre will also diminish with time. All of the AIDA software was written in a Unix/C environment from the beginning, first under HP-UX and later ported to GNU/Linux. A block-diagram of the AIDA software and user interfaces appears in Figure 5.1. See [*Nilsson*, 1994] for a more detailed description of AIDA.

5.2.3 Station software

The present ALIS stations are to a large extent controlled by station-control programs running in the station computer (SC). As long as MS-DOS was used as the operation system for the station computer (Section 2.2.6) a huge application program (`HENRIK`) controlled the station. Due to the many and absurd technical limitations of MS-DOS, this program had problems meeting the required specifications, especially with respect to speed, reliability and the data-handling capacity. As GNU/Linux emerged as a reliable and free multi-tasking operating system, it was quickly realised that a change of operating-system at the stations was top priority. Around 1997, `HENRIK` was quickly ported to GNU/Linux; the resulting program was called `arnljot`. Although this was a major improvement, it was still a ported huge MS-DOS program including large amounts of code written exclusively to bypass MS-DOS limitations. To remedy this, a major rewrite of the code was initiated, removing all "MS-DOS-artifacts", as well as splitting the program in three parts: `aniara` handling the overall station control and communication with the control centre; `mima`, controlling the imager; and `nipu` handling the NIPU, (Section 2.2.2). These programs have been in routine operation since 1999.

`aniara` supervises most functions at the station and provides an interface to AIDA. Among many other things, `aniara` handles alarm conditions, stores configurations, and acknowledges "sanity-checks" sent from the Housekeeping Unit (Section A.4) after verifying that the station computer is operating properly. A simple text-oriented user interface to ALIS, mainly intended for system maintenance is also provided by `aniara`. As AIDA is slowly phased out, `aniara` will most likely take over some of its functionality.

`mima` is the imager control program. It boots up the camera-control unit (Section 3.3.2), configures the imager (Section 3.3.3), retrieves the image-data as well as creates and saves FITS images onto the local disks (Section 2.2.5). This program is thus responsible for putting all the supplementary information into the FITS header (integration-time, filter, UTC, viewing direction, CCD-temperatures, etc.).

`nipu` is a program for controlling and booting the NIPU. This program is used to calibrate the FPS and CPS, select filters (Section 3.5) and viewing-directions (Section 3.6).

Apart from the software discussed above, it is also worth mentioning the following software packages at the station:

CCU-software: Vendor-provided Transputer binaries for the camera-control unit (Section 3.3.2). This code is uploaded by `mima` during the imager boot-up phase.

HU-firmware: The Housekeeping Unit (Section A.4) firmware is written in assembler and stored in an Erasable Programmable Read-Only Memory (EPROM). It provides low-level interfaces to various GLIP systems (Appendix A), watchdog functions for the station computer, as well as alarm operating system at the stations, dominated. Following the major OS upgrade to GNU/Linux, most of these software problems have now been eliminated. The importance of reliable and free operating systems cannot be over-estimated. Many man-years of programming efforts could have been saved if proprietary software could have been avoided in the first place.

Regarding the user-interfaces, it seems inevitable that an effort will be required to create a web-oriented standard user interface for ALIS. AIDA will probably be depreciated in favour of moving this functionality to the stations. This will also increase redundancy of the ALIS control system. At the stations a simple and flexible approach seems to be to let each major functionality to be represented by an application program. An interesting development is the networked "parameter-server" that can be used to configure ALIS as well as to retrieve status information in a consistent way over the entire network of stations and user-interfaces.

The lag between the desired and present control system for ALIS is in the order of 1–2 man-years. Finally it should never be forgotten that software development is an evolutionary process that requires continuous upgrades and maintenance.

Chapter 6

Scientific results from ALIS

> “Vetenskapsmannen är en byggmästare. Att samla vetenskapliga uppgifter kan jämföras med att samla stenar till ett hus; en hög med uppgifter är inte mer “vetenskap” än en hög stenar är ett hus. Obearbetade vetenskapliga resultat är bara en död stenhög” *Kristian Birkeland*

> “Wovon man nicht sprechen kann, darüber muß man schweigen”
> *Ludwig Wittgenstein*

This chapter attempts to provide a summary of the scientific results obtained from the analysis of data from ALIS. It is important to stress that this can only be a brief review of published scientific results in order to demonstrate the scientific applicability of ALIS in particular, and of multi-station imaging in general. The reader is urged to read the original papers for more complete and detailed information about the scientific results summarised.

Interesting results often emerge from unexpected directions. HF pump-enhanced airglow was not mentioned among the scientific objectives in the early ALIS papers. However, this topic existed as an auxiliary scientific objective until 16 February 1999, when the first unambiguous observations of this phenomenon at high-latitudes were made. Since then it has been the main scientific objective of the ALIS measurements. Hence, a large portion of this chapter (Section 6.4) is therefore devoted to these observations.

It is essential for a proper interpretation of the data-sets to do coordinated observations involving as many independent measurement systems as possible. ALIS has participated in a number of coordinated campaigns involving instrumentation such as the tri-static European Incoherent SCATter radar (EISCAT), the EISCAT Heating facility in Tromsø, the American FAST, POLAR and MSX satellites, and the German lee-wave campaign studying polar stratospheric clouds etc.

The author’s main role has been to supervise and make the observations with ALIS and supporting instruments, retrieve, calibrate and validate the datasets, as well as to assist with data-analysis and interpretation of the data-sets. Most ALIS data-analysis software, and in particular the software for triangulation and tomography-like analysis has been designed and written by Björn Gustavsson. He also performed most of the data-analysis. Many other coauthors (see the bibliography) contributed to the physical interpretations of the data-sets obtained that ALIS would be able to produce 2-D maps of the altitude-distribution of the different auroral emissions. This would represent a pseudo 3-D image of the aurora. To develop techniques for visualising the variations in time and space of 3-D aurora was characterised as "an interesting but non-trivial exercise*". While the latter still lies in the realm of the future, ALIS-images have frequently been used for obtaining heights and volume distributions through triangulation and tomography-like inversion techniques. The progress in this field is reported in Section 6.3 and references therein.

Relation between electron and proton aurora: The main auroral particle species are electrons and protons. The intensity of the more diffuse proton aurora is much lower than the electron aurora. In order to study the relation between these two types of aurora, it was suggested to use the N_2^+ 1Neg. (4278 Å) and H_β (4861 Å) emission lines [see for example *Galand*, 2001, and references therein]. Although ALIS would be well-suited for studies of proton aurora, no measurements have been carried out to date.

The relation between the neutral wind and the aurora: Auroral intensifications appear to be related to rapid variations in the thermospheric neutral wind on a time scale which excludes contribution from the ion-drag force. This objective was added in *Steen et al.* [1990] and some initial studies were carried out (Section 6.5.6).

Non-auroral studies: It was envisioned that ALIS would make mainly auroral observations during dark periods. The system would also be available for other types of measurements. One such type of measurement is to study the formation of Polar Stratospheric Clouds (PSC) which is important for the understanding of ozone depletion. The results of some of these studies are summarised in Section 6.6.1. It was later proposed [*Steen et al.*, 1990] to study gravity wave modulation of airglow emissions. However, no such studies have been carried out to date. It was also speculated that ALIS could be used for other studies, for example high-altitude flashes, clouds and comets, etc. ALIS acquired some images of the Hale-Bopp and the Hyakutake comets; however these data have not yet been analysed. In summary, observations of HF pump-enhanced airglow quite unexpectedly ended up as the main topic for ALIS.

The majority of published ALIS results to date concerns studies of HF pump-enhanced airglow and therefore constitutes the main part of this chapter. When ALIS measurements stopped for the season each year due to the midnight sun period, one detector participated in a joint study to attempt daytime auroral imaging using an imaging spectrometer. This generated some interesting first results, as outlined in Section 6.5.5. Another sidetrack that might become productive in the future is the study of meteor trails. Some rather promising observations have already been carried out (Section 6.6.2).

*The problem is not so much the visualisation itself, but rather that human perception has evolved to interpret 2-D surfaces of 3-D objects. Evolution has never required an understanding of a true 3-D distribution.

Package name	*Description*
`ALISFIX`	Loads images into Matlab, converts the FITS headers to a common format.
`ALISMOVIE`	Generates mpeg movies containing a single-frame overview of all stations.
`TOMO`	Iterative 3D-Tomography toolkit. Stand-alone version.
`TOMOMEX`	The same as `TOMO`, but compiled as a Matlab "mex" file.
`TOMOWS`	A Matlab API for the `TOMOMEX` package. Includes some graphical user interfaces for plotting
`ALISDB`	A set of scripts used to create arrays of structures describing ALIS images. These can be used to create static web-pages with quicklook overviews. The package can also be used as a pre-processor for the `TOMO` package.
`alisim`	A universal tool to preprocess, correct and display ALIS FITS images.
`ITERATOR`	Creates fast files for Matlab from a Matlab expression. Typically 6–16 times faster for the ALIS optical camera model.
`ALIS-SQL`	A searchable database for all ALIS images with download, viewing of quick-look images, etc. in use at `http://petrydpc.itm.mh.se/alis/`. Uses `alisim` to read the database and create quick-looks.
`fits_toolbox`	Tools to read, modify and write FITS headers.

Table 6.2: Summary of data analysis tools written by Peter Rydesäter, available at `http://petrydpc.itm.mh.se/tools/`. See also *Rydesäter* [2001] for more information.

Auroral classification scheme

Main morphological feature	Secondary morphological feature	Temporal feature	Vortex feature
Auroral arc one dimension is significantly larger than the other	Non-diffuse Diffuse Multiple (2,3,...) Rayed Striated Corona Dark aurora Enhanced Partly clouds Intensity	Active Quiet Pulsating	Spiral (E.g. WTS, omega, torch) Fold Curl
Fragmental auroral structure	Non-diffuse Diffuse Multiple (2,3,...) Rayed Striated Corona Dark aurora Enhanced Partly clouds Intensity	Active Quiet Pulsating	Fold Curl
Diffuse aurora covering a larger region	Dark aurora Partly cloudy Intensity	Pulsating	
Unidentified aurora			

Table 6.3: An auroral classification scheme (after a proposal by Å. Steen) used by the manual classification program for ALIS data. ("Dark aurora" stands for a class of phenomena commonly known as "black aurora")

Early on in the ALIS project, an auroral classification scheme was suggested (by Åke Steen, see Table 6.3). A classification program (developed by Petrus Hyvönen and later Mats Luspa) was written. The program was used to manually, but relatively quickly, classify the images according to the classification scheme in Table 6.3. This classification was very useful but time-consuming due to the large number of images from many stations. The quality of the image-classification was also dependent on the operator. This classification method was therefore abandoned, and investigations started to find automated methods of image classification.

In an exploratory study carried out by *Waldemark et al.* [1997]; *Eide et al.* [1997] Pulse Coupled Neural Networks (PCNN) were evaluated as a preprocessor for classifying image-data from ALIS. The PCNN is a biologically inspired neural network based on findings in the visual cortex of small mammals. The algorithm has been successfully applied in the field of mammography [*Kinser and Lindblad*,

6.3 Tomography and triangulation

Many earlier experiments have used multi-station measurements combined with triangulation techniques to estimate the height of the aurora (Section 1.1.1). Computer Tomography (CT) has its most well-known applications in the field of radiology† [*Cormac*, 1963a,b]. A similar method was applied by *Solomon et al.* [1984] to estimate the airglow distribution as measured by space-borne photometers. An emission distribution was characterised by *Jones et al.* [1991] by using data from a rocket and three ground-based scanning photometers. *Na and Lee* [1991] estimated ionospheric electron densities from radar measurements by the use of tomographic methods. *McDade and Llewellyn* [1994] presented methods to estimate airglow distributions from limb-scanning satellite measurements. By the use of image data from two monochromatic TV-cameras in Antarctica with a separation of 20 km *Aso et al.* [1990] studied the auroral emission distribution in slices.

6.3.1 Methods, initial studies and simulations

One primary scientific objective of ALIS was to provide the possibility to reconstruct the 3D auroral volume emission by applying tomographic inversion techniques on spectroscopic high-resolution images of aurora, airglow and related phenomena [*Steen*, 1989]. An initial study based on simulated ALIS-data was performed by *Gustavsson* [1992]. Later, the problems of auroral tomography were discussed during an auroral tomography workshop in Kiruna [*Steen*, 1993]. A more detailed model simulation study [*Gustavsson*, 1998] concluded that the capability to achieve results with acceptable horizontal and vertical resolution, exists. This paper also suggests a useful way to define a stopping criteria for iterative tomographic methods by combining adaptive low-pass filtering and feasibility tests, and concludes that "it is possible to achieve feasible reconstructions with the modified Multiplicative Algebraic Reconstruction Technique (MART)." An introductory overview of ground-based tomography, including a further investigation of resolution and error sensitivity is presented in *Gustavsson* [2000, Chap. 3] concluding that "the result of the tomographic inversion cannot retrieve fine scale internal structures. However, estimates of the spatial distribution of ionospheric emissions which, in general, have a comparatively simple shape, can be accurately obtained". The chapter also presents a strengthening of the statistical stopping criteria of *Veklerov and Llacer* [1989].

6.3.2 Summary of results from computer tomography of ALIS-data

At an early stage a close scientific and technical collaboration was established with colleagues at Kyoto University, and later at the National Institute for Polar

†Incidentally, the term "tomography" existed in radiological applications decades before computerised tomography became a real possibility. See, for example, *Lodin* [1935]; *Weinbren* [1946], and other references discussed in *Backlund* [1956]. Typically a series of X-ray exposures were obtained while the X-ray tube and film-cassette rotated around the patient. Back then, the tomographic inversion had to be performed by the brain of the radiologist observing these series of X-ray images.

6.4 HF pump-enhanced airglow

By transmitting a powerful high-frequency (HF) ("short-wave") radio signal into the ionosphere it is possible to modify the ionosphere given that the ionospheric conditions are favourable (i.e. high enough electron concentration, and little or no auroral activity). Such experiments may excite plasma processes on a wide range of temporal and spatial scales [*Leyser et al.*, 2000]. It is possible to produce enhanced optical emissions, which are far to weak to be detected by the unaided human eye, but that can be detected with sensitive imagers and photometers. These optical emissions can be used as a diagnostic tool to study electron energisation during driven plasma turbulence. For example, it is possible to study what the roles of heating and electron acceleration are for dissipating the turbulence [*Leyser et al.*, 2000]. The naturally occurring airglow emissions at 6300 Å and 5577 Å (from the two lowest excited states of oxygen, $O(^1D)$ and $O(^1S)$) can be enhanced by transmitting a high-powered short-wave radio signal into the ionospheric F-region plasma. The low noise and high quantum-efficiency of the ALIS imager (Chapter 3) makes ALIS an ideal instrument for studying optical effects from active ionospheric experiments.

HF pump-enhanced airglow ‡ has been studied at low latitudes (Arecibo, Puerto Rico) since the early 1970s by *Carlsson et al.* [1982] and *Bernhardt et al.* [1989]. At mid-latitudes, experiments have been carried out in: Platteville, U.S.A., [*Sipler and Biondi*, 1972; *Haslett and Megill*, 1974], Moscow, Russia, [*Adeishvili et al.*, 1978], and in Sura, Russia [*Bernhardt et al.*, 1991]. However, at high (auroral) latitudes, there was only one previous report of HF pump-enhanced airglow before 1999 made by *Stubbe et al.* [1982].

The airglow enhancement has been attributed to excitation of metastable states of atomic oxygen by energetic electrons accelerated in plasma instabilities, [*Perkins and Kaw*, 1971; *Weinstock and Bezzerides*, 1974; *Weinstock*, 1975; *Gurevich et al.*, 1985] and by energetic electrons from the tail of the heated thermal electron plasma [*Mantas*, 1994; *Mantas and Carlson*, 1996; *Gurevich and Milikh*, 1997]. Electron collisions with energies above 3.5 eV yield the excited $O(^1D)$ metastable state, which radiates at 6300 Å [*Bernhardt et al.*, 1991]. The second excited metastable state $O(^1S)$, which radiates at 5577 Å, is obtained for electron energies from about 4.5 eV and upwards. For comparison, the ionospheric background electron temperature is typically 0.1–0.2 eV. Further, it has been proposed that the $O(^1D)$ state may be thermally excited and that the scarcity of observations of simultaneous 6300 Å and 5577 Å enhancements imply that acceleration of electrons may require special experimental and ionospheric conditions that are not often fulfilled [*Mantas and Carlson*, 1996].

‡As long as the enhancements were only observed in the $O(^1D)$ (6300 Å) and occasionally in the $O(^1S)$ (5577 Å) emission lines, the natural term was "HF pump-enhanced airglow". With the recent observations in the N_2^+ 1Pos. (6600 Å) emission [*Djuth et al.*, 1999], and N_2^+ 1Neg. (4278 Å) and $O(3p^3P)$ (8446 Å), a more correct term would be something like "HF pump-enhanced optical emissions" or maybe "Radio-induced optical emissions". However, the old term "HF pump-enhanced airglow" will be retained in this text for compatibility with earlier papers.

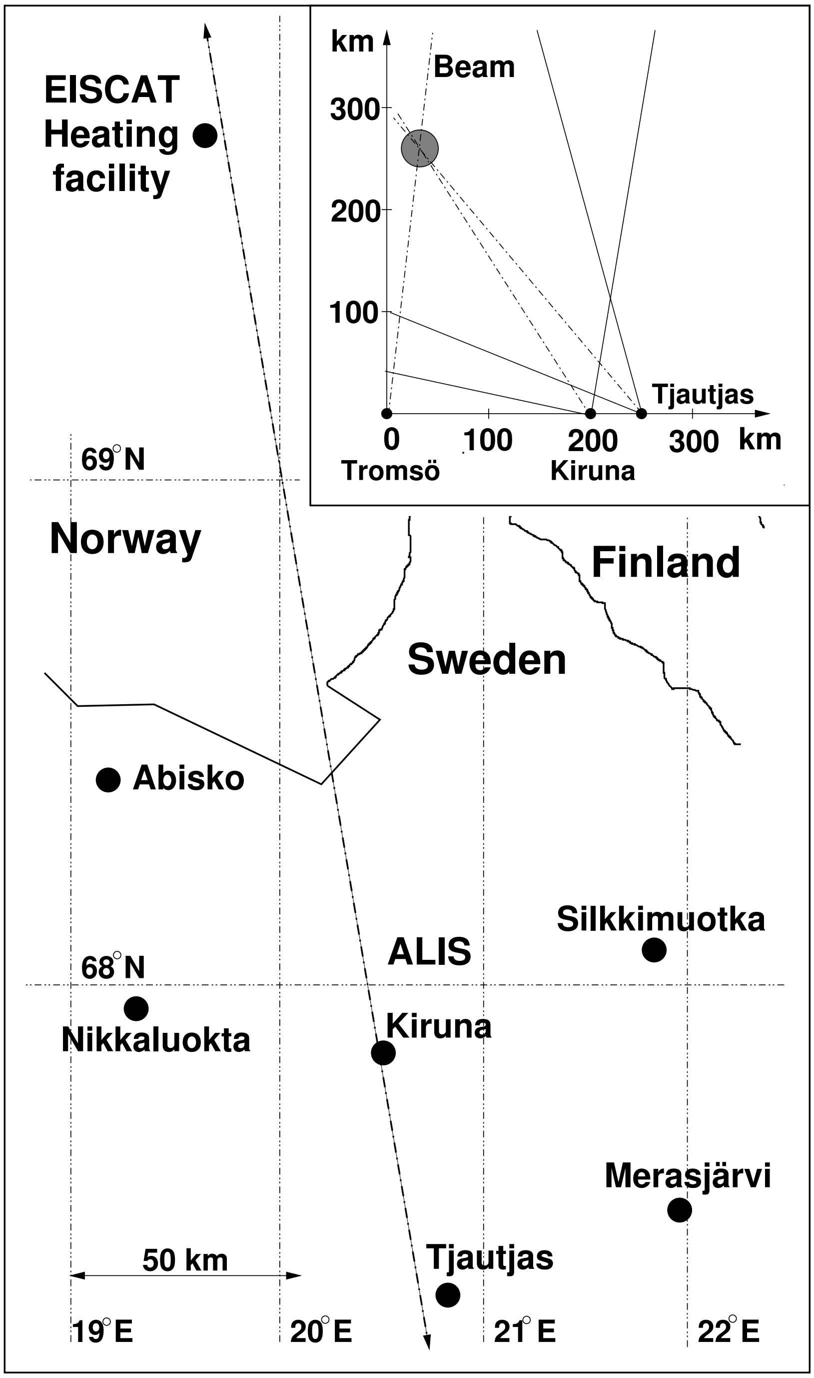

Figure 6.2: Geometry of the HF pump-enhanced airglow. Some of the ALIS stations (see text) observed pump-enhanced airglow over the EISCAT Heating facility. *Inset:* A vertical cut along the Tromsø–Kiruna meridian. The dot indicates the anticipated region of enhanced airglow and the solid lines indicate the field-of-view of the cameras. [After Figure 1 in *Brändström et al.*, 1999]

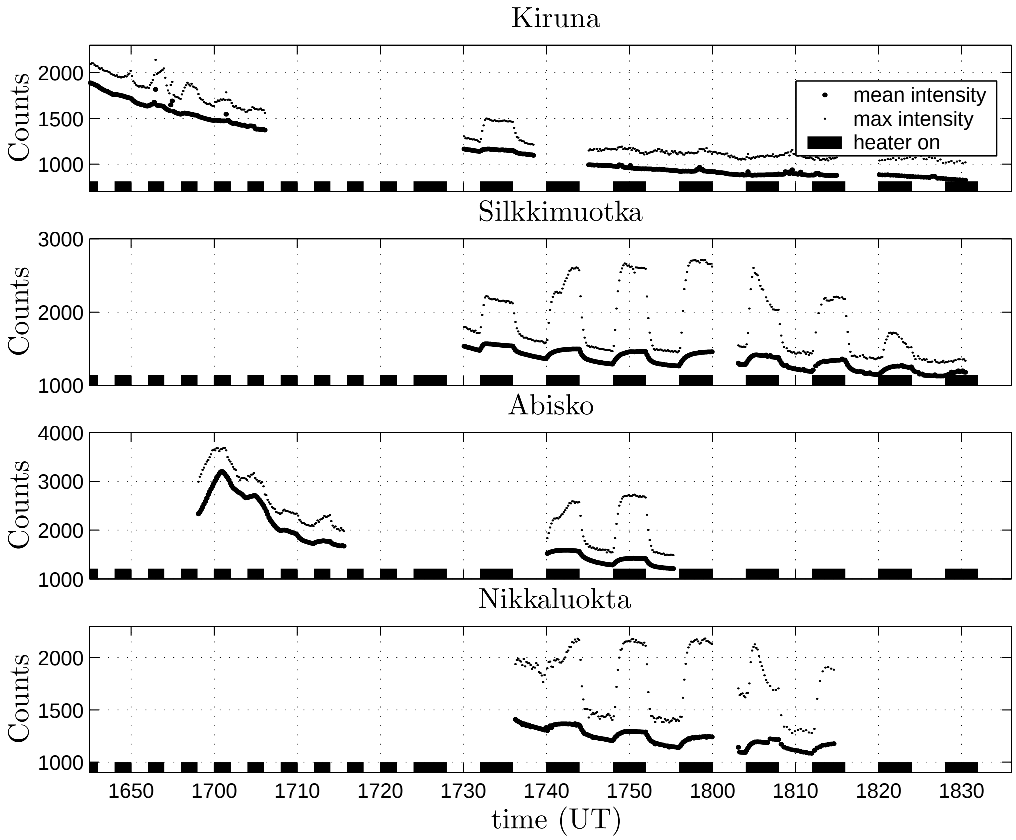

Figure 6.3: Maximum and average column emission of the 6300 Å airglow as seen from four stations. The intensity modulations correlate well with the transmitter-on/off cycles. After 17:40 UTC the Kiruna camera was directed to local zenith, imaging the natural background airglow. [After Figure 1 in *Gustavsson et al.*, 2001a]

in the ionospheric F-region above the transmitters). The transmitters (or "HF-pump") were cycled on/off with a duty cycle of 50%. Between 16:32 and 17:22 UTC the transmitters were cycled 2 min on/2 min off. Between 17:24 and 18:32 UTC this was changed to 4 min on/4 min off.

When the transmitters were cycled 2 min on/2 min off, weak airglow enhancements were observed [*Brändström et al.*, 1999; *Leyser et al.*, 2000; *Gustavsson et al.*, 2001a]. Starting at 17:32 UTC and continuing until 18:30 UTC (transmitters 4 min on/4 min off) pump-enhanced airglow was observed by all ALIS stations in operation. Due to occasional thin clouds and technical problems, some data-losses occurred. In Figure 6.3 the maximum intensity of the 6300 Å emission is plotted against time for each image from the four stations observing between 16:40 and 18:40 UTC.

The airglow intensity has an *e*-folding growth time of about 60 s after transmitter-on, and decays with an *e*-folding decay time of about 35 s after transmitter-off. After the growth time following transmitter-on, the maximum intensity of the emission appears to have a different temporal evolution at different transmitter-on/off periods. This feature may be due to irregularities in the

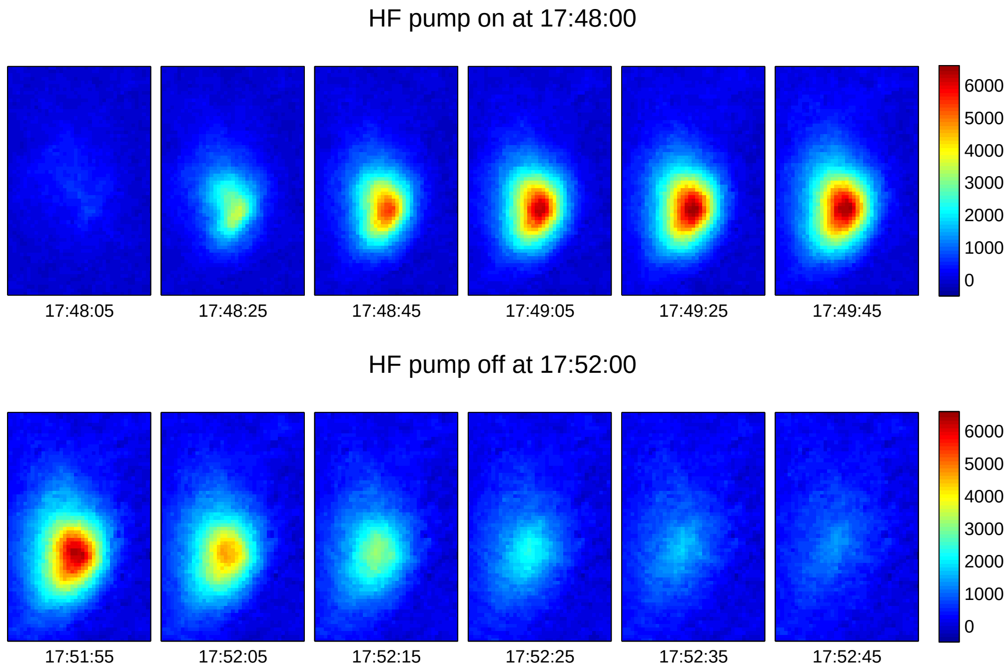

Figure 6.5: A series of images of enhanced 6300 Å airglow recorded at the Silkkimuotka station for the period 1748–1752 UTC. The upper panel displays an image sequence just after transmitter-on, and the lower panel shows images near transmitter-off. [After Figure 3 in *Leyser et al.*, 2000]

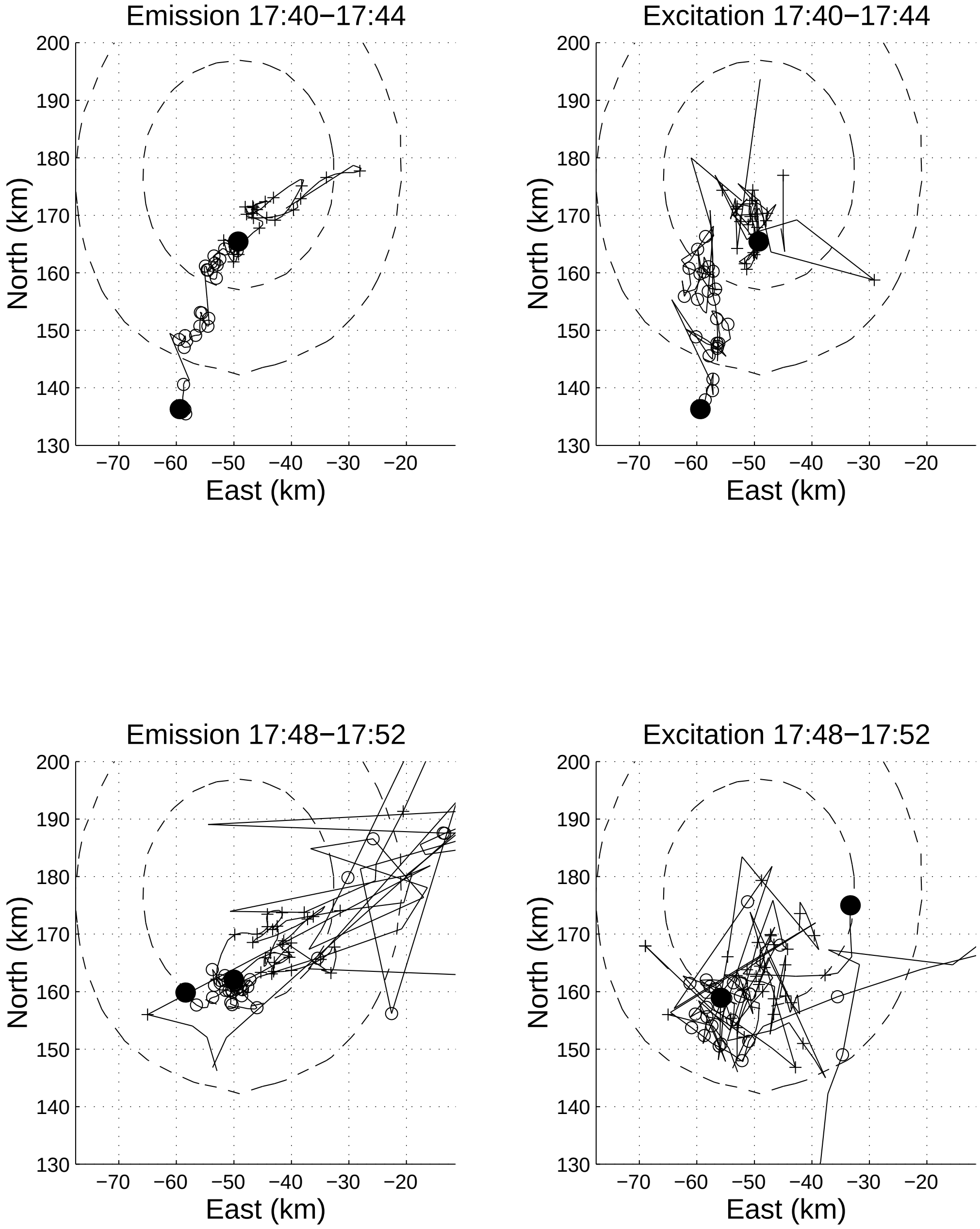

Figure 6.7: Upper left: trajectories of the centres of 6300 Å airglow emission, starting at the black points. Upper right: centres of $O(^1D)$ excitation. Lower left: centres of 6300 Å airglow emission. Lower right: centres of $O(^1D)$ excitation. There are 10 s between the markers in all panels, and all distances are relative to Kiruna. The dashed contours are the -1 and -3 dB projections of the HF-pump beam. [After Figure 4 in *Gustavsson et al.*, 2001a]

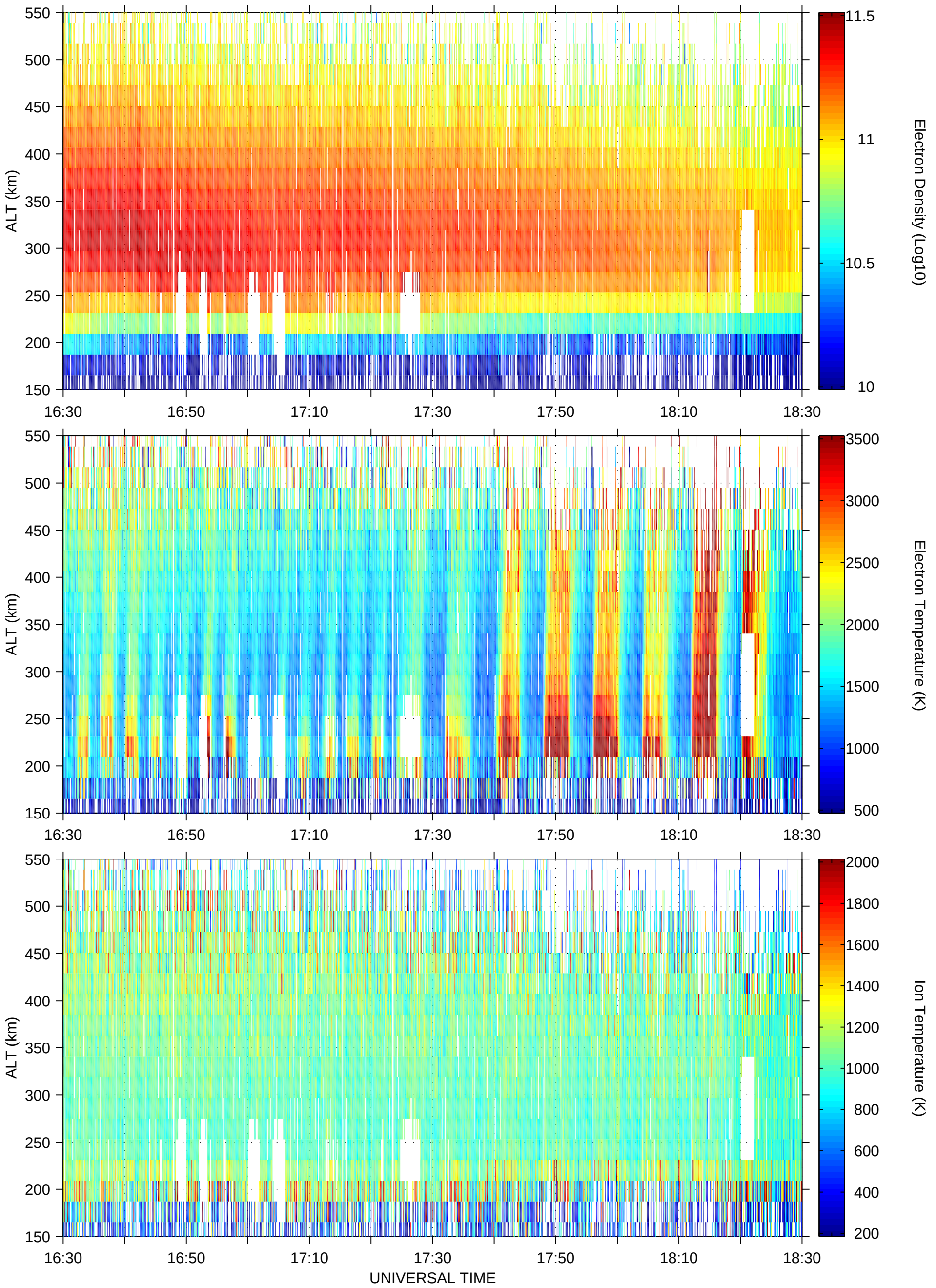

Figure 6.9: EISCAT UHF radar measurements of electron density (top panel), electron temperature (middle panel) and ion temperature (lower panel) on 16 February 1999. The data are for altitude gates spaced 22.5 km apart, which were analysed with 5 s time resolution. The blank areas below 350 km altitude are regions where the ion-line was enhanced by the HF-pump wave, causing the standard analysis to be invalid. [After Plate 3 in *Gustavsson et al.*, 2001a]

ficantly shorter than the 110 s lifetime of the $O(^1D)$ metastable state [*Solomon et al.*, 1988]. However, at 240 km altitude, the effective life time of the $O(^1D)$ emission is reduced due to collisional quenching by excitation of vibrational states in N_2 and O_2 to as low values as 30 s [*Sipler and Biondi*, 1972; *Bernhardt et al.*, 1991]. Thus, the observed decay time is consistent with the effective life time of the $O(^1D)$ state being reduced by quenching [*Leyser et al.*, 2000].

Sergienko et al. [2000] used EISCAT measurements of the electron temperature to estimate the position and magnitude of the heating source. The magnitude of a modelled electron heating source was adjusted to give the best fit to the observed time-behaviour of the electron temperatures at all altitudes. This procedure led to a determination of the position and magnitude of the electron-heating source at 220 km altitude and 6×10^4 eVs^{-1} cm^{-3} respectively. A good agreement with the measured and calculated electron temperatures were obtained. The next step was to compare modelled and measured column emission rates of the $O(^1D)$ (6300 Å) line. Assuming a thermal excitation mechanism led to large overestimates of the modelled column emission rates as compared to an accelerated electron excitation mechanism. The paper shows that the assumption of abnormal electron heating generated by the transmitted wave leads to a possible explanation of the observed electron-temperature variations, but cannot account for the observed airglow variations. A process resembling acceleration by Langmuir turbulence (where the electrons above 2 eV are non-Maxwellian with a uniform energy distribution from 3–10 eV) might be an alternative explanation for airglow enhancements. This modelling was done according to the analysis by *Bernhardt et al.* [1989] and by calculating the production rate of the $O(^1D)$ state by electron impact according to the Monte Carlo model for electron transport into the atmosphere by *Ivanov and Sergienko* [1992].

It was, however, later found out that the electrons are more likely accelerated by upper hybrid turbulence [see *Leyser et al.*, 2000] instead of Langmuir turbulence. For example, if the pump-frequency is close to a multiple of the electron gyro-frequency, the optical emissions in 6300 Å and 5577 Å becomes very faint [*Kosch et al.*, 2002a] while the Langmuir turbulence is very strong. This is also consistent with results from tomographic inversion, which resulted in a too low altitude for Langmuir-turbulence. [*Leyser and Gustavsson*, 2003]

The most complete treatment of the observations from 16 February 1999 (so far) is presented in *Gustavsson et al.* [2001a]. This paper presents the first estimate of the volume distribution the HF pump-enhanced airglow emission obtained from a tomography-like analysis of the image data. Where data from three stations exists (17:40–17:56 UTC), the tomography-like inversion procedure gives reliable results [see *Gustavsson et al.*, 2001a, for details]. For periods with data from only two stations a stereoscopic triangulation method was employed to determine the position of the enhanced airglow region. In Figure 6.10 the result of the tomography-like inversion is presented. The shape of the excitation varies from prolate along the magnetic field to slightly oblate. Also, the existence of two separable regions is clearly seen in the figure. These results were validated by back-projecting images from the reconstructed volume and comparing them to the original images. Comparing the images [see *Gustavsson et al.*, 2001a] gives a typical maximum error of ±10%. Thin drifting clouds in Abisko as well as uncertainties in the relative sensitivities (Chapter 4) of the cameras contribute to the errors.

There are significant differences between the two pulses, as shown by calculating the "centres of emission and excitation" (Figure 6.7). The north-eastward drift of the "centre of emission" agrees well with the FPI measurements of the neutral wind. These intensity variations and drift patterns indicate that the energy dissipation of the HF-pump wave depends on the background ionosphere.

Calculating the altitude-averaged lifetime according to *Bernhardt et al.* [1989] an effective lifetime of 25 ± 2 s is obtained during the pulses and 30 ± 2s for the first minute after the pumping. Applying these results, *Gustavsson et al.* [2001a] made a model-independent estimate of the altitude average excitation distribution according to *Bernhardt et al.* [1989] displaying a systematic pattern: initially a patchy structure appears, after 15–25 s the excitation grows in a smaller region, where the surrounding region either saturates or decreases, as shown in Figure 6.11. These results show how nicely multi-station spectroscopic imaging of HF pump-enhanced airglow can visualise the complexity and temporal evolution of the pump-ionosphere interaction. Clearly, many more experiments are needed to fully understand the underlying physics.

For periods with image data from only two stations, triangulation with manual identification of corresponding points was employed. This gave an estimate of the maximum emission altitude varying from 230–240 km at 17:32–18:08 UTC, but from the transmitter-on period starting at 18:12 UTC, the height was 250–260 km (Figure 6.6). A reasonable estimate of the error is ± 3 km. Periods with the largest spread in altitude (17:32, 18:04 UTC) occurred when a rise in altitude of the enhanced ion line was observed. The paper also contains a discussion of temporal and intensity variations and a section on theoretical airglow modelling.

From the analysis of the data-set from 16 February, in part summarised above, *Gustavsson et al.* [2001a] make a plausible claim that *the enhanced airglow is not excited by the high-energy tail of a purely Maxwellian electron distribution* and raise a number of questions:

- What physical processes control the complex drift pattern?
- What physical process controls the transition from the initial complex excitation structure?
- During what physical conditions can more than one region of strong $O(^1D)$ excitation coexist?

A brief summary of all results obtained hitherto, including some so far unpublished results, is provided in *Leyser et al.* [2002].

A recent publication [*Gustavsson et al.*, 2003] reports on the first nearly simultaneous observations of HF pump-enhanced airglow at $O(^1D)$ 6300 Å and $O(^1S)$ 5577 Å. These results were obtained during 21 February 1999 at 4.04 MHz, transmitting vertically with an ERP of 73 MW and an 8 minutes transmitter-on/off cycling period. ALIS station 5 in Abisko alternated between 5577 Å and 6300 Å during the same heater pulse. The regions of enhanced airglow are nearly identical, suggesting that the sources of the emissions are co-located in the ionospheric F-region. During the same transmitted pulse an estimated maximum column emission rate of about 40–60 Rayleighs in 6300 Å and with a maximum column emission rate of about 10–20 Rayleighs in 5577 Å were observed. These preliminary results indicate that an intensity-ratio of 5577 Å and 6300 Å of about 0.3–0.4 implies that the excitation is caused by a non-thermal electron population. Previously obtained intensity ratios were 0.05–0.3 [*Haslett and Megill*, 1974], and 0.08 [*Bernhardt et al.*, 1989].

HF pump-enhanced airglow in the N_2^+ 1Neg. 4278 Å emission was observed in photometer data from 2001 by *Kaila* [2003b]. In March 2002 ALIS observed HF pump-enhanced airglow in N_2^+ 1Neg. 4278 Å. In this experiment the transmitted wave was stepped up and down in frequency through the third harmonic of the ionospheric electron gyro frequency. The airglow was simultaneously imaged with one CCD camera operated at 6300 Å by M. Kosch in Skibotn, and the mobile ALIS station (Section A.8) located at the same place. The ALIS camera recorded emissions in 5577 Å as the frequency was stepped downward through the gyro harmonic, and weaker 4278 Å emissions as the transmitted frequency was stepped up again. This is the first time that pump-enhanced ionisation of the thermosphere has been directly observed. Furthermore, the frequency dependence of the 4278 Å emission gives input to theoretical modelling of electron acceleration for HF-frequencies near the harmonics. It is important in future experiments to be able to reconstruct the volume distribution of the N_2^+ 1Neg. emission and compare with the volume distribution of for example $O(^1D)$ to study the role of the underlying plasma dynamics perpendicular and parallel to the geomagnetic field [*Leyser et al.*, 2002]. Therefore it is essential to obtain more multi-station measurements with ALIS in the future.

6.5 Auroral studies

Although ALIS was built for auroral observations, and consequently most of its observing time was spent on auroral observations, the amount of published scientific results in this field have been sparse. One explanation is that once the HF pump-enhanced airglow experiments proved successful, it was deemed far more productive for a small group to spend time publishing these results. Other contributing factors are the technical problems affecting the maximum framerate (Section 3.3.4). Furthermore, as ALIS is a new type of instrument, much remains to be learned about how to exploit it in the optimal way. The amount of data is also somewhat limited as auroral studies often are dependent on a variety of coordinated observations with other instruments.

When planning coordinated studies with satellites as well as ground-based radars and optical instruments, many criteria need to be fulfilled; near new-moon, clear skies, the satellite magnetic footprint needs to be reasonably close to the ground-based instruments, radar observing-time needs to be applied for and scheduled [*Hedin et al.*, 1999]. Furthermore, the probability of observing the desired auroral phenomena must be maximised for the ground-based sites taking part in the study. For campaigns involving satellite passes, slow magnetic midnight passes are optimal. Yet, fulfilling all of these criteria for a successful observation might take a very long time. Therefore patience, long-term stability and flexibility in changing the scientific objectives are key-issues. An auroral

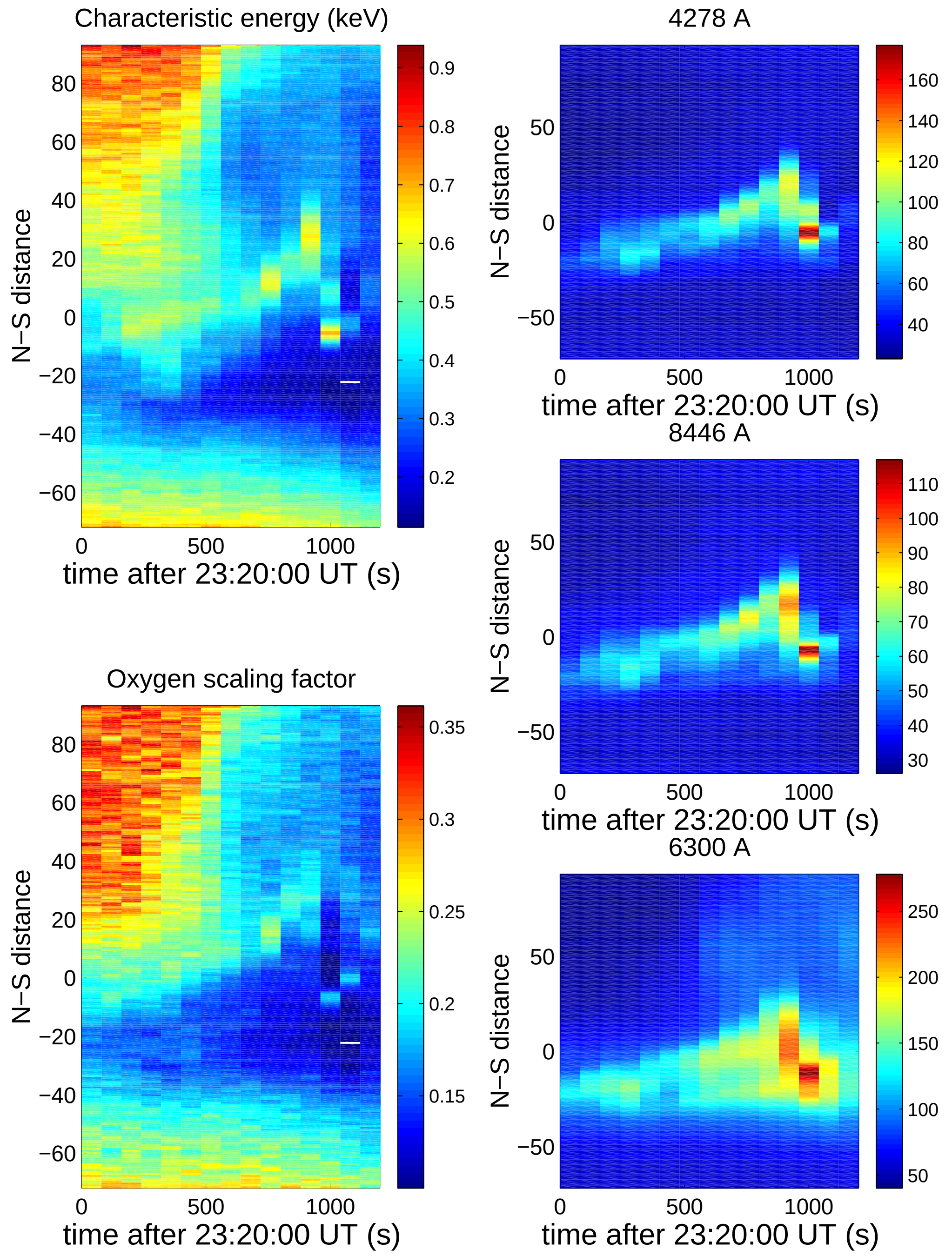

Figure 6.12: The right column displays meridional cuts through images from the Kiruna ALIS station. These "keograms" are projected to an altitude of 120 km and the axes are in km relative to Kiruna. As can be seen the arcs drift slowly northward while brightening. After 900 ± 10 s a fold sweeps eastward and the arc rapidly moves south and fades. The left columns shows characteristic energy (top) and oxygen scaling factor (bottom) as calculated from the spectroscopic ratios of I_{8446}/I_{4278} and I_{6300}/I_{4278}. [After Figure 6 in *Gustavsson et al.*, 2001b]

6.5.2 Coordinated observations with satellite and radar

During 7, 8 and 16 February 1997, ALIS, a five-channel, meridian scanning photometer [*Kaila*, 2003c], and EISCAT performed simultaneous observations during several auroral events when the FAST satellite [*Carlson*, 1992] passed in orbits with close magnetic projections to the ground-based instruments.

A preliminary collection of data from these observations was presented by *Brändström et al.* [1997a]. Later these events were also discussed by *Andersson* [2000, Chapter 4] A recent, more comprehensive study is in the preparation-phase, as briefly outlined below from an abstract by *Sergienko* [2003].

On 16 February 1997 the FAST satellite passed through the auroral oval over Northern Scandinavia one hour before a local substorm onset. The magnetic projection of the satellite orbit was within the field-of-view of ALIS. Given the high temporal resolution of FAST particle detectors combined with the sensitivity and spatial resolution of ALIS, studies of fine auroral structures became an interesting possibility. The FAST electron spectrogram displays three well-defined regions with clear borders between them. The most polarward region is a multiple inverted-V structure with an electron characteristic energy of 3–5 keV, while the middle region is characterised by homogeneous Maxwellian electron spectra with a characteristic energy of about 3.5 keV. Chaotic, weak fluctuations in the precipitating electron energy flux are also observed. The third, most equatorward region, involves two different populations of electrons. The first of them is an extension of the particles from the second region while the other population consists of energetic electrons (about 10 keV) with a perceptible periodic structure in the precipitating part of the particle flux.

The auroral data from ALIS correlate nicely with the electron spectrum peculiarities, as observed by FAST. The most poleward region of the electron spectra corresponds to the bright auroral arcs moving towards the equator, while the second part of the electron spectra conjugates with a region where the short-lived auroral rays and small patches appear chaotic against the weak diffuse background. In the equatorward parts of the auroral images, a very regular spatial luminosity structure, consisting of thin and weak auroral stripes is seen. A sample image of the auroral situation during the FAST pass at 20:10:00 UTC appears in Figure 6.14.

Calculations of the emission intensities with an auroral 5577 Å emission model using the measured electron spectra have given a good quantitative agreement between the structured high energy electrons and the auroral stripes. The stripes stretch along the geomagnetic latitudes, have a width less than 2 km, and are separated by the background luminosity by approximately the same distance. The intensities of the stripes vary in longitude and with time, but their positions do not change in latitude, at least not during the 15 minute observation by ALIS. Possible formation mechanisms for the regular striped auroral structures will be discussed in another publication in preparation [*Sergienko*, 2003]

6.5.3 Auroral vorticity

The east-west elongated auroral arc is frequently destroyed by an instability process involving the development of a series of vortex structures of various scales.

Vorticity, ζ, is the measure of rotation in a fluid, $\zeta = \nabla \times \mathbf{u}$ (where $\mathbf{u}$ is the fluid velocity). *Pudovkin et al.* [1997] published a theoretical and experimental review of data connected with vorticity in the magnetospheric plasma and on its signatures in the auroral dynamics. Early ALIS images were used in this paper to exemplify what can be learned from studying vortex structures in the aurora. Such studies can yield an abundant information on the physical state of the magnetospheric plasma as well as the processes developing in it. For example, by observing auroral forms with high temporal and spatial resolution, it is possible to determine the distribution of the electric field and field-aligned currents in the magnetosphere. The shape of auroral vortices, carry information on the nature of the Magnetohydrodynamical (MHD) instabilities responsible for the excitation of the observed turbulence. Subsequent experimental work by for example *Trondsen* [1998, and references therein] is an excellent example of research in this field. Due to technical problems affecting the maximum achievable temporal resolution (Section 3.3.4), ALIS has not been perfectly suited to continue studies in this field.

6.5.4 Studies of the ionospheric trough

An example showing that ALIS sometimes can provide usable supporting measurements, even when not operated in a scientific mode is presented by *Hedin et al.* [1999, 2000]. In this study of the main ionospheric trough, all the EISCAT radars were for the first time operated in a four-beam configuration close to the meridian plane in order to obtain a wide area of observation without the loss of temporal resolution [*Hedin et al.*, 2000]. This combined "meta-radar" has a huge fan-like observation area, of about 70°N–80°N in geographic latitude [*Hedin et al.*, 2000]. Supporting measurements were provided by the FAST satellite and ALIS. During the night of 14 March 1997, ALIS was only operated occasionally since there were no significant aurora, and the conditions at some stations were partly cloudy. The images were obtained randomly in order to check cloud conditions etc. However, some images happened to be acquired at relevant times for the trough study, displaying faint, diffuse auroral structures around the time when the trough poleward boundary passed over the field-of-view of ALIS. The position of the diffuse aurora obtained from ALIS was consistent with extrapolated data from the more direct measurements by EISCAT [*Hedin et al.*, 2000]. This observation of the trough was found to be typical as it had all the common features as compared to earlier studies. Calculations of the apparent southward motion of the trough were consistent with it having an oval shape. The trough was seen to be wider towards magnetic midnight. The paper concludes by stating that "the earlier proposed linear equations for trough motions are shown not to be valid over the latitude range in question".

6.5.5 Daytime auroral imaging

The problem of isolating atmospheric airglow and auroral emissions from scattered sunlight has been solved in a number of ground-based experiments, such as: *Noxon and Goody* [1962]; *Bens et al.* [1965]; *Barmore* [1977]; *Cocks et al.* [1980]; *Conde and Jacka* [1989]; *Conde et al.* [1992].

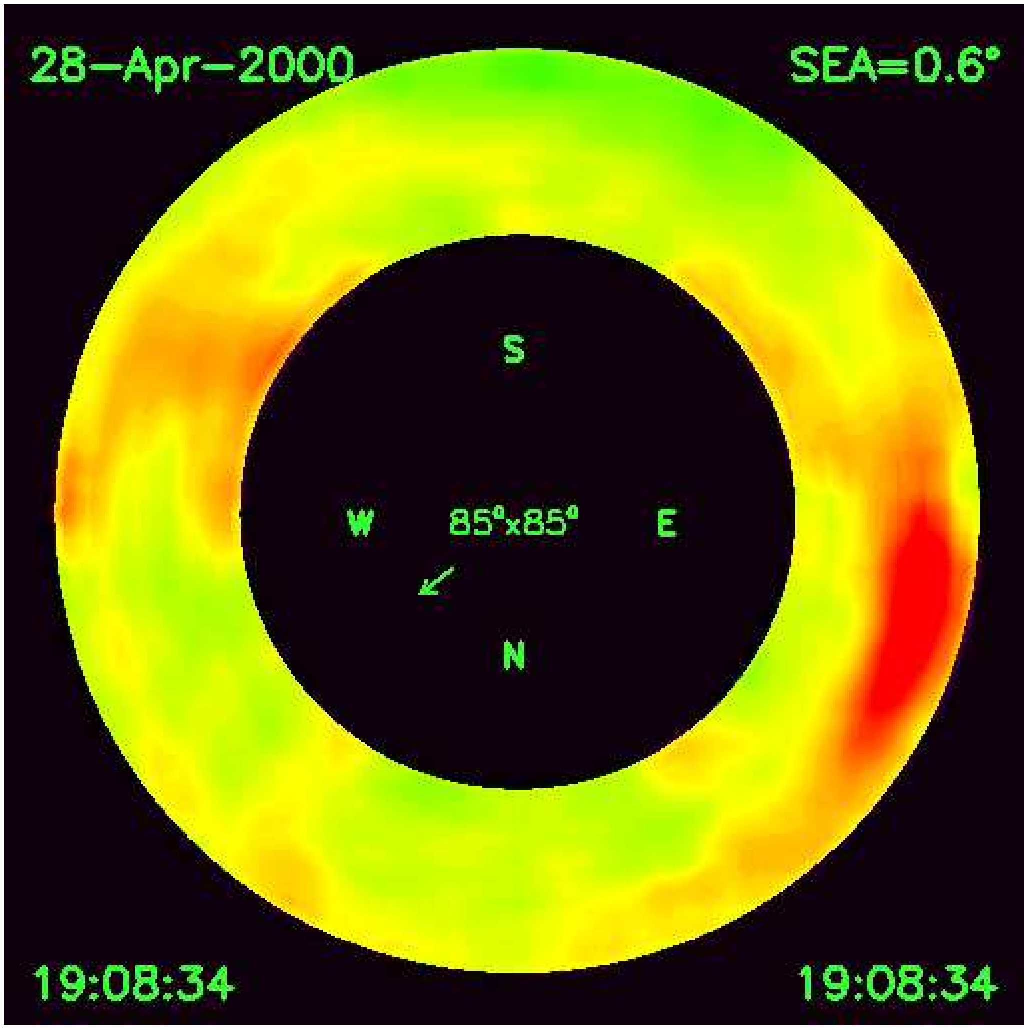

Figure 6.15: Daytime auroral image in 6300 Å acquired on April 28, 2000 at 19:08:34 UTC. The solar elevation angle was 0.6°. Bright features of the $O(^1D)$ 6300 Å emission-line are seen in north-east as well as in south-west. (Courtesy of David Rees)

distribution during three events, 9, 11 and 16 January 1997 [*Steen et al.*, 1997b]. Measurement techniques and the derivation of a composite colour image (derived from three images obtained with narrow-band interference filters for the three main auroral lines 6300 Å, 5577 Å and 4278 Å) are presented in *Steen et al.* [1999b] and *Enell et al.* [1999c]. According to *Steen et al.* [1999b] "it would, at least in principle be possible to invert the particle size distribution in the PSC by measuring the absolute colour variation, 3-D surface location, wind parameters and temperature, using an optical transport model". *Enell et al.* [1999b] states that, in certain cases, it might be possible to retrieve the particle size distribution in a section across the PSC from narrow-band images in several wavelengths. An example of time development of an altitude contour of PSC cloud-bases calculated by triangulation was also presented in this paper.

A feasibility study regarding the use of multi-station imaging systems for studies of PSC physics was presented by *Enell et al.* [2000], proposing a method to solve for particle sizes using bistatic multi-wavelength observations. As it has not yet been possible to apply this method to real measurements, numerical simulations for an ideal case (single scattering, spherical particles) work with reasonable results, even if random noise is added. Despite these positive results, a major complication is that light is scattered not only from the cloud particles, but also from the entire atmospheric column observed. A background correction, assuming a smoothly varying atmospheric background must therefore be applied. An example of a background correction by quad-tree decomposition is discussed by *Enell et al.* [1999a]. Should this method prove to be practically applicable, an important issue might be to determine the probability that actual PSC incidence gives rise to visually observable mother-of-pearl clouds, for example for interpretation of historical reports of PSC sightings. Such studies would be of interest for modellers of atmospheric chemistry and radiative transfer.

Enell et al. [2003] presented a case study of the development of visible PSCs observed by ALIS. The paper concerns automatic and manual altitude determination of PSC observations made on 9 January 1997 from two ALIS stations (Figure 6.16). It is shown that semi-automatic detection of stratospheric clouds is possible, and that short-term dynamics such as altitude variations can be tracked. The PSCs, observed during twilight, were found to be moving within a stationary sloping surface, and some evidence was provided that they were lee-wave induced. *Enell et al.* [2003] suggests that in future studies "it would be desirable to image PSC with polarisation-sensitive devices in order to characterise the scattered light with a full set of Stokes parameters at different wavelengths. This might be a way to yield information about the particle shapes as well as the nature of the multiple scattered light illuminating the PSCs." Furthermore, imaging of PSCs under different conditions, i.e. direct or scattered sunlight, moon-light, and even extinction of starlight, deserves further experimental investigations. The PSC events summarised here were published by *Enell* [2002]. This work constitutes the main reference for PSC observations with ALIS.

6.6.2 Astronomical applications — water in a Leonid?

Vi missade på Mars, kom ur dess bana
och för att undgå fältet Jupiter
vi lade oss på kurvan ICE-tolv
i Magdalenafältets yttre ring,
men mötte stora mängder leonider
och väjde vidare mot Yko-nio.
Vid fältet Sari-sexton uppgav vi försöken
att vända om.

Harry Martinsson, Aniara

Early on it was realised that ALIS might be usable for spectroscopic studies of certain astronomical objects, such as comets and meteoroids ejected from comets. Images were acquired of both the Hyakutake and Hale-Bopp comets, however none of these data-sets have yet been analysed.

Meteor showers are one of few processes taking place above the troposphere that are observable by the naked eye. This influx of extraterrestrial matter to Earth, on the order of 100 tons per day [*Love and Brownlee*, 1993] gives rise to the permanent layer of metal atoms in the 80–110 km altitude region [*Höffner and von Zahn*, 1999]. The study of these phenomena has important implications with respect to irregularities in long range radio communications, sporadic E-layers, as well as the survivability of artificial satellites, etc.

Modelling studies [*McNeil et al.*, 1995, 2001] combined with LIDAR observations [*Höffner and von Zahn*, 1999; *von Zahn et al.*, 1999] as well as observations by the GLO-1 instrument on the space-shuttle [*Gardner et al.*, 1999] have yielded significant new information on the mechanisms involved in the formation of meteor-trails and their properties.

When cosmic dust particles enters the Earth's atmosphere, heating and ablation of the material causes deposition of metals at altitudes between 80 and 110 km. As the atmospheric density increases exponentially along the particle trajectory, the ablation increases with decreasing altitude. On the other hand, due to atmospheric friction, the particle eventually reaches its terminal velocity, corresponding to a temperature lower than that needed for ablation to take place. Particle mass and particle velocity determine the altitude at which ablation takes place. Given high enough velocity (about 30 km/s) a particle ablates completely, otherwise parts of the material fall to ground unablated [*McNeil et al.*, 1998]. In essence this means that different elements are released from the meteor at different times, as demonstrated by *von Zahn et al.* [1999] using ground-based LIDARs.

ALIS could be used to study such differential ablation phenomena in meteor trails. The easiest meteoroid constituents to observe are the quite common sodium (Na) and calcium (Ca). These elements have strong emission lines at 5893 Å and 4227 Å [*Ceplecha and Rajchl*, 1963]. The evaporation is a temperature-dependent process for the different constituents. According to the differential ablation model there is a distinct altitude difference of several kilometres for the sodium and calcium deposition distributions. This should be quite easily seen with two or more ALIS stations equipped with the proper filters, especially for slow meteors. However, there are other practical problems concerning observa-

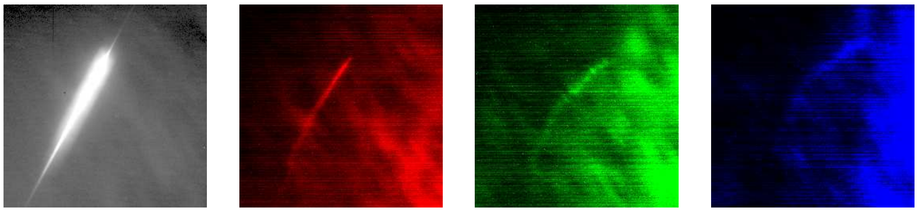

Figure 6.17: Portions of ALIS raw-data images of a meteor trail acquired on November 19, 2002. From left to right: (1) A 20 s exposure starting at 03:48:00 UTC in 4227 Å. (2) 10 s exposure at 03:48:00 UTC in 5893 Å (3) Same filter and integration time, but exposed at 03:48:30 UTC and (3) at 03:49:00 UTC. The false colours correspond to the colours in Figure 6.18

in Figure 6.17.

In Figure 6.18 projected altitude profiles for the images in Figure 6.17 appear.

Figure 6.19 shows the meteor-trail projected in altitude versus horizontal distance scale as observed through the two filters and with intensity profiles for both wavelengths. The relatively high intensity, the length of the trail as well as the short life time of the 4227 Å component were unexplained from the beginning. The 5893 Å component was seen in three consecutive images ranging over 1.5 minutes while the strong 4227 Å emission line was seen only within one 20 seconds exposure. The 4227 Å echo became visible already from 160 km altitude while the other one appeared at about 130 km altitude.

Similar optical observations of high-altitude Leonids have been reported from 1998 Leonids by *Spurny et al.* [2000] and there is still no good explanation for them. While their observations were made in white light, the rather wide passband of the filter used for the ALIS-observations might provide a hint as to a possible origin of these unusual high and bright Leonids. The 280 Å bandwidth of the 4227 Å filter corresponds to a corrected passband of about 4077 Å to 4356 Å (Equation 3.45). *Dressler et al.* [1992] report luminescence measurements of $N_2^+ + H_2O$ supra-thermal charge transfer collisions and have measured hydrogen atom Balmer series and N_2^+ emissions at high energies overlapping the passband of the ALIS observations. This observation can thus restrict the origin of these high-altitude meteors to one possible explanation. The water is still bound to some minerals in these young meteors. By reaching temperatures of above 1500 K which occurs already at about 130 km altitude in the meteor impact process, the water is suddenly released in a fast and bright process.

This explanation was found in March 2003. Therefore the value of observing water from meteoroides, cannot yet be evaluated, especially in the perspective of the present observing instrument ALIS. The analysis of this case continues and a manuscript is in preparation [*Pellinen-Wannberg et al.*, 2003].

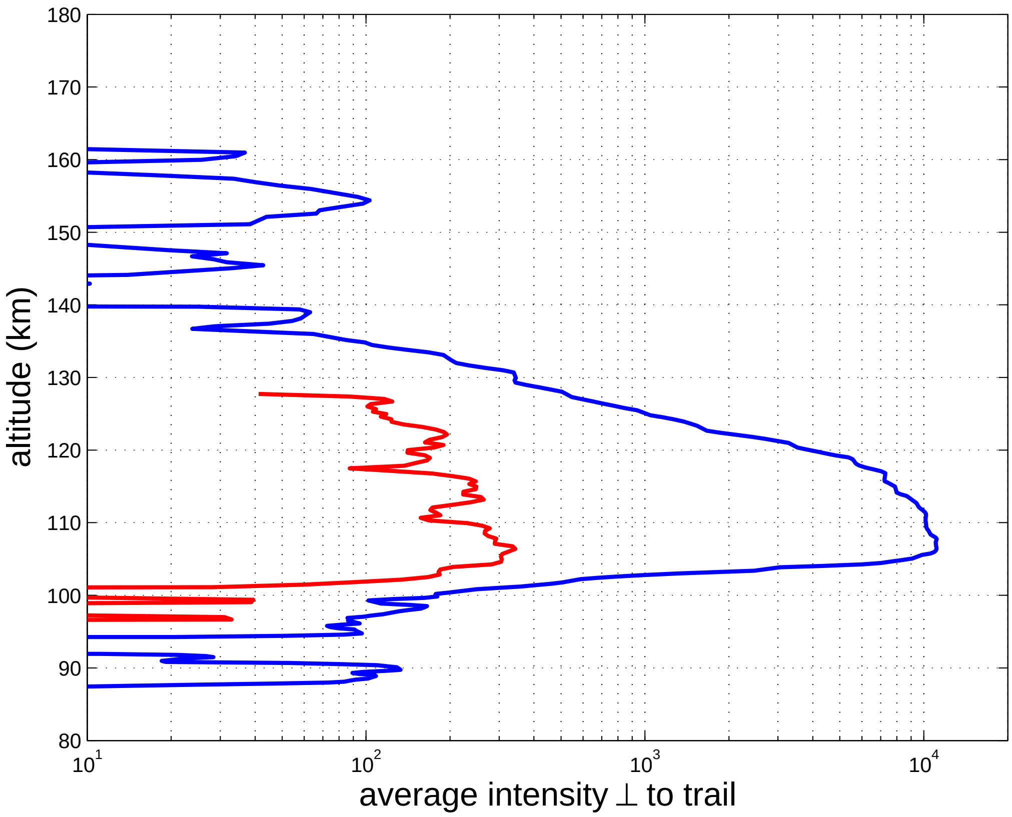

Figure 6.19: Altitude vs. average intensity perpendicular to the meteor trail in 5893 Å (red) and 4227 Å (blue). Note that the image in 4227 Å was saturated causing a cropping of the peak intensity, despite this, the altitude of the maximum intensity should be correctly estimated.

Chapter 7

Concluding remarks

> "Cur invideamus posteritati nostris laboribus frui?
> Majori laudi ducteur Seculo nostro observationes veras ad posteritatis memoriam transmisisse, quam falsas & facile refellendas hypotheses.
> Utinam priora Secula rerum naturalium experientias potius, quam varias opiniones nobis reliquissent!" *Celsius [1733]*

This report has attempted to provide a thorough documentation of the ALIS-project. Naturally, the focus of this work has been on the design, operation and calibration of the instrument, as this has been the main occupation of this author for more than one decade. Apart from ALIS, which provides imaging spectroscopic absolute-measurements of column emission rates, there has been some work carried out related to colour imaging of aurora, as is briefly described in Appendix C.

Since April 2001, only occasional campaigns related to the study of HF pump-enhanced airglow have been carried out with 1–2 stations that were operated manually. As there has recently emerged increased interest in a more extensive operation of ALIS, an outline of the required actions, as well as some ideas for the future appear in Appendix D.

Chapter 6 provided a survey of the versatile scientific applications of a multi-station low-light imaging system such as ALIS. Although many results already have been obtained, scientific questions that have arisen from this work require further analysis of existing data-sets as well as new measurements.

At present, the scientific highlights from ALIS include the first unambiguous observations of HF-pump enhanced aurora [*Brändström et al.*, 1999] and the first tomographic estimate of volume distribution of HF-pump enhanced airglow emissions [*Gustavsson et al.*, 2001a]. The task of following up some of the new scientific questions raised by these observations would alone motivate the continued operation of ALIS for many years. The recent promising observations of Leonid meteor-trails (Section 6.6.2) might also prove to be a fruitful field of future studies with ALIS.

As a spin-off effect, the combined use of the ALIS detector together with an imaging spectrometer resulted in the first daytime ground-based optical image of the aurora which was acquired on 2 May 1999 [*Rees et al.*, 2000].

It can therefore undoubtably be said that there exist strong multi-disciplinary scientific arguments for the continued operation of ALIS.

Appendix A

The Instrumentation Platform

> "It might be the warriors who get the glory, but it's the engineers who build societies" *B'Lanna Torres*

Any scientific instrumentation, regardless of whether it is manual or automatic, ground-based or space-borne, needs some basic supporting infrastructure in the form of:

- Structural support of the instrument, for example the satellite platform or a measurement structure with instrument stand.
- Environmental subsystems, keeping environmental parameters (for example temperature) within acceptable limits.
- Power supply and conditioning devices.
- Control subsystems. Anything from a simple switch to a sophisticated telecommand system.
- Monitoring subsystems. Anything from eyeball observations of an instrument reading to a complex telemetry system.
- Communication] subsystems.
- Data processing and storage subsystems.

For space-borne instruments, many of these functions are provided by the spacecraft platform. In the ground-based case many of these requirements are often more relaxed due to a less-hostile environment and the proximity to the general infrastructure of human civilisation. However if unmanned measurement stations are deployed in a sparsely-populated area with a sub-arctic climate, some requirements on the instrument platform becomes as demanding as in the space-borne case. Thus the ALIS-project required a closer examination of the basic infrastructure than most ground-based facilities in the field. The required basic infrastructure for low-light imaging stations could to a large extent also be used by other instruments (not necessarily optical), or even in entirely different contexts. Thus, these efforts to provide a housing for the ALIS stations resulted in the concept of a Ground-based Low-light Imaging Platform (GLIP) which constitutes the major part of an ALIS station.

Acronym	Explanation	See also
AIS	ALIS Imager Subsystem	Chapter 3
CCD	Charge Coupled Device	
CCH	CCD Camera Head	Section 3.3.1
CCU	Camera Control Unit	Section 3.3.2
CPC	Camera Positioning system Control unit	Section 3.6
CPS	Camera Positioning System	Section 3.6
ECU	Environmental Control Unit	Section A.2
FW	Filter Wheel	Section 3.5.1
FWC	Filter-Wheel Control Unit	Section 3.5.1
GPS	Global Positioning System	Section A.5
HU	Housekeeping Unit	Section A.4
NIPU	Near-Sensor Interface and Processing Unit	Section 2.2.2
PDU	Power Distribution Unit	Section A.3
PWR	Power subsystem, the electrical installation of the GLIP	Section A.3
SC	Station Computer, the main computer at the GLIP	Section 2.2.1

Table A.1: Explanation of acronyms in Figure A.1.

a circular hole for the dome made this design complicated and ended up heavy and difficult to keep water-proof. Based on this experience, an improved roof was designed as described below.

The optical system could be said to start with the observing window. From the optical point of view, no window at all apart from the front lens itself would be the best solution. However in this case the imager must either be fixed, or the entire instrument housing must be mounted in a positioning system. The latter solution would be difficult to realise at a reasonable cost in the harsh climate. This fact, combined with the requirement of a pointable camera, led to the compromise of a half-spherical plexi-glass dome. Such domes have long been in wide use for auroral observations. The transmittance curve of the plexi-glass is shown in Figure A.2.

The bottom part of the HALIS is an iron frame (2 m $\times$ 2 m $\times$ 0.75 m) firmly anchored in such a way that the frame rests $\approx$ 0.5 m above the ground. In this way the wind can blow under the floor, preventing snow from piling up around it, while also stopping some animals from reaching the station house (Figure A.3). This design requires a well-insulated floor.

A quadratic structure of dimensions 2 m $\times$ 2 m $\times$ 1.5 m is attached onto the iron frame by means of four bolts. The structure is made of two layers of construction plywood, separated by a 5 cm layer of thermal insulation. The door is 1 m $\times$ 1.2 m.

Inside the structure the imager-stand, consisting of four iron rods, is directly attached to the corners of the iron frame. The imager is thus not affected by vibrations in the structure caused by strong winds, etc.

The removable roof is made of plastic reinforced with glass-fibres and thermal

Figure A.3: The GLIP in Tjautjas (4) showing how snow is prevented from building up around the station.

ditions. Therefore visits to the stations should be avoided close to measurement periods.

A.2 Environmental subsystems

Two electrical heaters (2×1 kW) heat the station. Defrosting of the dome can be enhanced by enabling heating spirals in the base of the dome (200 W) and an additional heated air-stream (2 kW). The power required for heating and defrosting might seem high, but is explained by the quite high thermal losses through the thin plexi-glass dome and, also by the unpredictable weather in the region, where a heavy snowfall might be followed by clear skies and good observing conditions in less than one hour. The station is protected from overheating by triple safety systems on the heating devices as well as by a cooling fan.

All environment control devices (heaters, dome-heater, auxiliary heater, cooling-fan), as well as the illumination and electrical outlets used during service visits to the GLIP, can be remote-controlled via the housekeeping unit (Section A.4). If the housekeeping unit fails, the environment control settings fall back to safe hardware-defined values.

During the midnight sun period, the black surfaces visible through the dome are exposed to intense sunlight and might reach high temperatures (up to about 100°C has been measured.) As ALIS is not imaging during this season, the domes are replaced with opaque covers during summertime. This also keeps the need for cleaning the domes (and thus the risk of scratches) to a bare minimum, by not exposing the dome to bird-droppings and insects. For summertime operations an air-conditioning device (cooler) is required so as not to exceed the temperature specifications of the equipment inside the dome.

A.3 Power subsystems

Although the original ALIS paper [*Steen*, 1989] stated that some stations would have to generate their own power, all GLIPs deployed so far have been located close to commercial power lines.

In Sweden, a typical electricity account gives access to 3×16 A at 230/400 V AC which provides much more than sufficient electrical power (about 11 kW) for heating and powering the GLIP. Thus only the energy cost has been of concern.

The electrical installation in the GLIP has more fuses than a typical household installation in order to minimise the loss of function caused by blown fuses.

The incoming power lines pass through the mains switch, energy meter and surge protection circuits before entering the main fuse box. There is a relay box for remote-controlling the heaters, defrosters, etc. (see Section A.2) from the housekeeping unit (Section A.4). Three thermostats are used for fail-safe temperature control if the housekeeping unit should fail to control the temperature properly. There are a number of outlets (230 V/10 A) for equipment and a three-phase outlet (3×10 A 230/400 V). Figure A.5 shows some of this equipment.

The Power Distribution Unit (PDU) (Figure A.6) distributes mains power to most subsystems at the station. The PDU contains eight independent outlets

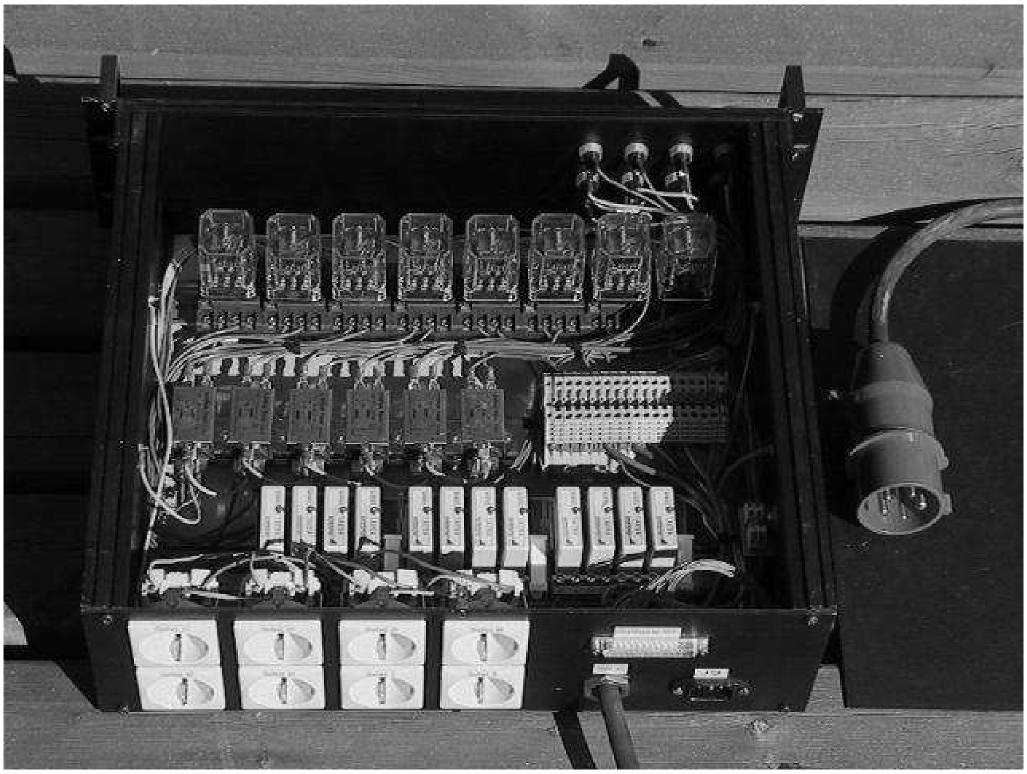

Figure A.6: Rear view of the Power Distribution Unit. The fuses are seen on the front panel (top), the relays for remote control are on the upper row, below them are surge filters and a terminal board. The bottom row contains the power sensors. The outlets are mounted on the back panel.

of networked micro-controllers, possibly with a GSM telephone as a redundant communication link.

A.5 Timing

Timing and synchronisation of measurements at the different stations are critical for essentially all scientific measurements. The timing-system must be decentralised since the GLIPs are not necessarily online all the time during a measurement. Several possibilities were considered, such as frequency references at each station, the Omega navigation system, the Global Positioning System (GPS) etc. Since GPS provided superior accuracy and reliability at an affordable cost, this system was selected for the GLIPs (Figure A.8). The first GPS receiver used in ALIS

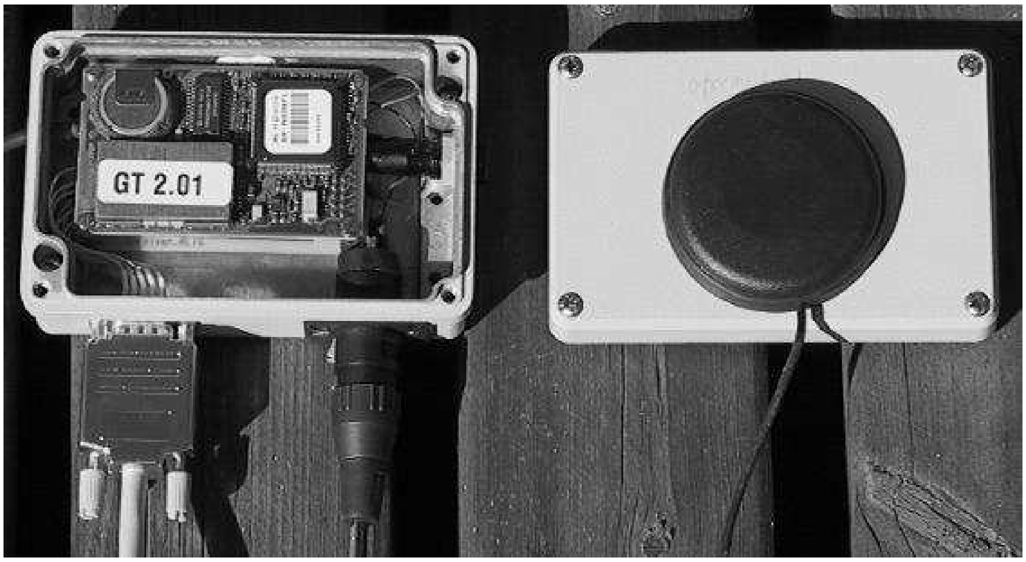

Figure A.8: The GPS receiver currently used in ALIS. Left: Receiver board with connectors for RS-232 and power (12 V DC). Right: GPS antenna.

was contained on an ISA-board that was plugged into the station computer. Later GPS units were external, communicating over RS-232. Both versions had a 1 Pulse Per Second (PPS) TTL-level output for precision timing. Early on the GPS devices had their own software, but they are now controlled by the Internet standard network time protocol (ntp) [*Mills*, 1992]. The ntp daemon (ntpd) running at each station interfaces directly to the output of the GPS receiver, as well as to other time-servers on the Internet, synchronising the PC clock to better than 1 ms precision against UTC. A software Phase-Locked Loop (PLL) implemented in the ntpd software allows timing to be preserved with good accuracy during periods when the timing sources are lost. While presently not needed, it is possible to further enhance timing accuracy to better than $1 \mu s$ by using the 1 PPS signal from the GPS-receiver, giving almost atomic-clock precision to the stations. The GPS-receiver also provides information about the geographical position of the station.

manned during the observations, no housekeeping unit, power distribution unit, communications, etc. were required. However if an unmanned, remote-controlled configuration had been desired, this equipment could easily have been installed. A mobile generator was also included, so the station was independent of mains power. This station operated with good results in the years 1999–2003.

Appendix B

Data for the ALIS imagers

The following tables list a selection of items from the vendor-provided CCD test reports, as well as some measurements provided by the camera manufacturer. (Table B.5 is identical to Table 3.2). See Chapter 3 for more information.

Parameter	Symbol	ccdcam1	Unit	Notes
Read noise	$\langle n_{e_r^-} \rangle$	9.74	e^-_{RMS}	a) b) 8@13$\mu s/pixel$
Dark current	$\overline{n}_{e_d^-}$	853	$e^-_{RMS}\ s^{-1}$	at 20°C.
Full well	$N_{e^-_{max}}$	272	ke^-	
Quantum efficiency	Q_E	≥ 35	%	4000 Å
Quantum efficiency	Q_E	84.96	%	5500 Å, at $-10°C$.
Quantum efficiency	Q_E	≥ 60	%	7000 Å

Table B.1: Some parameters for the CCD in ALIS-imager ccdcam1 (Tk1024AB, serial No. 1541BR0104) as measured by the CCD-manufacturer. All values at $-90°C$ unless otherwise noted. Notes: a) quadrant with highest value. b) same parameter, as measured by camera manufacturer.

Parameter	Symbol	ccdcam2	Unit	Notes
Read noise	$\langle n_{e_r^-} \rangle$	7.65	e^-_{RMS}	a) b) 7.9@10.5$\mu s/pixel$
Dark current	$\overline{n}_{e_d^-}$	12.28	$e^-_{RMS}\ s^{-1}$	at $-15°C$
Full well	$n_{e^-_{max}}$	281	ke^-	b) 230ke^- c)
Quantum efficiency	Q_E	82.3	%	4000 Å
Quantum efficiency	Q_E	88.4	%	5500 Å, at $-15°C$
Quantum efficiency	Q_E	89.4	%	7000 Å
Quantum efficiency	Q_E	48.7	%	9000 Å

Table B.2: Some parameters for the CCD in ALIS-imager ccdcam2 (Tk1024A, serial No. 1743BR10-03R) as measured by the CCD-manufacturer. All values at $-45°C$ unless otherwise noted. Notes: a) quadrant with highest value. b) same parameter, as measured by camera manufacturer. c) quadrant A -3% linearity.

Parameter	Symbol	`ccdcam6`	Unit	Notes
Read noise	$\langle n_{e_r^-} \rangle$	< 6	e^-_{RMS}	a)
Dark current	$\overline{n}_{e_d^-}$	< 3.3	$e^-_{RMS}\ s^{-1}$	a) at $-31.0°$
Full well	$n_{e^-_{max}}$	370	ke^-	a)
Quantum efficiency	Q_E	90	%	5500 Å a) b)

Table B.6: Some parameters for the CCD in ALIS-imager `ccdcam6` (SI003A/T-4 serial No. 6403GCR14-B2) as measured by the *camera* manufacturer. a) No CCD test report, measured by camera manufacturer. b) No Q_E measured, assuming a lower value (Figure 3.1) [author's note]

Appendix C

Related work

"Hier stehe ich und kann nicht anders." *Martin Luther*

When ALIS began operating, an "aiming-system" appeared as desirable. This was planned to consist of a simpler white-light video-rate camera intended mainly to assist the ALIS operator. Two old low-light TV-cameras were used for this purpose at the ALIS operations centre. However it was always desired to have real-time digital colour images available, even if ALIS was operated from a remote place. For many years this appeared as impossible or too expensive. Around 1999 commercially-available digital still- and video colour cameras began to reach the required sensitivity. This initiated a study, mainly intended to replace the present all-sky imager in Kiruna, but also with interesting implications for ALIS. This appendix briefly describes these efforts.

It is, however, of great importance to note that the imagers discussed here are in no way comparable to the ALIS imagers. A colour CCD camera can never be used for absolute measurements of column emission rates as it contains its own colour filters. On the other hand, the colour cameras can be of great value for providing overview information of the morphology and dynamics. Also, colour images and movies of auroral phenomena tend to be much more appealing for public outreach purposes, compared to the more scientifically useful, but "unexciting" monochromatic images.

C.1 A new digital all-sky camera

An all-sky camera has been operating in Kiruna since the International Geophysical Year in 1957 [*Stoffregen*, 1962]. In 1977 the camera was replaced with a new more automated camera [*Hyppönen et al.*, 1974]. This camera is still in operation, but a replacement was strongly desired as the data storage medium is 16 mm colour film, a medium soon to become obsolete, as well as expensive to develop and copy and difficult to digitise, and thus complicated to make available and distribute to the scientific community and general public. In Finland all 16 mm all-sky cameras have already been replaced by advanced new cameras with filter-wheels and narrow-band interference filters similar to ALIS, but with all-sky optics and intensified CCDs [*Syrjäsuo*, 2001]. Furthermore, a non-intensified spectroscopic all-sky imager is described by *Ejiri et al.* [1999] (see also Section 1.1). Here an

Figure C.2: Example image from the new all-sky camera prototype 2001-03-19 19:10 UTC. A digital version of this image can be downloaded from: `http://www.irf.se/~urban/28am`

suggested that it should be replaced by a newer model (Fuji FinePix S2Pro). This model has an IEEE-1394 interface (aka. “Firewire”) instead of USB. As the new all-sky cameras are intended to operate continuously at least during the hours of darkness, exposing on average one image per minute, a major concern for both cameras tested is the long-term mechanical reliability of the shutter. So far no major problems have been encountered after a couple of months of operation. However it is highly desirable to have a spare camera in order to avoid data-gaps during maintenance operations. This work is to a large extent carried out by Arne Moström (programming) and Torbjörn Lövgren (photographer). For further information see `http://www.irf.se/data.html`

C.2 Colour video recordings of aurora

A new generation of semi-professional digital video (DV) camcorders have proved sensitive enough for almost real-time recordings (3–4 frames/s) of auroral phenomena [*Yamauchi*, 1999; *Brändström et al.*, 2001b]. One such camera (Sony DCR VX-2000E PAL) was procured by the author. The sensitivity for auroral scenes at 3 exposures/s was found to be of the same order as the unaided human eye (i.e. roughly 1 kR at 5577 Å). Several hours of auroral footage were recorded and the image quality is acceptable for TV-broadcasting and auroral visualisation for the general public (for example Swedish Television has broadcasted such material on two occasions). It has proved possible to record weak diffuse, pulsating

Figure C.3: Sample frame from a auroral video obtained with a commercial mini-DV camcorder displaying green, red and blue aurora. A meteor-trail is seen in the lower middle part of the image. A digital version of this image can be downloaded from: `http://www.irf.se/~urban/28am`

Appendix D

Continued operations with ALIS

> "Determinismens huvudskäl är kausalitetslagen.
> Indeterminismens huvudskäl är ansvarskänslan." *Dag Hammarskjöld*

The design work on ALIS started in 1990. Thus most of the technology of the system is about ten years old and consequently the need for upgrades and technical maintenance has increased. Unfortunately, this has not been possible, mainly because of budgetary constraints. As the measurement season of 2000/2001 ended, ALIS was put into hibernation, mainly to give the author a chance to finish this report, but also due to a shortage of staff and funding. Since then, 1–2 ALIS imagers have occasionally been operated manually, primarily for studies of HF pump-enhanced airglow. In the fall of 2001 funding covering operation and some technical maintenance was received for the period 2002–2004.

From a scientific point of view, a continued and enhanced operation of ALIS can be motivated solely on the new questions raised by the observations of HF pump-enhanced airglow (Section 6.4). The recent promising observations of meteor trails (Section 6.6.2), as well as continued auroral studies (Section 6.5) also constitute strong arguments for a prolonged operation of ALIS.

This short appendix outlines how to assess the present status of ALIS in order to make a plan for bringing ALIS back into full operation. It is assumed that the present funding situation is stable for 2003/2004, and that performing new measurements, as well as analysing existing data, will enable a sustained funding at the present level, or higher. The most limited resource for ALIS has always been the staff. Here it is assumed that a stable group of at least 3–4 physicists, with a thorough scientific and technical knowledge of ALIS, is available to at least 50% for engineering and programming tasks, as well as general maintenance. (Ideally ALIS should have access to an electronics engineer and one programmer. However given the present situation this is not considered economically feasible.)

D.1 Assessing the present status of ALIS

Finding out the present status of ALIS is the inevitable first step in making a plan. As ALIS was closed, the status of the system was reported in [*Brändström*, DVD-R (Recordable DVD) to keep down the number of discs. (see also Section 2.2.5)

Operating systems: The operating systems for the control-centre computers must be upgraded to newer versions due to security and compatibility issues. At the stations it is preferable to keep the present operating systems as long as the old station computers are in use.

The control centre: At least two computers need to be replaced at the ALIS control centre since they are past their technical lifetime. At the operations centre no immediate replacements are required. Some computer screens should be replaced to improve working conditions.

Environmental subsystems: These systems should be usable for many more years (Section A.2).

Power subsystems: All stations should be equipped with UPS units for powering the instrumentation. Some stations lack good surge protection devices. A safety check should be carried out for all power subsystems, especially the PDUs.

Housekeeping units: Although obsolete, all housekeeping units (Section A.4) should be usable for many more years. Replacement will be required eventually as the current housekeeping units are only capable of handling dial-up lines. New housekeeping units can easily be built in the same way as the NIPU replacement micro-controllers.

GPS units: No changes anticipated, all timing units (Section A.5) should be working.

The mobile station: The van (mobile station, see Section A.8) is critical for some scientific objectives.

Software: Most ALIS software (Chapter 5) should be working. At the stations, some bug-fixes and upgrades of `mima` and `aniara` would be appropriate. Somewhat larger programming efforts are required in order to get a web-based and user-friendly new user-interface for ALIS. This could be carried out as a student project, but is not crucial to the operation of ALIS in the near future (one year). The NIPU replacement, as well as some other hardware upgrades, will require new control software as well as modifications to existing programs.

After performing these upgrades the block-diagram of a GLIP will change slightly, as indicated in the upgraded block-diagram of Figure D.1.

D.1.1 The ALIS imagers

Since ALIS closed down in 2001, two imagers with supporting systems have participated in observations with good results. All ALIS imagers were taken to Oulu in 2002 for the calibration workshop (see Section 4.2). Although the CCUs are becoming obsolete, the CCDs and camera heads are still state-of-the-art in the field. Therefore prolonging their operational lifetime as long as possible is strongly to be desired. Procuring new imagers is not possible within the current budgetary limits. Two imagers (`ccdcam1,6`) are immediately usable for observations. Three imagers (`ccdcam3,4,5`) developed reliability problems during the Oulu visit in 2002. These problems are most likely solvable with moderate efforts. One imager (`ccdcam2`) had problems with ice-formation on the CCD, probably due to a breach in the hermetically-sealed CCD compartment. Instructions has been received from the manufacturer how to resolve this. However this is a delicate procedure involving a risk of damaging the CCD. Preferably this procedure should be carried out by the camera manufacturer.

A thorough testing of all imagers is required before being able to assess their status. Yet it appears feasible to have 4–6 imagers operational within about six months. On a longer time-scale (about five years) the CCUs at least must somehow be replaced, but this requires additional funding. The remaining subsystems related to the imager are discussed below:

Calibration: A cleaning of the optical systems, as well as focusing and calibration of each imager, is important to maintain and improve the data quality. This is estimated to take 2–3 nights per imager.

Interference filters: The change of filter transmittance with time due to aging is at present unknown, as is the filter transmittance as a function of pixel coordinates (Section 4.2.3). Measuring the transmittance could be made locally, but the monochromator system [*Vaattovaara and Enback*, 1993] must be modernised. For example, this can be done as a student final-year project.

Filter-wheels: One filter wheel (on `ccdcam5`) is experiencing mechanical problems. The remaining filter-wheels are operational, but all angular encoders are likely to fail in the near future (due to an aging laser-diode) Therefore these must be replaced, preferably as the NIPUs are replaced. As the filter-wheels are essential for successful measurements, this is a high-priority task.

Camera positioning system: All CPS units are subject to the same angular encoder problems described above. However replacing these angular encoders is not nearly as high priority as the filter-wheels. It is possible to lock some CPS units in a fixed observing position until new angular encoders can be installed. Furthermore as the filter-wheels are upgraded, spare angular encoders for the CPS are released. A mechanical maintenance and adjustment of all units are also strongly recommended.

D.2 Summary

In the near future (1–2 years) it is of highest priority to enable measurements with as many stations as possible, given the present budget and staff. This implies no major upgrades, and only performing a selection of the most critical maintenance tasks as discussed above. To increase the time for analysis and publication of data,

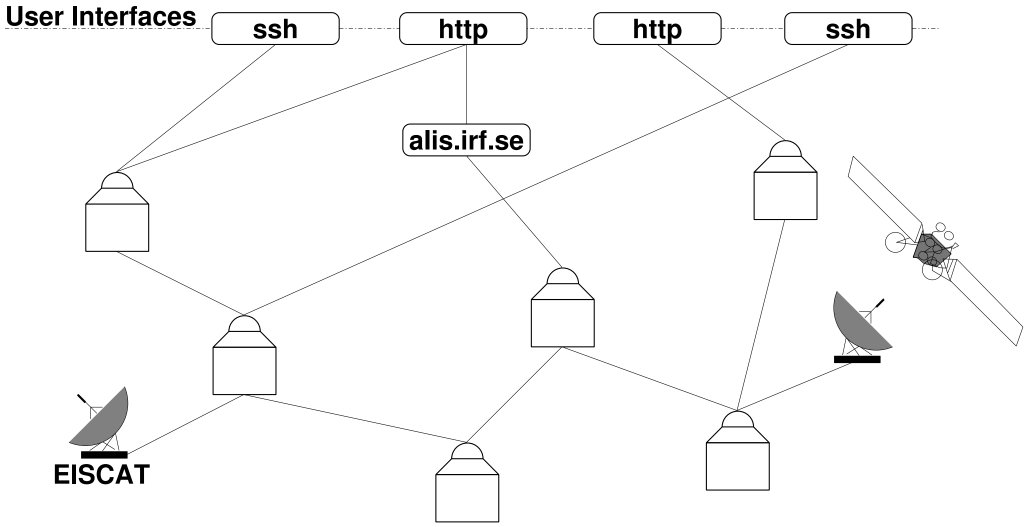

Figure D.3: A decentralised future ALIS: As the ALIS stations will most likely gain permanent Internet access in the future, the functions of the control centre will be decentralised to the stations. Connections to other stations, as well as other instruments (exemplified by EISCAT and a satellite) can then also be initiated as required.

tion of instruments could be quickly enrolled into simultaneous observations of a particular phenomena.

In the future perhaps scientific instruments will be placed on a standardised General Instrument Platform (GIP), which can be either ground-based, airborne, or placed on a spacecraft. Networks of such GIPs could then be spontaneously created, configured and controlled for specific scientific studies. Developing such ideas might enhance the availability and usage of the existing plethora of scientific instrumentation, in the same way as the world-wide-web enhanced simplified Internet usage.

Bibliography

Adeishvili, T. G., A. V. Gurevich, S. B. Lyakhov, G. G. Managadze, G. M. Milikh, and I. S. Shlyuger, Ionospheric emisson caused by an intense radio wave, *Sov. J. Plasma Phys.*, *4*, 721–726, 1978.

Alpatov, V., Å. Steen, and U. Brändström, Fractal analysis of the ALIS auroral images, 1996a, (draft manuscript).

Alpatov, V. A., A. A. Matveev, C.-F. Enell, B. Gustavsson, and U. Brändström, Investigations of the polar atmosphere with the use of dynamical characteristics of the processes and self-organizing neural networks on ground-based multi-position optical observations, in *Proceedings of the EGS General Assembly*, 2000.

Alpatov, V. V., U. Brändström, Å. Steen, and B. Gustavsson, Fractal analysis of auroral images from ALIS, (poster presentation), 1996b, The third international substorm conference (ICS3), Paris, France.

Andersson, L., Acceleration processes in auroral region, Ph.D. thesis, Swedish Institute of Space Physics, 2000, (IRF Scientific Report 270 ISBN: 91-7191-914-7).

Anger, C. D., S. K. Babey, A. L. Broadfoot, R. G. Brown, L. L. Cogger, R. Gattinger, J. W. Haslett, R. A. King, D. J. McEwen, J. S. Murphree, E. H. Richardson, B. R. Sandel, K. Smith, and A. Vallance Jones, An ultraviolet auroral imager for the Viking spacecraft, *Geophys. Res. Lett.*, *14*, 387–390, 1987.

Ångström, A. J., *Recherches sur le Spectre Solaire*, W. Schultz, Uppsala, 1868.

Ångström, A. J., Spectrum des Nordlichts, *Pogg. Ann.*, *137*, 161–163, 1869.

Aristotle, *Meteorologica*, vol. I, chap. 5, (ancient text), ca. 340 B.C.

Aruliah, A. L., A. D. Farmer, D. Rees, and U. Brändström, The seasonal behaviour of high-latitude thermospheric winds and ion velocities observed over one solar cycle, *J. Geophys. Res.*, *101*, 15,701–15,711, 1996.

Aso, T., M. A. Hashimoto, T. Ono, and M. Ejiri, On the analysis of aurora stereo observations, *J. Geomag. Geoelectr.*, *42*, 579–595, 1990.

Birkeland, K., *The Norwegian aurora polaris expedition 1902–1903. Volume I On the cause of magnetic storms and the origin of terrestrial magnetism. First section*, vol. 1, A. W. Brøggers bogtryckeri, Christiania (Oslo), Norway, 1908.

Birkeland, K., *The Norwegian aurora polaris expedition 1902–1903. Volume I On the cause of magnetic storms and the origin of terrestrial magnetism. Second section*, vol. 1, A. W. Brøggers bogtryckeri, Christiania (Oslo), Norway, 1913.

Brandy, J. H., and J. E. Hill, Rapid determination of auroral heights, *Canad. J. Phys.*, *42*, 1813–1819, 1964.

Brown, N. B., T. N. Davis, T. J. Hallinan, and H. C. Stenbaek-Nielsen, Altitude of pulsating aurora determined by a new instrumental technique, *Geophys. Res. Lett.*, *3*, 403–404, 1976.

Brändström, B. U. E., T. B. Leyser, Å. Steen, M. T. Rietveld, B. Gustavsson, T. Aso, and M. Ejiri, Unambigous evidence of HF pump-enhanced airglow, *Geophys. Res. Lett.*, *26*, 3561–3564, 1999.

Brändström, U., Reduction of CCD images from ALIS, ALIS internal note, 2000, (Intended for CCD-course).

Brändström, U., ALIS, a brief technical summary of the current situation, ALIS internal note, 2001a.

Brändström, U., ALIS stängt för säsongen, email to alis_folk@irf.se 2001-04-11, 2001b, (in Swedish).

Brändström, U., and Å. Steen, Report on the ALIS project, in *Proc. 19th Annual European meeting on atmospheric studies by optical methods, Kiruna, Sweden*, edited by Å. Steen, pp. 310–321, Swedish Institute of Space Physics, Kiruna, Sweden, 1992, IRF Scientific Report 209.

Brändström, U., Å. Steen, B. Gustavsson, L. Andersson, I. Häggström, A. Westman, A. Pellinen-Wannberg, T. Aso, K. Kaila, C. W. Carlson, D. Klumpar, and C. Catell, Preliminary results from coordinated measurements by FAST and groundbased optical and radar facilities, in Northern Scandinavia, during active auroral conditions, in *Proceedings of the 24th annual European Meeting on Atmospheric Studies by Optical Methods*, pp. 41–46, Sentraltrykkeriet A/S Bodø, 1997a, ISBN 82-994583-0-7.

Brändström, U., Å. Steen, B. Gustavsson, D. Rees, and M. J. Harris, Preliminary results from a comparision of observations of thermospheric neutral wind patterns and auroral emissions, in *Proceedings of the 24th annual European Meeting on Atmospheric Studies by Optical Methods*, pp. 37–40, Sentraltrykkeriet A/S Bodø, 1997b, ISBN 82-994583-0-7.

Brändström, U., Å. Steen, P. Rydesäter, B. Gustavsson, and T. Aso, ALIS, a multi station imaging facility with possibilities of future VI applications, in *Ninth workshop on Virtual Intelligence / Dynamic neural networks*, edited by

Crutzen, P. J., and F. Arnold, Nitric acid cloud formation in the cold Antarctic stratosphere: a major cause for the springtime "ozone hole", *Nature*, *324*, 651–655, 1986.

Csorba, I., *Image Tubes*, Howard Sams, Indianapolis, Indiana, 1985.

Davis, T. N., and G. T. Hicks, Television cinemaphotography of Auroras and preliminary measurements of auroral velocities, *J. Geophys. Res.*, *69*, 1931, 1964.

de Mairan, J. J. D., *Traité Physique et Historique de l'Aurore Boréale*, Imprimerie Royale, Paris, 1733, (2ns ed., 1754).

Delbouille, L. G., L. G. Roland, and L. Neven, *Photometric atlas of the solar spectrum from 3000 to 10000 Å*, Institute d'Astrophysique de l'Universite de Liege, Cointe-Ougre, Belgium, 1973.

Djuth, F. T., P. A. Bernhardt, C. A. Tepley, J. A. Gardner, M. C. Keley, A. L. Broadfoot, L. M. Kagan, M. P. Sulzer, J. H. Elder, C. Selcher, B. Isham, C. Brown, and H. C. Carlson, Large airglow enhancements produced via wave-plasma interactions in sporadic *E*, *Geophys. Res. Lett.*, *26*, 1557–1560, 1999.

Dressler, R. A., J. A. Gardener, R. H. Salter, and E. Murad, Luminescence measurements of $Ar^+ + H_2O$ and $N_2^+ + H_2O$ suprathermal charge transfer collisions: Product state distribution from $H_2O^+\tilde{A}^2A_1{-}\tilde{X}^2B_1$ analysis, *J. Chem. Phys.*, *96*, 1062–1076, 1992.

Eather, R. H., *Majestic lights the aurora in science, history and the arts*, AGU (American Geophysical Union), Washington D.C., 1980, ISBN: 0-87590-215-4.

Eather, R. H., Low light level imaging design, *Tech. rep.*, Air Force Geophysics laboratory, USAF, Hanscom AFB, Massachusetts USA, 1982, AFGL-TR-82-0308.

Eide, Å. J., V. Becanovic, U. Brändström, C. Holmström, M. Larsson, I. M. Lillesand, T. Lindblad, C. S. Lindsey, Å. Steen, and J. Waldemark, Pulse coupled neural network pre-processing of aurora images, in *AI Applications in Solar Terrestial Physics*, vol. WPP-148, pp. 201–205, European Space Agency, 1997.

Ejiri, M., M. Okada, M. Tsutsumi, M. Taguchi, and S. Okano, All sky imager observation of aurora and airglow at south pole station : Initial results, in *Proceedings of the 25th annual European Meeting on Atmospheric Studies by Optical Methods, Granada, Spain*, pp. 54–57, 1998.

Ejiri, M., T. Aso, M. Okada, M. Tsutsumi, M. Taguchi, N. Sato, and S. Okano, Japanese research project on Arctic and Antarctic observations of the middle atmosphere, *Adv. Space Res.*, *24*, 1689–1692, 1999.

Elvey, C. T., and W. Stoffregen, Auroral photography by all-sky camera, *Ann. IGY.*, *5*, 117–151, 1957.

Gurevich, A. V., and G. M. Milikh, Artificial airglow due to modifications of the ionosphere by powerful radio waves, *J. Geophys. Res.*, *102*, 389–394, 1997.

Gurevich, A. V., Y. S. Dimant, G. M. Milikh, and V. V. Va'skov, Multiple acceleration of electrons in the regions of high power radio-wave reflection in the ionosphere, *J. Atmos. Terr. Phys.*, *47*, 1057–1070, 1985.

Gustavsson, B., A study of feasible tomographic inversion techniques for ALIS, *Tech. Rep. 039*, Swedish Institute of Space Physics, Kiruna, Sweden, 1992, ISSN 0284-1738.

Gustavsson, B., Private communication, 1997.

Gustavsson, B., Tomographic inversion for ALIS noise and resolution, *J. Geophys. Res.*, *103*, 26,621–26,632, 1998.

Gustavsson, B., Three Dimensional Imaging of Aurora and Airglow,, Ph.D. thesis, Swedish Institute of Space Physics, Kiruna, Sweden, 2000, (IRF Scientific Report 267), ISBN: 91-7191-878-7.

Gustavsson, B., Private communication, 2003.

Gustavsson, B., T. Sergienko, M. T. Rietveld, F. Honary, Å. Steen, B. U. E. Brändström, T. B. Leyser, A. L. Aruliah, T. Aso, and M. Ejiri, First tomographic estimate of volume distribution of enhanced airglow emission caused by HF pumping, *J. Geophys. Res.*, *106*, 29,105–29,123, 2001a.

Gustavsson, B., Å. Steen, T. Sergienko, and B. U. E. Brändström, Estimate of auroral electron spectra, the power of ground-based multi-station optical measurements, *Phys. Chem. Earth*, *26*, 189–194, 2001b.

Gustavsson, B., B. U. E. Brändström, Å. Steen, T. Sergienko, T. B. Leyser, M. T. Rietveld, T. Aso, and M. Ejiri, Nearly simultaneous images of HF-pump enhanced airglow at 6300 Å and 5577 Å, *Geophys. Res. Lett.*, *29*, 2003, paper No. 10.1029/2002GL015350.

Hallinan, T. J., H. C. Stenbaek-Nielsen, and C. S. Deehr, Enhanced aurora, *J. Geophys. Res.*, *90*, 8461–8475, 1985.

Hammarskjöld, D., *Vägmärken*, Albert Bonniers Förlag AB, 1963, (In Swedish, reprinted 1999 ISBN:9100571121).

Hammarskjöld, D., *Markings*, Knopf, New York, 1964, (transl. by Leif Sjöberg and W. H. Auden, ISBN: 039443532X).

Haslett, J. C., and L. R. Megill, A model of the enhanced airglow excited by RF-radiation, *Radio Sci.*, *9*, 1005–1019, 1974.

Hecht, J. H., A. B. Christensen, D. J. Strickland, and R. R. Meier, Deducing composition and incident electron spectra from ground-based auroral optical measurements: Variation in oxygen density, *J. Geophys. Res.*, *94*, 13,553–13,563, 1989.

Johansson, H., Station software for ALIS, *IRF Tech. Report 036*, Swedish Institute of Space Physics, 1991, ISSN 0284-1738.

Jones, A. R. V., R. L. Gattinger, F. Creutzberg, F. R. Harris, A. G. McNamara, A. W. Yau, E. J. Llewellyn, D. Lummerzheim, M. H. Rees, I. C. McDade, and J. Margot, The ARIES auroral modelling campaign: Characterization and modelling of an evening auroral arc observed from a rocket and a ground-based line of meridian scanners, *Planet Space Sci.*, *39*, 1677–1705, 1991.

Jones, A. V., *Aurora*, vol. 9 of *Geophysics and astrophysics monographs*, D. Reidel Publishing Company, 1974, ISBN: 90-277-0272-1.

Kaila, K., Optical instrumentation of Oulu, `http://spaceweb.oulu.fi/projects/optical` and Private communication, 2003a.

Kaila, K., Private communication, 2003b, data analysis and publication in progress.

Kaila, K., Private communication, 2003c, (See also `http://spaceweb.oulu.fi/projects/optical`).

Kaila, K. U., An iterative method for calculating the altitudes and positions of auroras along the arc, *Planet. Space Sci.*, *35*, 245–258, 1987.

Kaila, K. U., and H. J. Holma, Absolute calibration of photometer, *Phys. Chem. Earth*, *B(25)*, 467–470, 2000.

Keo Consultants, Kiruna telecentric lens systems, 1994, vendor-provided documentation.

Keo Consultants, Telecentric lens for Kyoto university, 1997, vendor-provided documentation.

Kinser, J. M., and T. Lindblad, Detection of microcalcifications by cortical stimulation, in *Proceedings EANN'97 Neural networks in engineering systems*, edited by A. Bulsari and S. Kallio, pp. 203–206, 1997, ISBN: 952908667-9.

Kosch, M. J., T. Rietveld, M., S. Å, and T. Hagfors, HF-Induced Airglow: Double Patches, *Phys. Chem. Earth*, *25*, 475–581, 2000a.

Kosch, M. J., T. Rietveld, M., T. Hagfors, and T. B. Leyser, High-latitude HF-induced airglow displaced equatorward of the pump beam, *Geophys. Res. Lett.*, *27*, 2817–2820, 2000b.

Kosch, M. J., M. T. Rietveld, A. J. Kavanagh, C. Davis, T. Yeoman, F. Honary, and T. Hagfors, High-latitude pump-induced optical emissions for frequencies close to th third electron gyro-harmonic, *Geophys. Res. Lett.*, *29*, 27–1–274, 2002a.

Kosch, M. J., M. T. Rietveld, T. Yeoman, K. Cierpka, and T. Hagfors, The high-latitude artificial aurora of 21 February 1999: An analysis, *Adv. Polar Upper Atmos. Res.*, 2002b, (in press).

McNaught, R. H., and D. J. Asher, Variation of Leonid maximum times with location of observer, *Meteorit. Planet. Sci.*, *34*, 975–978, 1999.

McNeil, W. J., E. Murad, and S. T. Lai, Comprehensive model for the atmospheric sodium layer, *J. Geophys. Res.*, *100*, 16,847–16,855, 1995.

McNeil, W. J., S. T. Lai, and E. Murad, Models of thermospheric sodium, calcium and magnesium at the magnetic equator, *Adv. Space Res.*, *21*, 863–866, 1998.

McNeil, W. J., R. A. Dressler, and E. Murad, Impact of a major meteor storm on earth's ionosphere: A modeling study, *J. Geophys. Res.*, *106*, 10,447–10,465, 2001.

McWhirter, I., Imaging photon detectors and their use with single and multiple fabry-perot etalon systems for atmospheric wind measurements, Ph.D. thesis, University College London, London, 1993.

Meier, R. R., D. J. Strickland, J. H. Hecht, and A. B. Christensen, Deducing composition and incident electron spectra from ground-based auroral optical measurements: a study of auroral red line processes, *J. Geophys. Res.*, *94*, 13,541–13,552, 1989.

Mills, D. L., Network time protocol (version 3) specification, implementation and analysis, Request for Comments: 1305, 1992, ftp://ftp.rfc-editor.org/in-notes/rfc1305.txt.

Mohn, H., Perlemorskyer, in *Christiania Videnskabs-Selskabs Forhandlinger*, vol. 2, A. W. Brøggers bogtryckeri, Christiania (Oslo), Norway, 1893.

Na, H., and H. Lee, Orthogonal decomposition technique for ionospheric tomography, *Int. J. Imaging Syst. Technol.*, *3*, 354–365, 1991.

NASA, *Definition of the Flexible Image Transport System (FITS)*, NASA/Science Office of Standards and Technology, Code 633.2, NASA Goddard Space Flight Center, Greenbelt MD, USA, 1999, nOST 100-2.0, http://fits.gsfc.nasa.gov/fits_documentation.html.

Nilsson, L., OPERA operations program for ALIS version 1.0, *Internal Note 024*, Swedish Institute of Space Physics, Kiruna, Sweden, 1994.

Nilsson, L., and B. Nyström, OPERA operations program for ALIS version 1.0, *IRF Tech. Rep. 037*, Swedish Institute of Space Physics, Kiruna, Sweden, 1992, ISSN 0284-1738.

Noxon, J. F., and R. M. Goody, Observations of day airglow, *J. Atmos. Sci.*, *19*, 342–343, 1962.

Okano, S., S. Takeshita, and M. Taguchi, Absolute calibration system at NIPR for aurora/airglow measurements using an 1.9 m integrating sphere, in *Proceedings of the 24th annual European Meeting on Atmospheric Studies by Optical Methods*, Sentraltrykkeriet A/S Bodø, 1997, ISBN: 82-994583-0-7.

Rees, D., M. Vyssogorets, N. P. Meredith, E. Griffin, and Y. Chaxell, The doppler wind and temperature system for the ALOMAR observatory: Design and initial results, *J. Atmos. Terr. Phys.*, *58*, 1827–1842, 1996.

Rees, D., R. W. Smith, F. Sigernes, K. Henriksen, U. Brändström, W. B. Wickwar, N. D. Lloyd, and M. Harris, Observations of thermospheric wind patterns in the vicinity of the polar cusp from a doppler imaging system, in *Proceedings of the 24th annual European Meeting on Atmospheric Studies by Optical Methods*, Sentraltrykkeriet A/S Bodø, 1997, ISBN: 82-994583-0-7.

Rees, D., U. von Zahn, G. von Cossart, K.-H. Fricke, W. Eriksen, and J. A. McKay, Daytime LIDAR measurements of the stratosphere and mesosphere at the ALOMAR observatory, *Adv. Space Res.*, 1999, proc. COSPAR meeting, Nagoya, July 1998, accepted.

Rees, D., M. Conde, Å. Steen, and U. Brändström, The first daytime ground-based optical image of the aurora, *Geophys. Res. Lett.*, *27*, 313–316, 2000.

Rees, M. h., and D. Luckey, Auroral electron energy derived from ratio of spectroscopic emissions 1. model computations, *J. Geophys. Res.*, *79*, 5181, 1974.

Rietveld, M. T., H. Kohl, H. Kopka, and P. Stubbe, Introduction to ionospheric heating at Tromsø —I. Experimental overview, *J. Atmos. Terr. Phys.*, *55*, 577–599, 1993.

Romick, G. J., and A. E. Belon, The spatial variation of auroral luminosity—II, *Planet Space Sci.*, *15*, 1695–1716, 1967.

Rydesäter, P., and B. Gustavsson, Investigation of smooth basis functions and an approximated projection algorithm for faster tomography, *Int. J. Imaging Syst. Technol.*, *11*, 347–354, 2001.

Rydesäter, P., Processing of multi-station auroral image data, Lic. thesis, Applied Physics and Electronics, Umeå University, Umeå, Sweden, 2001, ISBN: 91-7305-149-7.

Rydesäter, P., Å. Steen, U. Brändström, and B. Gustavsson, Classifying auroras using artificial neural networks, in *Ninth workshop on Virtual Intelligence / Dynamic neural networks*, edited by M. L. P. Thomas Lindbladh and J. Kinser, vol. 3728, pp. 115–120, Royal Institute of Technology, Stockholm, Sweden, The International Society for Optical Engineering, 1998, ISBN 0-8194-3202-4.

Rydesäter, P., B. Gustavsson, U. Brändström, and Å. Steen, Lossy compression of scientific images of aurora, in *Proc. of 28th Annual European Meeting on Atmospheric Studies by Optical Methods*, Sodankylä Geophysical Observatory, 2001, (in press).

Scourfield, M. W. J., and N. R. Parsons, Auroral pulsations and flaming — Some initial results of a cinematographic study using an image intensifier, *Planet Space Sci.*, *17*, 1141, 1969.

Seneca, *Quaestiones Naturales*, vol. I, chap. 14–15, (ancient text), ca. 63.

Steen, Å., and P. N. Collis, High time-resolution imaging of auroral arc deformation at substorm onset, *Planet. Space Sci.*, *36*, 715–732, 1988.

Steen, Å., P. N. Collis, and I. Häggström, On the development of folds in auroral arcs, *J. Atmos. Terr. Phys.*, *50*, 301–313, 1988.

Steen, Å., U. Brändström, and K. Kaila, A scientific and technical description of ALIS, in *Proc. NSSR Annual meeting Bolkesjø, Norway*, pp. 153–164, Nordic Society for Space Research, 1990.

Steen, Å., U. Brändström, and B. Gustavsson, ALIS — a multi station imaging system at high latitude with multi disciplinary scientific objectives, in *Proceedings 13th ESA Symposium on European Rocket and Balloon Programmes and Related Research*, pp. 261–266, ESA, 1997a.

Steen, Å., B. Gustavsson, and U. Brändström, Temporal variation of 2D altitude distributions of lee-wave generated polar stratospheric clouds, in *Proceedings of the 4th European symposium of polar stratospheric ozone*, 1997b.

Steen, Å., B. Gustavsson, U. Brändström, T. Aso, and M. Ejiri, OI 846.6 nm auroral imaging, in *Proceedings of the 25th annual European Meeting on Atmospheric Studies by Optical Methods, Granada, Spain*, pp. 90–95, Instituto de Astrofísica de Andalucia, Granada, Spain, 1999a.

Steen, Å., B. Gustavsson, C.-F. Enell, and U. Brändström, PSC dynamics investigated by multi-station imaging — techniques, results and prospects, in *Air pollution research report. Mesoscale processes in the stratosphere*, edited by K. Carslaw and G. Amanatidis, vol. 69, pp. 239–242, European Comission, 1999b, ISBN 92-828-4629-6.

Stenbaek-Nielsen, H. C., and T. J. Hallinan, Pulsating auroras: Evidence for non-collisional thermalization of precipitating particles., *J. Geophys. Res.*, *84*, 3257–3271, 1979.

Stoffregen, W., All-sky camera auroral research during the third geophysical year 1957–1958, *Tellus*, *7*, 509–517, 1955.

Stoffregen, W., An all-sky camera for auroral research, description and operational manual, *Tech. rep.*, Uppsala Jonosfärsobservatorium, 1956.

Stoffregen, W., ed., *I.G.Y. ASCAPLOTS*, vol. XX (part 1) of *Annals of the international geophysical year*, Pergamon Press, Oxford, London, New York, Paris, 1962.

Størmer, C., Bericht über eine Expedition nach Bossekop etc., *Vid. Selsk. Skr. Math. Nat. Kl.*, 1911, Christiania (Oslo), Norway.

Størmer, C., Photogrammetrishe bestimmung der Höhe von irisierenden Wolken (Perlmutterwolken) am 30. Dezember 1926., *Geofysiske Publikasjoner*, *5*, 1–8, 1930.

Størmer, C., *The Polar Aurora*, Clarendon Press, Oxford, 1955.

Veklerov, E., and J. Llacer, Feasible images and practical stopping rules for iterative algorithms im emission tomography, *IEEE Trans. Medical Imaging*, *8*, 186–193, 1989.

von Zahn, U., M. Gerding, J. Höffner, W. J. M. Neil, and E. Murad, Fe, Ca and K atom densities in the trails of Leonids and other meteors: Strong evidence of differential ablation., *Meteorit. Planet. Sci.*, *34*, 1017–1027, 1999.

Waldemark, J., V. Becanovic, U. Brändström, C. Holmström, M. Larsson, T. Lindblad, C. S. Lindsay, and Å. Steen, Investigation of useful image preprocessing for analysis of aurora images, in *Proceedings EANN*, 1997.

Wannberg, G., The G2-system and general purpose alternating code experiments for EISCAT, *J. Atmos. Terr. Phys.*, *55*, 543–557, 1993.

Weinbren, M., *A manual of tomography*, H. K. Lewis & Co., 1946.

Weinstock, J., Theory of enhanced airglow during ionospheric modifications, *J. Geophys. Res.*, *80*, 4331, 1975.

Weinstock, J., and B. Bezzerides, Theory of electron acceleration during parametric instabilities, *Phys. Rev. Lett.*, *32*, 754–758, 1974.

Widell, O., and H. Henricson, Intercalibration of low light level sources, in *Proc. of 28th Annual European Meeting on Atmospheric Studies by Optical Methods, Oulu, Finland*, Sodankylä Geophysical Observatory, 2001, (in press).

Wilcke, J. C., *Tal om de nyaste förklaringar öfver Norr-Skenet, hållet, i Kongl. Maj:ts höga närvaro, för dess vetenskaps-academie, vid praesidii nedläggande, den 7 Febr. 1778*, Johan Georg Lange, Stockholm, 1778.

Yamauchi, M., Private communication, 1999, (see also `http://www.irf.se/pics/YamaAuroraVideo/`).

Index of acronyms

Index of notation

Index